

SURFACE MODIFICATION OF CARBON FIBERS

Improvement of the dissipative properties of carbon fiber reinforced plastics

Dissertation zur Erlangung des akademischen Grades

- Dr. rer. nat. -

Eingereicht an der Fakultät für Naturwissenschaften der Universität Paderborn

von

Anna Becker-Staines

geboren am 23.03.1989 in Redkaja Dubrawa (Altai)

Universität Paderborn
Fakultät für Naturwissenschaften
Department Chemie
Coatings, Materials & Polymers



Erstgutachter: Prof. Dr. Wolfgang Bremser

Zweitgutachter: Prof. Dr. Thomas Tröster

Acknowledgement

An dieser Stelle möchte ich mich bei Prof. Wolfgang Bremser und Thomas Tröster bedanken, die es mir ermöglicht haben diese Arbeit anzufertigen. Diesen Dank möchte ich auch an Oliver Seewald und Oliver Strube weiterreichen.

Für ein tolles Arbeitsklima sorgen nicht nur die Chefs, sondern auch die Kollegen. Daher gilt ein großer Dank auch an die „Mini-Me“s und die epischen Büro-Abende. Obwohl ich einige „Leiden“ durchstehen musste, sehe ich mit Freuden auf die Bürozeit mit Arthur Oswald, Daniel Appel und David Wedegärtner zurück. Meinen anderen Kollegen aus dem Arbeitskreis möchte ich ebenfalls meinen Dank ausdrücken und darüber hinaus im Speziellen erwähnen: Kathi, Manuel, Anne, Tobi, Deniz, Christian, Meike, Swetlana. Und meinen Studenten Cüneyt, Jana und Lea möchte ich für ihre ausgezeichnete Zusammenarbeit und Leistung danken.

Meiner Familie und meinem Ehemann steht der größte Dank zu. Ich kann mich glücklich schätzen über eure Liebe und eure Unterstützung. Danke an Viktor Becker, Nina Becker, Stefanie Becker und Colin Staines.

Abstract

“The future is now”

- BMW

BMW set pioneer steps towards the reduction of the carbon footprint for daily life in the automotive sector. Our present-day tasks in innovation are not just technology and economy related, but involve demands concerning ecology, sustainability and resource conservation. Today's technological designs combine innovation with sustainability, and focus in the overall transportation industry not just on alternative fuel sources but also on lightweight construction. The idea of weight reduction of structural components describes lower fuel consumption and therefore, lower CO₂ emissions. One of the most promising materials for lightweight designs are carbon fiber reinforced plastics. Carbon fibers show impressive properties in terms of low density and high strength and are therefore, a popular choice for lightweight construction.

This study developed from a technical issue: Is it possible to develop a CFRP component, which is optimized in its frictional behavior, while it keeps its excellent density to strength ratio? Although CFRP compounds have remarkable mechanical properties, their deformation behavior leads to problems; including the formation of internal stress and brittle shock absorption. This is caused by the tightly bound construction of composites in combination with the low elongation ability of carbon fibers, which also makes it difficult to perform forming processes, like compression and bending. The present study shows a new approach regarding this topic, which focuses on the energy dissipation ability of CFRP composites. An elastic modulus optimization through fiber-plastic interphase modification was performed. The modification of the fiber-plastic interface allows the creation of an interphase with improved energy dissipation, ductile-like failure behavior, elastomeric character, enhanced plastic deformation behavior and low friction. This approach promises a reduction in internal stress, enhanced shock absorption and lower defect formation during manufacturing and processing.

This study presents an unprecedented approach regarding the manipulation of the fiber-plastic interphase of CFRP composites with polydimethylsiloxane. PDMS is a well-known material in terms of low friction and its use as slip additive. Due to hydrodynamic friction, PDMS is a promising material for the objective of this study. Different coating methods were used for the deposition of PDMS onto carbon fibers: covalent bonding and physical adsorption of macro-sized PDMS structures. PDMS was successfully coated on carbon fibers and analyzed chemically and mechanically. A second approach, covered by this study, describes the manipulation of the fiber-plastic interface through the interaction in complex formation.

Contents

Chapter 1: Introduction	1
1.1. Carbon Fibers	2
1.1.1. Carbon Fibers: Structure and Manufacture	3
1.1.2. Carbon Fibers: Properties.....	4
1.2. Carbon Fiber Reinforced Plastics	5
1.2.1. Carbon Fiber Reinforced Plastics: Epoxy Resins as Matrix Component.....	6
1.2.2. Carbon Fiber Reinforced Plastics: Reinforcement and Breakdown.....	7
Chapter 2: Surface Modification of Carbon Fibers.....	11
2.1. Object of Investigation and Concept of Dissertation.....	14
2.2. Materials for Modification of Carbon Fiber Surface.....	17
2.3. Impact of Coating on Surface Chemistry and Chemical Analysis	19
2.3.1. Scanning Electron Microscopy	19
2.3.2. Atomic Force Microscopy.....	20
2.3.3. Contact Angle Analysis.....	21
2.3.4. Corrosion Analysis.....	23
2.4. Impact of Coating on Fiber-Plastic Interface and Mechanical Analysis	24
2.4.1. Micromechanical Analysis	24
2.4.2. Macromechanical Analysis	30
Chapter 3: Covalent PDMS Coating on Carbon Fibers	33
3.1. Experimental.....	34
3.2. Chemical Composition of Carbon Fiber Surface	38
3.3. Physical Appearance and Nanomechanical Analysis of Carbon Fiber Surface	39
3.4. Polarity and Wettability of Carbon Fiber Surface	45
3.5. Corrosion Potential of Carbon Fibers	47
3.6. Fiber-Plastic Interface Characterization	50
3.7. First Impressions of Carbon Fiber Reinforced Plastics	59
3.8. Summary.....	65

Chapter 4: PDMS Microgel on Carbon Fibers.....	69
4.1. Experimental.....	70
4.2. Optical Analysis of PDMS Microgel Deposition onto Carbon Fibers	71
4.3. Fiber-Plastic Interface Characterization	72
4.4. Summary.....	74
Chapter 5: PDMS Janus Particles on Carbon Fibers.....	77
5.1. Experimental.....	79
5.2. Optical Analysis of PDMS-Janus Particle Deposition onto Carbon Fibers	80
5.3. Fiber-Plastic Interface Characterization	81
5.4. Summary.....	83
Chapter 6: Cyclodextrin on Carbon Fibers	85
6.1. Experimental.....	87
6.2. Analysis of β -Cyclodextrin coated Carbon Fiber Surface.....	88
6.3. Fiber-Plastic Interface Characterization	89
6.4. Summary.....	91
Chapter 7: Summary of Dissertation.....	95
Bibliography	101

Chapter 1: Introduction

Green energy, fuel consumption and CO₂ emissions are trend-setting keywords in our modern era. As they rise in importance as social ideals, they win attention not just in the environmental sector, but also in political debates, economical advertisement and industrial regulations. As a result, the use of lightweight construction strategies increased drastically in the last decades and thus the application of multimaterial components and hybrid structures. Since the lightweight concept is defined as low weight in combination with excellent mechanical properties, hybrid materials, like carbon fiber reinforced plastics, are present in industries such as aerospace,¹⁻³ automotive,⁴⁻⁶ construction⁷⁻⁹ and sports¹⁰⁻¹².

Hybrid structures, also called composites, are heterogeneous combinations of different materials, which have superior properties than their pure single structures. Smart design and up to date production techniques are necessary to generate high performance compounds. In general, composites can include a huge variety of material combinations, such as laminates (e.g. nacre ¹³), porous materials (e.g. zeolites ¹⁴) or fiber reinforced materials (e.g. wood ¹⁵). Nowadays, fiber reinforced plastics are one of the most important composite materials in the transportation industry. The combination of fibers and plastics create structures, which are lightweight, resource efficient, emission reductive, corrosion resistant and high strength. As for the fiber part, carbon fibers are gaining more and more importance, since they have the best ratio of low density and high strength. ¹⁶

1.1. Carbon Fibers

Compared to other fillers, e.g. natural fibers and inorganic particles, carbon fibers are a fairly new material, ¹⁷ and its demand is rising daily (Fig 2). The reason for the growing importance in industrial and commercial use of carbon fibers are the outstanding properties: low density, chemical and thermal stability, high tensile strength and high elastic modulus.

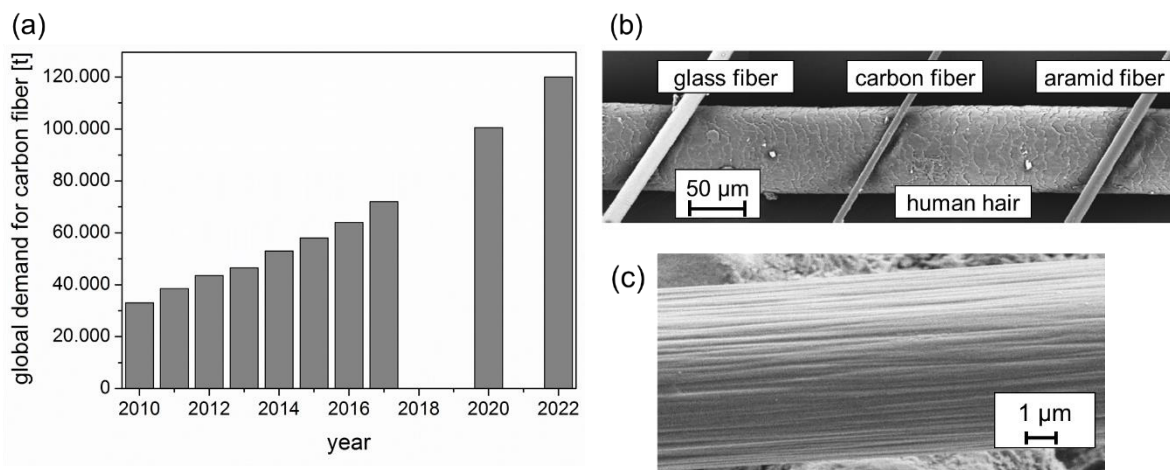


Fig 1: (a) Global demand for carbon fibers (estimated values for 2016 - 2022). ¹⁸ (b) Scanning electron microscopy image of comparison between glass fibers, carbon fibers, aramid fibers and human hair. ¹⁶ (c) Scanning electron microscopy image of a carbon fiber.

In general, materials show higher strengths in their fiber form than in any other formation. This is mainly caused by the size effect, as described by the theory of brittle failure based on the Weibull distribution: the smaller the volume of the material, the less strength-reducing defects exist. As for carbon fibers, the bond-dissociation energy and the structure and orientation of the crystal lattice are unique and increase the tensile strength on top of the geometrical factors. ¹⁶

1.1.1. Carbon Fibers: Structure and Manufacture

Carbon fibers are made of graphite, and thus graphene layers, which means the carbon atoms are sp^2 hybridized and the crystal lattice is defined as hexagonal. The graphene layers themselves are crystalline, the carbon atoms are bonded covalently and the bond-dissociation energy is 614 kJ/mol. However, between the graphene layers, there are just weak van der Waals forces and π -interactions present.¹⁹ Macroscopically, the fiber structure can be described as anisotropic, turbostratic and non-crystalline.²⁰

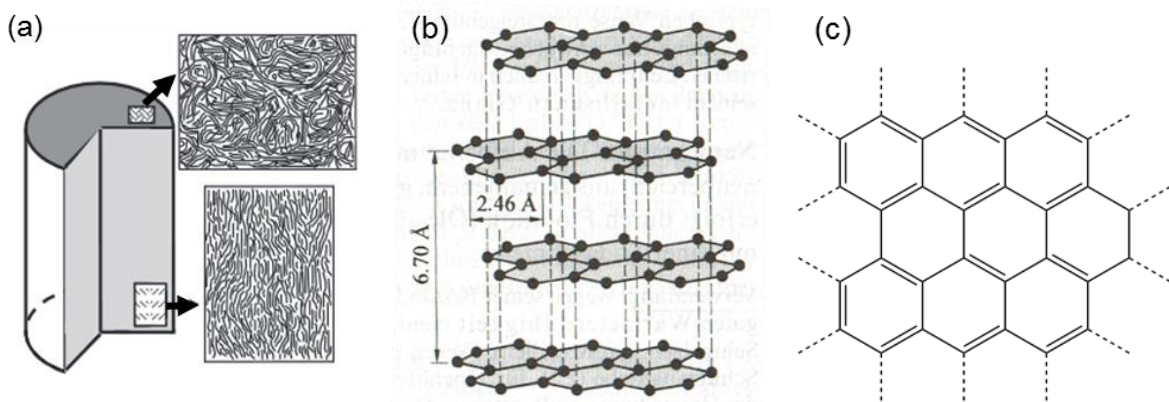


Fig. 2: (a) Schematic illustration of the structure and graphene layer assembly of high strength carbon fibers.²⁰ (b) Primitive cell of hexagonal graphite crystal structure.¹⁹ (c) Valence structural formula of one possible mesomeric structure of a graphene layer.

Most of the properties of carbon fibers depend on the manufacturing process, since impurities, defects and graphene layer organization are defined by the production procedure.^{16,21,22} The main component of carbon fibers is carbon, but depending on the materials and processing, nitrogen and oxygen are also present. Nowadays, polyacrylonitrile is mainly used as precursor for carbon fiber production. Several treatments are used to obtain carbon fibers from PAN fibers (Fig. 3). First, the fibers are treated at 200 to 300 °C in air, so cyclization and dehydrogenation take place. The following carbonization process describes the loss of impurities and formation of graphite layers at 1500 to 3000 °C in inert atmosphere and under tension.

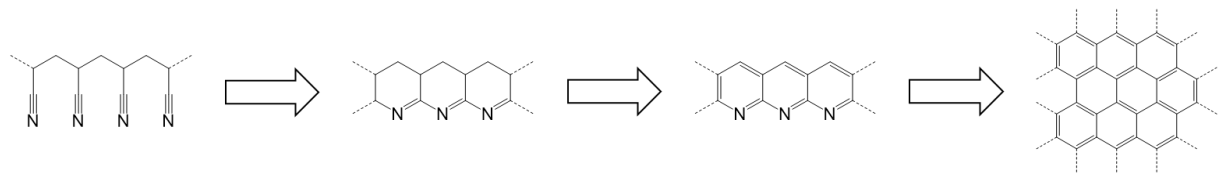


Fig. 3: General reaction procedure during the manufacturing of PAN based carbon fibers: cyclization, dehydrogenation and carbonization.^{16,22,23}

Depending on the process parameters, different mechanical properties can be obtained, e.g. high tenacity (HT) or high modulus (HM) fibers. In general, higher treatment temperatures and higher drawn tension increase the organization of the graphene layers (parallel to the fiber

direction) and thus, increase the elastic modulus. After manufacturing, the carbon fibers are treated under oxidizing conditions, so oxygen-containing groups are introduced to the fiber surface. These act as reaction centers for sizing or further processing. The surface treatment can be performed either in oxidizing acids or thermally in air. If a sizing is requested, the coating material has to be compatible with the plastic that is used in the composite.

1.1.2. Carbon Fibers: Properties

Carbon fibers have outstanding properties, due to their molecular structure and geometry. The most important characteristics for industrial and commercial use are the low density of 1.8 g/cm^3 in combination with high elastic modulus (HM) and high tensile strength (HT). Since both mechanical properties can be set and varied through the parameters of the production process,²⁰ carbon fibers can be specifically designed for their final purpose and use. Further advantages¹⁶ of carbon fibers are their fatigue strength, high rigidity, chemical and thermal stability, compatibility with synthetic polymers and biomaterials, and thermal and electric conductivity.

Due to their anisotropic structure, carbon fibers have different properties parallel or perpendicular to the fiber. Since the graphene layers are organized parallel to the fiber, the strong covalent bonds within the graphene layer lead to high strengths parallel to the fiber. However, the graphene layers can slide against each other, due to weak van der Waals forces between the layers and this causes lower strengths perpendicular to the fiber. The anisotropic behavior can also be observed for the thermal and electric properties, since the π -electrons are delocalized within the graphene layers, but not perpendicular between them.¹⁶

Tab. 1: Comparison of different fiber materials and their mechanical properties. [Note: the table sums up rounded values for all fibers. Depending on the modulus (for carbon: HT or HM; for glass: E or S) and environmental conditions (for natural fibers) the mechanical values can vary strongly]

	density [g/cm ³]	tensile strength [GPa]	elastic modulus [GPa]	elongation at break [%]	ref.
aramid fiber	1.4	3.0	100	3.5	16,24
jute fiber	1.4	0.6	20	1.3	16,24
carbon fiber	1.7	4.0	300	1.5	16,21,24,25
spider silk	-	1.0	10	27	25,26
steel (bulk)	7.8	1.5	20	0.8	25
coir fiber	1.2	0.2	5	28	24
glass fiber	2.5	3.5	75	2.7	16,24

There are, nevertheless, disadvantages of using carbon fibers for composites. The primary complication is the brittleness of carbon fibers. Additionally, carbon fibers have an elongation

to failure of just approx. 1 %, low compressive strength, are the most expensive commercial fiber material and their rigidity makes them complicated to process in compounds with e.g. tight radii. Due to their electric conductivity, carbon fibers cannot be used as insulation material and cannot be used in direct contact with most metals, otherwise corrosion processes can take place in the presence of an electrolyte; exceptions are titanium and stainless steel.¹⁶

1.2. Carbon Fiber Reinforced Plastics

Carbon fibers are an essential component for high performance composites. Due to their geometry, they cannot be used as pure single structures, but have to be embedded in a matrix: the fibers are fixed in a solid shape and the construct is called “carbon fiber reinforced plastic”. Although carbon fibers are expensive, their excellent properties allowed them to become a well-established material in several industries and on the global market.



Fig. 4: (a) “The future is now”. The BMW i3 is a famous example for the use of carbon composites in the automotive sector. The electric vehicle uses carbon fiber reinforced plastics as lightweight components.²⁷ (b) The Boeing 787 Dreamliner is a pioneer in the aircraft industry and made up of multimaterial design, thereof 50 % advanced composites, including CFRPs.^{28,29}

The task distribution between fibers and matrix is defined clearly: the carbon fibers absorb mechanical loads and the plastic forms the composite’s shape and secures the fibers’ position within the hybrid structure. Commercially available CFRP composites are mostly delivered as prepgres. This term describes a fabric with alternating aligned layers of laminates, in which the fibers of each layer can be unidirectional or woven. The fibers are pre-impregnated and the plastic is partially cured. This allows easy handling during delivery, storage and processing but also includes special requirements for the prevention of early curing. Although the matrix is the weak point of the composite, it is of necessary use for the transfer of mechanical loads to and between the fibers and the separation of the fibers from the environment.¹⁶ Of course, the plastic should be chosen to fit the composite’s later use, but ideally, the plastic’s properties also compensate the disadvantages of the carbon fibers.

CFRPs have to be used economically. Smart utilization of CFRPs can mean, that the composites are placed in high loaded areas as local reinforcements in structural components. This way, metals are not completely replaced by CFRPs in multimaterial design, but used less and mostly as a support or carrier material. CFRP reinforced metals are produced by either curing the prepreg directly on the metal or using an additional adhesive. The conventional process for the production of CFRP-metal composites describes a two-step hybridization: first, the metal sheet is being formed into the required shape and then, the CFRP component has to be formed onto the formed metal sheet. Both process steps need heat and time. Novel one-step hybridization approaches combine the simultaneous forming of CFRP and metal layers and lead to reduction of used energy (in form of heating), process time and cycle times. Therefore, efficient manufacturing objectives focus on combined forming of CFRP reinforced metal structures.^{30–32}

1.2.1. Carbon Fiber Reinforced Plastics: Epoxy Resins as Matrix Component

Theoretically, all plastics can be used for the construction of CFRPs; the most common plastics are epoxy resins as matrix material. These thermosetting resins are excellent adhesives and have good mechanical properties: tensile strengths of 50 to 90 MPa, elastic moduli of 3 to 8 GPa and fracture strains of 2 to 8 %.^{33–36}

Epoxy resins can be used as 1K or 2K systems. 1K systems are cured via hydroxyl and epoxy groups in condensation reactions. The 2K systems need curing agents like amines, acid anhydrides or carboxylic acids, for the polyaddition of the epoxy groups. The technically most relevant systems are the 2K resins of aromatic glycidyl ethers (Fig. 5 (a)) and the polymerization results in a thermally and chemically stable plastic, with low or even no shrinkage.³⁷ The cross-linking epoxy groups have a high ring strain and a reactive oxygen atom. Due to the polarity of epoxides, the two carbon atoms are electrophilic and undergo nucleophilic substitution reactions. The mechanism of the nucleophilic attack defines the structure of the reaction product. A strong nucleophile causes a base-catalyzed ring opening and the S_N2 reaction occurs on the less substituted carbon atom of the epoxide ring (Fig. 5 (b)). A weak nucleophile, on the other hand, does not attack the epoxide ring directly, but the ring opening is acid-catalyzed and the epoxide is first protonated and then attacked at the more substituted carbon atom in a S_N1 like reaction.³⁸

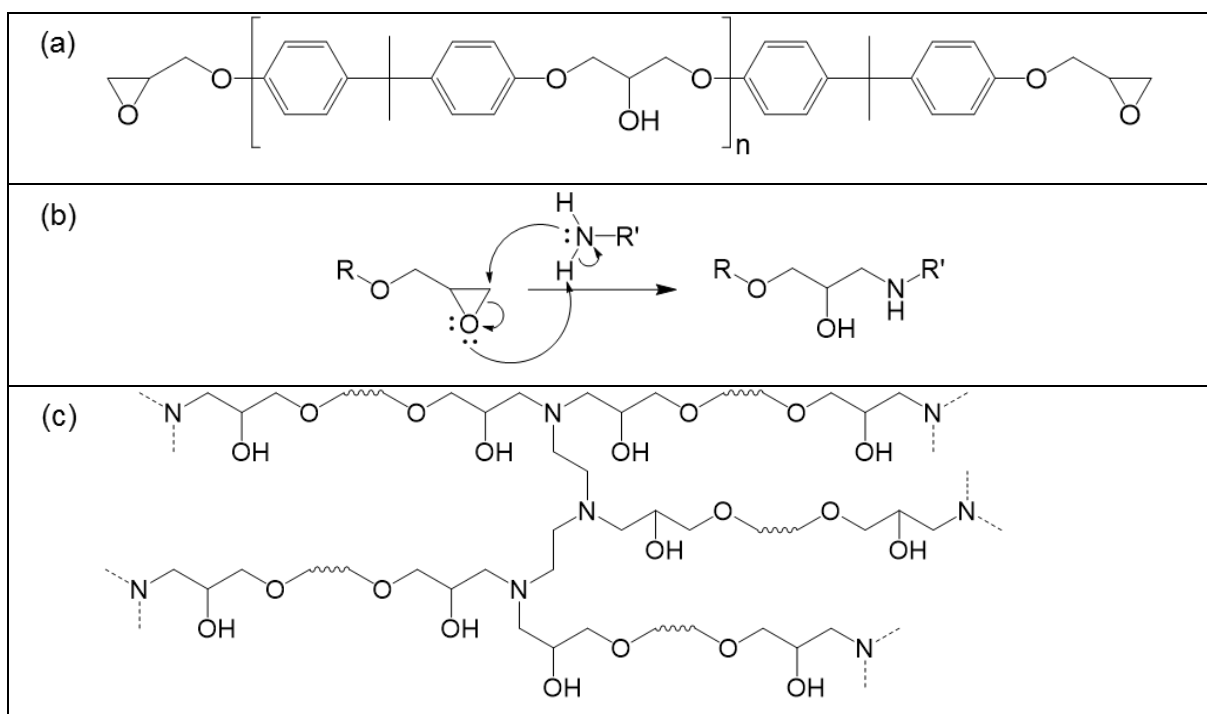


Fig. 5: (a) Molecular structure of an aromatic glycidyl ether resin. (b) S_N2 reaction mechanism of a glycidyl and an amino group. (c) Illustration of an amino cured epoxy resin network (used amine: diethylenetriamine).

The reaction rate is usually set by the curing agent: high basicity and less steric hindrance increase the curing agent's reactivity and therefore, increase the reaction rate. More importantly, the steric arrangement of the curing agent also determines the degree of cross-linkage: the more cross-linking groups are available in the curing agent, the higher the degree of cross-linkage (Fig. 5 (c)). An easy control of cross-linkage is given by amines; they are available in many varieties of aliphatic, cycloaliphatic or aromatic arrangements. The higher the degree of cross-linkage, the less elastic and the harder the plastic.³⁷

1.2.2. Carbon Fiber Reinforced Plastics: Reinforcement and Breakdown

CFRP composites combine two rigid and brittle materials to a hybrid structure, which is seemingly less rigid and brittle than its single structures. This reinforcement effect is caused by the structure of the composite and its influence on crack behavior and load distribution.¹⁶ A crack can grow unhindered in a pure material, and in case of this material being brittle, the component fails abruptly; but in a fiber reinforced material, the crack propagation stops at every single fiber and the mechanical load is then being redistributed to several neighboring fibers. More specifically, a crack does not break a fiber immediately, but has a notch effect on it. Depending on the severity of the induced stress on the fiber, the crack propagation stops or the fiber breaks and the crack continues growing until it reaches the next fiber. This failure behavior has two advantages: first, even if a few fibers break, it does not mean, that the entire composite

fails; and second, the crack propagation is slowed down, so that even brittle matrices do not fail abruptly.³⁹

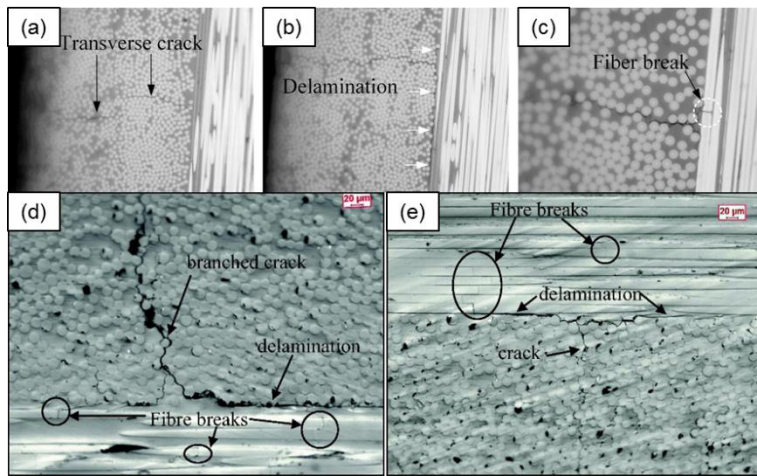


Fig. 6: Microscopic images of (a) a transverse crack, (b) delamination (and visible transverse crack) and (c) a fiber break in a carbon fiber reinforced epoxy resin.⁴⁰ (d & e) Microscopic images of transverse and branched cracks, delamination and fiber cracks in a glass fiber reinforced epoxy resin.⁴¹

The visible component separation between CFRP laminates is called delamination. The detachment of fibers and matrix can be caused by brittleness and rigidity of the single structures, low adhesive forces between fiber and matrix, external high-impact loads and high internal stress in the composite. Changing the elastic properties of the matrix is possible, if the degree of cross-linkage and the structure of the polymer network is variable. However, in most cases it is easier to switch the matrix component to a more ductile material. Not just the single materials but also their interfaces are important in the detachment process of a composite. The fiber-matrix interface has direct influence on the energy transfer between both components: the stronger the adhesion between them, the more energy is necessary for their separation. This means, strong adhesive forces between fiber and matrix lower the speed of crack propagation and lower the possibility of fiber-matrix separation and delamination. Nevertheless, this is just the case until a certain level (e.g. high impact) or kind (e.g. high frequency cycles) of external load occurs. However, high adhesive forces between fibers and matrix do not just have advantages, but can also cause internal stress. Since the single materials have different elastic properties and fracture strains, their deformation behavior differs under stress. A strong adhesion in case of two differently deforming materials can cause cohesive failure or creasing. These problems are also of high importance in processing of CFRP composites.

Chapter 2: Surface Modification of Carbon Fibers

The classical approach for the improvement of multimaterial structures is the enhancement of the strength of the individual components and their connection. Therefore, most research within the field of CFRPs focuses on a strong adhesion between fibers and plastic in hope of a better energy transfer and thus better mechanical properties. A strong bonding between fiber and plastic can be achieved by increasing the carbon fiber surface area and introducing functional groups to the carbon fiber surface. This surface activation removes contaminants and increases the wettability of the fiber, the amount of covalent bonds between fiber and plastic, and the mechanical interlocking between fiber and plastic. The typical methods for activation of the carbon fiber surface are oxidation processes, e.g. electrochemical oxidation,^{42,43} plasma,^{44–46} thermal treatment,^{47,48} but also chemical modification, e.g. with ammonia⁴⁹ or Diels Alder reagents.⁵⁰ This study focuses on the chemical oxidation of the carbon fiber surface with nitric acid.^{51–57}

Nitric acid is a strong oxidizing agent, which causes oxidation of the carbon atoms, starting on the edges of the graphene layers. Oxidation increases the quantity of all oxygen containing groups on the fiber surface, especially of hydroxyl groups and carboxylic acids. These functional groups increase the carbon fiber's polarity, and thus wettability, and the overall reactivity for covalent bonding. Further oxidation causes the formation of CO_2 , which is expelled as gas (Fig. 7 (a)). The carbon erosion can be observed as weight loss and increasing surface porosity, since the graphene layers are removed gradually (Fig. 7 (b)).^{42,51,52} The reaction yield, meaning the degree of oxidized carbon on the fiber surface, can be controlled by the nitric acid concentration, the treatment temperature and/or the oxidation time.

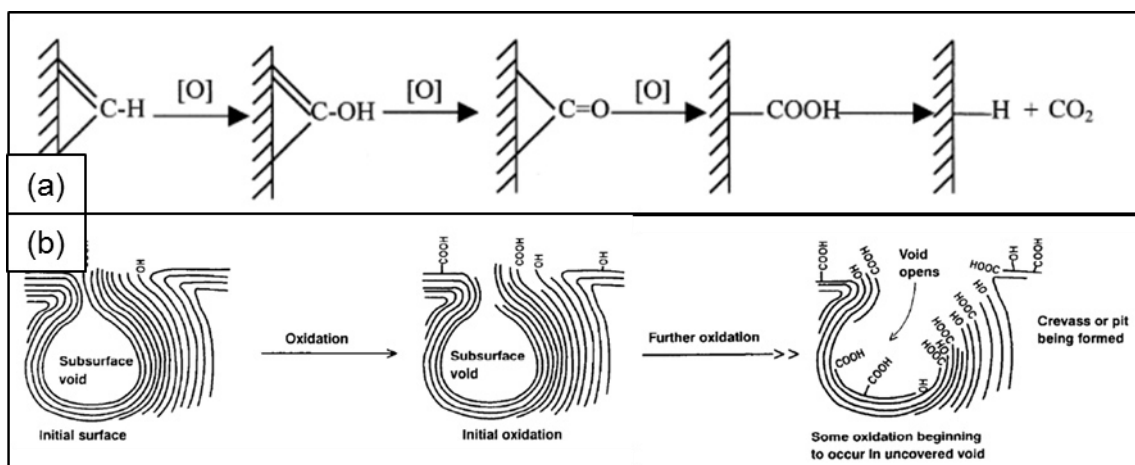


Fig. 7: Oxidation of graphene layers on carbon fiber surface through nitric acid. (a) Schematic overview of the gradual oxidation of carbon atoms on the carbon fiber surface.⁴² (b) Schematic illustration of the carbon erosion, increased surface area and porosity through oxidation.⁵¹

Oxidized carbon fibers can be directly used for CFRP composites. In a carbon fiber reinforced epoxy resin with an amine as curing agent, reactions can occur between the carbon fiber surface and the epoxy resin, but also between the fiber surface and the curing agent.^{51,52,58}

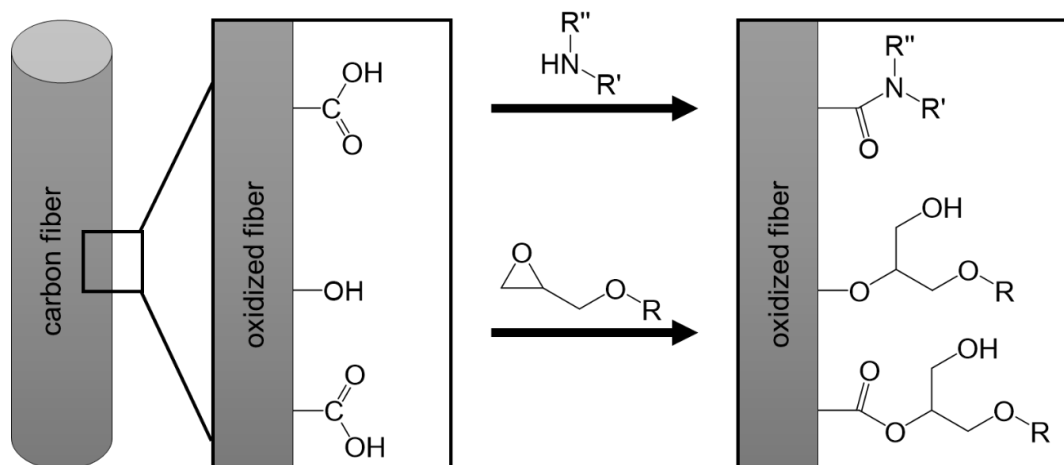


Fig. 8: Most relevant reactions between the oxygen-containing carbon fiber surface with the amine cross-linker and with the epoxy resin.

Further improvement of interfacial fiber-matrix adhesion is promised by sizing of carbon fibers. This process describes a coating of the carbon fiber with a polymer and is performed as the last step of carbon fiber production. The sizing protects the carbon fibers from environmental influences and stress due to transportation and processing. However, the use of polymers as sizing agents grants the incorporation of the carbon fiber surface into the polymeric network of the final CFRP composite. Meaning that, the new created interphase can be tailored precisely to the adhesive requirements of fiber and plastic. Classic examples for sizing agents are epoxy resins,^{59–61} polyurethane,^{61–63} vinyl ester resins,^{64,65} polyamide,^{61,63} polyimide,⁶³ acrylic acid,^{66,67} polymethylmethacrylate⁶⁸ and polystyrene⁶⁹. State-of-the-art sizing is not just defined as polymer coatings anymore, but may also include particle sizing, like nickel particles,⁷⁰ or hierarchical designs of carbon-carbon sizing using carbon nanotubes^{71–76} and graphene oxide^{77,78} or even combinations of sizing agents, e.g. carbon nanotubes with silane coating and zinc oxide nanorods⁷⁹. Creating an entirely new phase within a CFRP composite also opens new possibilities in terms of incorporated sensors and damage detection or self-healing mechanisms.^{80–82}

Most of these efforts enhance the fiber-matrix adhesion. This has a positive influence of the crack propagation in a damaged CFRP composite, due to higher separation energy of fiber and plastic, and better energy transfer between them. However, enhancement of the fiber-matrix adhesion leads to increased brittleness of the compound. Though tightly bound and therefore higher in strength, the compound is less elastic and more rigid, and therefore shows low shock absorption and impact stress.^{51,52} Not only is high brittleness not desired in many applications, it creates new problems in the manufacturing chain. Processing, like bending, folding or combined forming,^{30,31} are difficult, because of the composite's low deformation performance and tendency for creasing and kinking.^{83–88}

2.1. Object of Investigation and Concept of Dissertation

This study focuses on the fiber-plastic interface of CFRPs. Modification of the carbon fiber surface and coating it with a sizing agent, manipulates the interface interactions of fiber and plastic and therefore influences the CFRP's performance. Failure behavior is defined by various parameters, including strength, modulus, deformation and energy dissipation. Internal stress and external loads can damage a compound and lead to a breakdown. An external load is not necessarily caused by a crash, but most often introduced via processing during manufacturing. Tightly bound composites are high in strength, but also brittle and less elastic. Therefore, forming processes are difficult to perform, due to the CFRP's plastic deformation behavior. Processing of CFRPs include compression and bending and can be performed with or without a metal component. Longitudinal compression of CFRP composites lead to fiber kinking and the formation of kink bands.^{83,85,89} Creasing can be observed in bending processes, like combined forming^{30–32} or clinching^{90,91} of CFRP-metal composites.

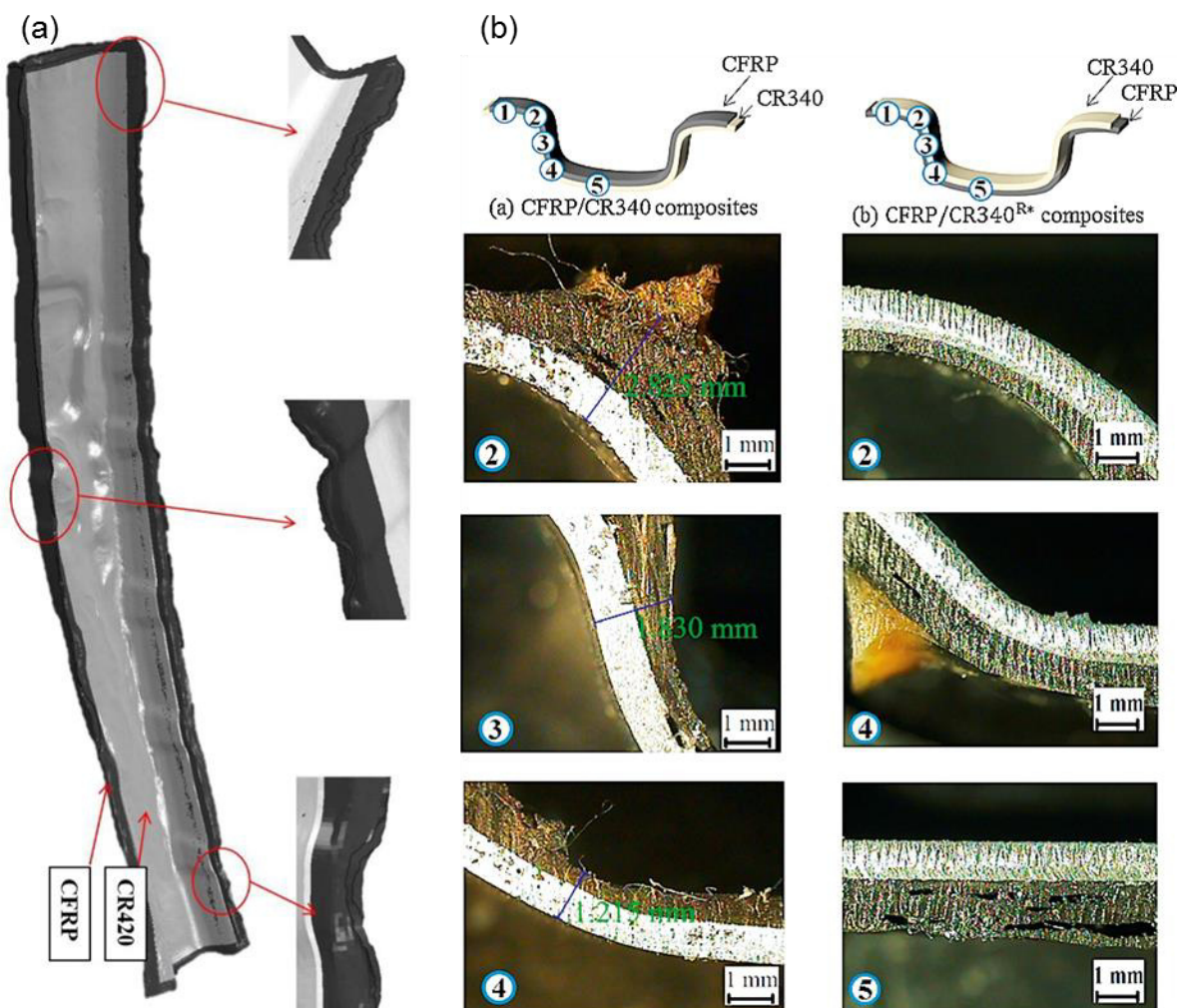


Fig. 9: Examples for CFRP failure during processing. (a) Wrinkling of CFRP-metal composite caused by one-step forming.⁹² (b) Comparison of different defects of CFRP-metal composites after deep drawing.⁹³

Improving the energy dissipation of CFRP composites can lead to better plastic deformation behavior, and therefore to enhanced shock absorption and to lower defect formation during manufacturing and processing. Reducing the internal stress between fiber and plastic, a ductile interphase can be applied. Ductility enables relaxation, which relieves internal stresses. If the interphase is more elastic than the fibers and the matrix, it can undergo plastic deformation, when an external load is applied. This way, the possibility of failure is lower, since the interphase is not brittle and the crack propagation cannot form local stress peaks. Meaning, the elastomeric interphase acts as a soft buffer. Successful approaches of elastomeric sizing were performed with copolymers of methyl acrylate and acrylonitrile,⁹⁴ DGEBA, butadiene acrylonitrile and methane diamine,⁹⁵ and carboxyphenylmaleimide and styrene⁹⁶.

Next to ductility and elastomeric properties, the ideal interphase for energy dissipation should lower the friction between the components. Friction describes the force between two objects, which are in direct contact with each other, and can be separated in a static and a kinetic part. Static friction is defined as the force, which is necessary to set one object in motion and kinetic friction describes the force, which is necessary for the object to stay in motion. The friction coefficient is material-dependent, but the friction resistance is defined by the adhesion of the objects and by the deformation behavior of the contact area.⁹⁷⁻⁹⁹ The fiber-resin adhesion and the deformation of the interphase are aimed to be modified in this work with the focus on hydrodynamic friction.

$$F_x = \mu_x \cdot F_N \quad (1)$$

- F_x static / kinetic friction force
- μ_x static / kinetic friction coefficient
- F_N normal force

This study focuses on polydimethylsiloxane as fiber coating, due to its interesting properties in terms of friction,¹⁰⁰ low surface energy,¹⁰¹ and thermal,¹⁰² electrical¹⁰³ and chemical stability¹⁰⁴. PDMS is widely known as cosmetic additive and lubricant, thanks to its inertness,¹⁰⁴ antifoaming properties¹⁰⁵ and lubricating effect¹⁰⁶. For coating purposes, the viscoelastic behavior¹⁰⁷ and hydrophobicity¹⁰⁸ of PDMS are also of high interest. The mechanical properties include high flexibility and high compressibility.^{109,110} All in all, a PDMS coating on carbon fibers promises a low friction, elastomeric sizing which acts as protective layer.

PDMS can be coated in different ways onto the carbon fiber surface. The best results should be obtained by covalent bonding of functionalized PDMS with the oxygen containing carbon fiber surface. For that, oxidized carbon fibers were treated in PDMS under high temperatures. Next to reaction time and temperature, different molar masses and molecular structures of PDMS were studied. A faster and more economical approach is the physical adsorption of micro-sized PDMS structures via dip coating. Here, two PDMS systems were studied: PDMS-microgel and PDMS-kaolinite-Janus-particles. The microgel was synthesized by cross-linking PDMS in presence of an emulsifier. The resulting product is an emulsion of PDMS spheres with sizes in the micro scale. The PDMS-kaolinite system describes two-faced lamellar particles, so called Janus particles¹¹¹. The clay^{112,113} acts as carrier particles for the PDMS phase, which is grafted on beforehand and can be easily applied on the carbon fiber via physical adsorption.

As an excursus, an other approach was used: cyclodextrins were covalently bonded on carbon fibers for the use as a different bonding system. Cyclodextrins are cyclic oligosaccharides and can form complexes with aromatic compounds. They have a hydrophilic exterior and a hydrophobic interior, which makes them soluble in water and able to incorporate hydrophobic compounds into their cavity.^{114,115} Since they can act as host molecules for aromatic compounds like the monomers of epoxy resins (Fig. 5 (a)), polymerizations can be performed with location specificity.

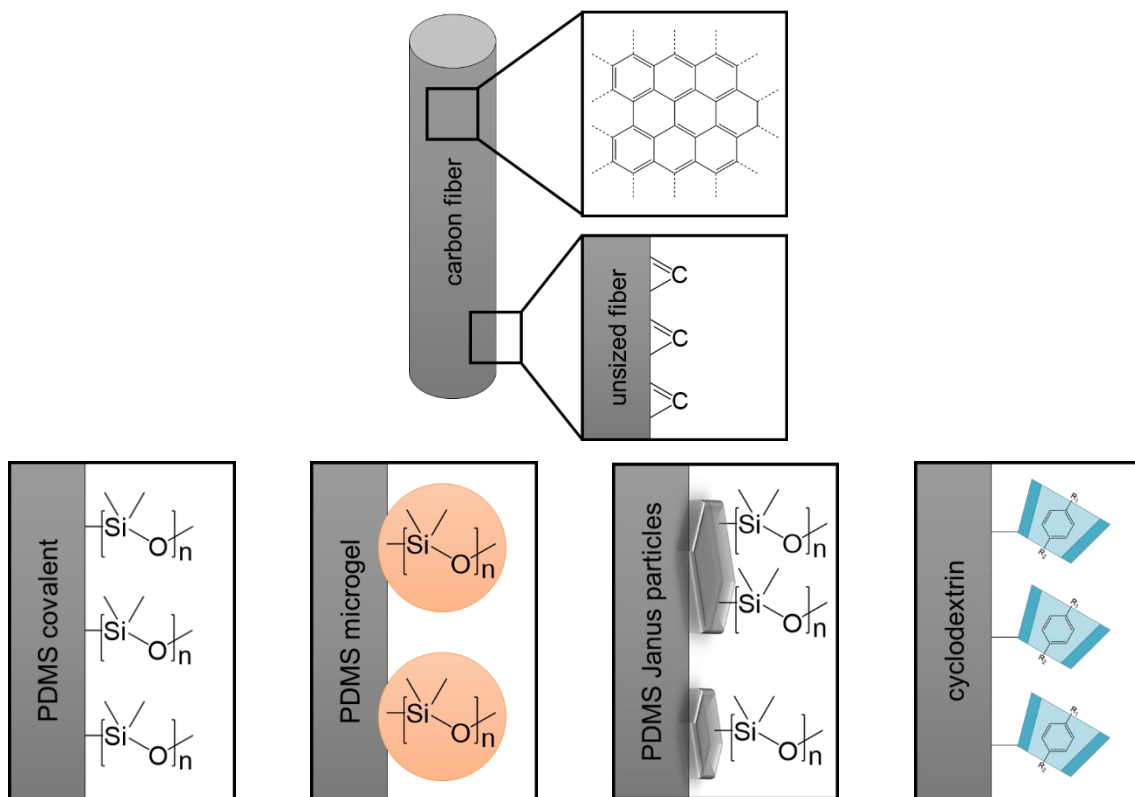


Fig. 10: Overview of coatings for carbon fibers.

The modification of the fiber-resin interface allows the creation of an interphase with improved energy dissipation, ductile-like failure behavior, elastomeric character, enhanced plastic deformation behavior and low friction. This approach promises a reduction in internal stress, enhanced shock absorption and lower defect formation during manufacturing and processing.

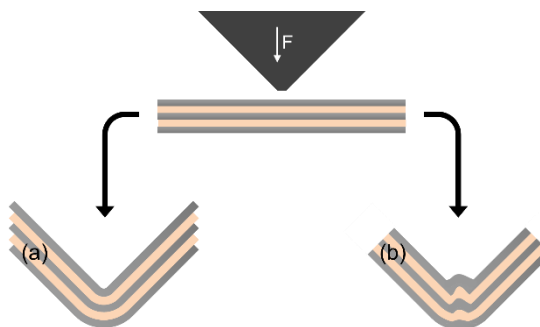


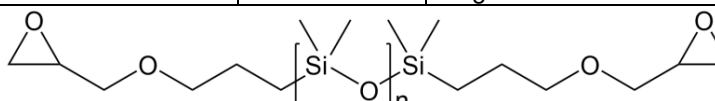
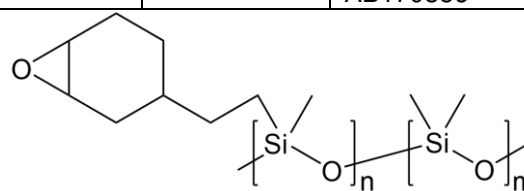
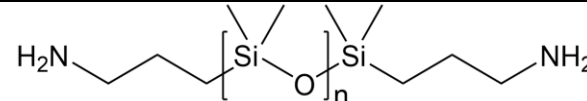
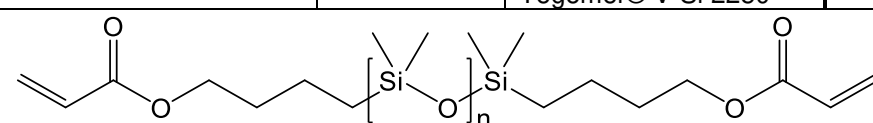
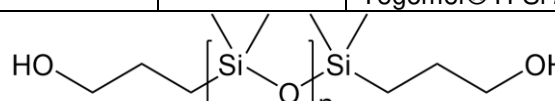
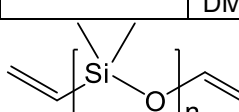
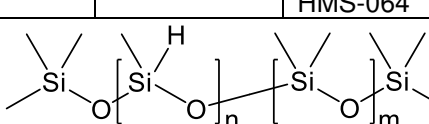
Fig. 11: Schematic illustration of an exemplary bending process of carbon fiber reinforced plastics. (a) Interlaminar sliding without damages to the composites. (b) Tightly bonded interfaces with creasing of the CFRP composite.

2.2. Materials for Modification of Carbon Fiber Surface

All coatings were grafted onto PAN-based, high strength, unsized carbon fibers (Sigrafil C30 T050 Uns SGL Carbon). Tetraethylenepentamine (Merck, $\geq 95\%$) and p-toluenesulfonyl chloride (ABCR, 98 %) were used for the improvement of the reactivity of the carbon fiber surface. For the covalent coating of PDMS, various PDMS species were used (Tab. 2): epoxy-, amino-, acryloxy- or hydroxy-functional as either bifunctional terminated or as copolymer. For the synthesis of PDMS microgel, an addition polymerization was performed. Different vinyl terminated and hydride functional PDMS were used (Tab. 2) and cured with a platinum-divinyltetramethyldisiloxane catalyst (ABCR, platinum content of 3 - 3.5 %) in the presence of an emulsifier Fluid 190 (Dow Corning). The synthesis of PDMS-kaolinite particles was performed by the use of kaolin SKT-13P (Bassermann minerals, multimodal), 3-aminopropyltriethoxysilane (ABCR, 97 %) and E2400-PDMS (Tab. 2). β -Cyclodextrin (Sigma Aldrich, 98 %) was used for the cyclodextrin coating on carbon fibers and its reactivity was improved by p-toluenesulfonyl chloride (ABCR, 98 %).

CFRP preparation was performed with a liquid epoxy resin BECKOPOX EP140 and EH637 by Allnex. Curing takes two days at room temperature. However, due to post cross-linking processes, all measurements were performed after two weeks. The polyurethane system PU3090A and PUH3090B by bacuplast Faserverbundtechnik was used as an additional plastic for the qualitative analysis of macromechanical behavior of CFRPs.

Tab. 2: PDMS species and their structures.

sample	PDMS species	molar mass [g/mol]	supplier	coating concept (Fig. 10)
E2400	glycidyl biterminated	2400	Evonik Tegomer® E-Si 2330	covalent, Janus
				
EB420	epoxy copolymer	420	ABCR AB155127	covalent
EB290	epoxy copolymer	290	ABCR AB170856	covalent
				
A5000	amino biterminated	5000	ABCR AB109371	covalent
A30000	amino biterminated	30000	ABCR AB111873	covalent
				
V2500	acryloxy biterminated	2500	Evonik Tegomer® V-Si 2250	covalent
				
OH2300	hydroxy biterminated	2300	Evonik Tegomer® H-Si 2315	covalent
				
V800	vinyl biterminated	800	Gelest DMS-V05	microgel
				
HB1900	hydride copolymer	1900	Gelest HMS-071	microgel
HB6000	hydride copolymer	6000	Gelest HMS-082	microgel
HB55000	hydride copolymer	55000	Gelest HMS-064	microgel
				

2.3. Impact of Coating on Surface Chemistry and Chemical Analysis

Changes in the chemical composition of the surface of carbon fibers lead to changes in their chemical and physical properties. PDMS coated carbon fibers changed from a graphitic surface to a silicone type surface. This change affects the topography and polarity of the carbon fiber surface. Topographical changes can be observed via optical analysis with scanning electron microscopy or with atomic force microscopy, linked with a nanomechanical analysis. Changes in polarity, and thus in surface energy and wettability, were analyzed with contact angle measurements. Although the carbon fiber bulk is not changed, the influence of their electric conductivity can be manipulated through a homogeneous coating with non-conducting PDMS. This is especially interesting for the application in CFRP-metal composites, in which corrosion is a limiting factor for performance. Corrosion analysis was performed with salt spray tests.

2.3.1. Scanning Electron Microscopy

The optical and topographical analysis was performed by scanning electron microscopy (SEM) with a Zeiss Neon 40 including energy-dispersive X-ray spectroscopy (EDX). Topographical changes on carbon fiber surface through coating were examined and optical analysis of fracture surfaces of CFRP samples was performed.

Uncoated fibers were used without further sample preparation, since they are electrically conductive. Coated fibers were sputtered with a film thickness of 3 to 5 nm to obtain electric conductivity of the fiber samples. The carbon fibers were placed directly on aluminium stubs and glued on the fiber ends with an electrically conductive adhesive. The SEM images were taken at working distances of 7 mm and an accelerating voltage of 2 kV. The EDX measurements were taken at an acceleration voltage of 5 kV and a working distance of 5 mm.

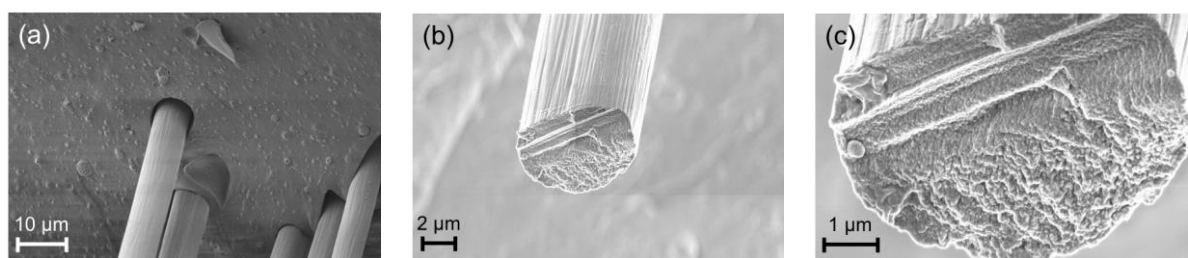


Fig. 12: Exemplary SEM images of carbon fibers, measured at (a) 1,500 times magnification and SE2-detector, (b) 5,000 times magnification and InLens-detector and (c) 15,000 times magnification and InLens-detector.

2.3.2. Atomic Force Microscopy

Further topographical analysis and nanomechanical analysis were performed by atomic force microscopy with a Bruker Dimension Icon PT (formerly Veeco). The PeakForce QNM mode (quantitative nanoscale mechanical characterization) enables high-resolution imaging including physical and mechanical data, like adhesion, deformation and dissipation. The adhesion image describes the negative peak force as a function of the separation between cantilever tip and sample, and defines the surface energy and polarity. In the dissipation image the dissipated energy is shown, which is calculated by the integration of the area between trace and retrace. It can provide information about energy losses through e.g. friction. The deformation image describes how deep the tip of the cantilever can penetrate the sample, and thus how soft the sample is. Additionally, surface area and porosity can be determined by AFM measurements. The surface area is defined by the actually detected area and the surface roughness is represented by the roughness average R_a . Because of the typical curvy surface of a fiber and the stretch marks,¹¹⁶ which are typical for PAN-based carbon fibers due to manufacturing, neither can R_a be zero nor the surface area be $1 \mu\text{m}^2$ (for a set measuring range of $1 \mu\text{m}^2$).

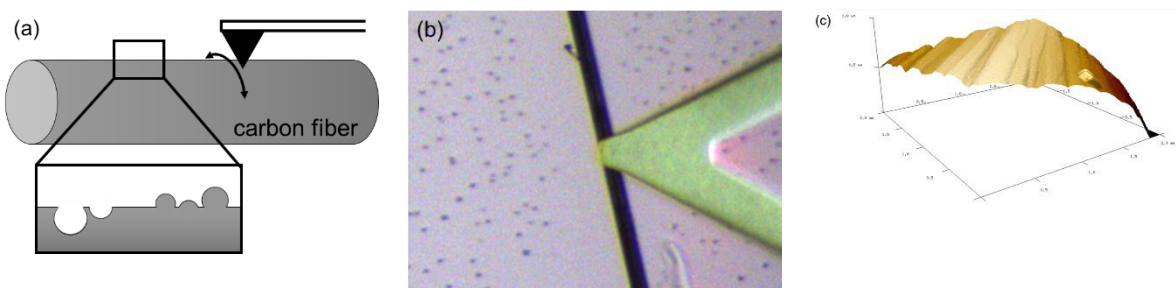


Fig. 13: (a) Schematic illustration of the lateral view and (b) digital image of the top view of the AFM measurement technique. (c) Exemplary 3D AFM height image ($2 \times 2 \mu\text{m}^2$) of a carbon fiber surface.

For the sample preparation, the carbon fiber bundles were separated into single fibers and the fiber ends were glued on glass substrates. The measurements were performed between the glue points. SNL-A cantilevers were used as probes. For scan sizes of $1 \mu\text{m}^2$, following scan parameters were used: scan rate was set to 0.5 Hz, PeakForce setpoint was set to 0.7 nN and the retrace images were taken with 512 lines.

2.3.3. Contact Angle Analysis

Contact angle measurements of single carbon fibers were performed with a Krüss Tensiometer K100SF. Contact angles can provide information about surface energy, polarity and wettability, and thus are a useful tool for examination of surface changes through surface modification.

Using the Wilhelmy plate method, the force, which occurs as a result of the interaction of liquid and immersed sample, is measured.^{117,118} As an example, a dynamic contact angle measurement of a PDMS coated carbon fiber is shown in Fig. 14. The advancing contact angle is measured during the wetting process (immersion in water) and the receding contact angle during the de-wetting process. The recorded force can be used to calculate the contact angle, if the surface tension of the liquid and the perimeter of the sample are known:

$$\theta = \arccos \left(\frac{F}{L \cdot \sigma} \right) \quad (2)$$

- θ contact angle
- F recorded force
- L wetted length, equals to the sample's perimeter
- σ surface tension of water

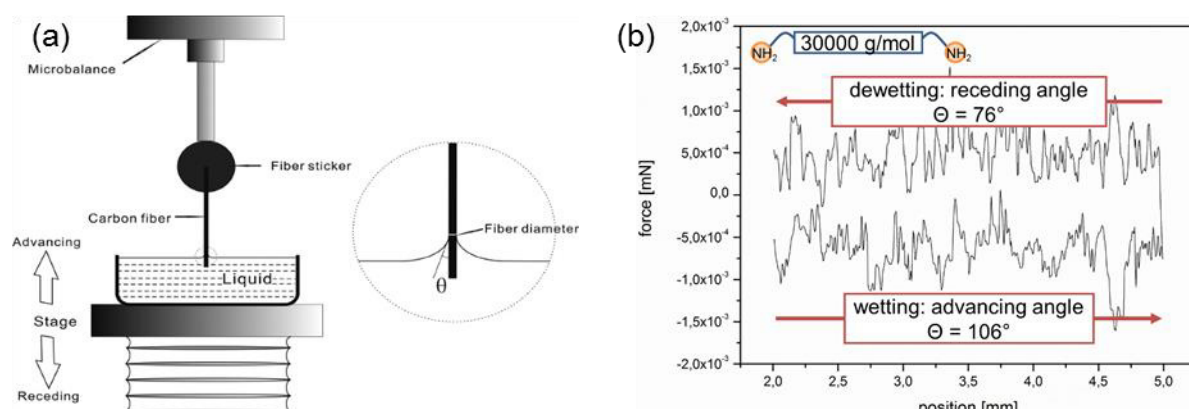


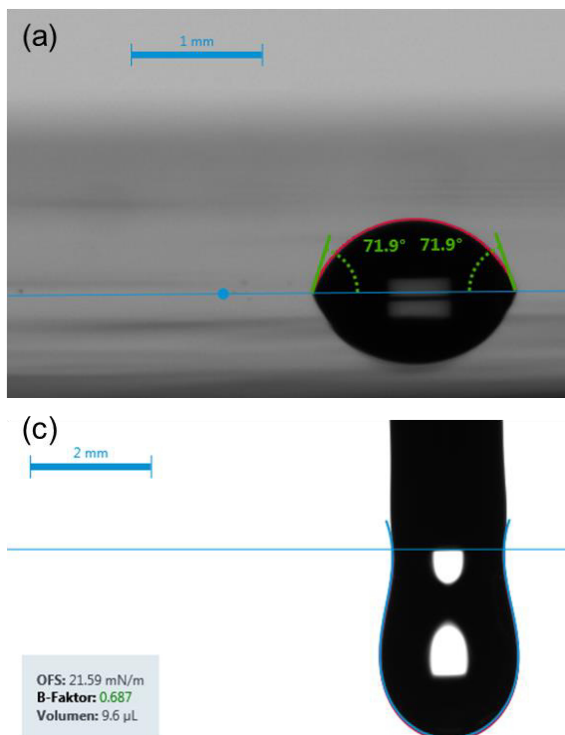
Fig. 14: (a) Schematic illustration of the K100SF tensiometer.¹¹⁹ (b) Representative example of dynamic contact angle measurement of a single carbon fiber coated with amino biterminated PDMS (A30000) with a molar mass of 30,000 g/mol. The measurement starts after the fiber is immersed in water (2 mm) to exclude influence of the cut surface and buoyancy.

In general, contact angles of carbon material depend strongly on oxygen content. An example for the variety of wettability of carbon is coal: lignite coal is hydrophilic and anthracite coal is a hydrophobic material.¹²⁰ Tab. 3 summarizes the wetting properties of different carbon material. According to application reports¹¹⁸ using the K100SF (published by Krüss), contact angles of unsized carbon fibers are 79 °.¹²¹

Tab. 3: Summary of contact angles of different carbon materials. (Note: contact angles of graphene are not absolute due to wetting transparency and exfoliation processes)

material	contact angle in water [°]	ref.
graphite	98	122
	94	123
graphene	127	122
	96	124
	92	125
graphene oxide	67	122
	63	126
carbon fiber	96	127
	79	121
	69	128

Contact angle measurements of the coating materials and matrix (for CFRP) were performed with a Krüss Drop Shape Analyzer DSA25. As matrix for the CFRP production, a liquid epoxy resin was used: BECKOPOX EP140 and EH637. For contact angle analysis, a smooth film of the epoxy resin was applied and cured on a steel sheet. The measurements were performed via sessile drop method with distilled water and diiodomethane; therefore, the surface free energy (SFE model: OWRK) could also be examined. For the determination of the surface free energy of the uncured matrix components and the coating materials, the pendant drop method was used. Analyzing the liquids provides information about wetting properties and wettability of coated carbon fibers.



(b) Tab. 4: Sessile drop analysis of cured BECKOPOX system EP140 and EH637.

θ (water) [°]	70.3
θ (diiodomethane) [°]	38.6
SFE [mN/m]	47.4
- dispersive	40.3
- polar	7.1

(d) Tab. 5: Pendant drop analysis of uncured BECKOPOX system EP140 and EH637 and PDMS polymer coatings.

sample	SFE [mN/m]
EP140	40.1
EH637	36.6
E2400	22.2
EB420	21.6
EB290	22.0
A5000	20.7
A30000	21.5

Fig. 15: Exemplary images of contact angle measurements via (a) sessile drop method for cured epoxy resin and (c) pendant drop method for liquid samples. The corresponding results are summarized in (b) Tab. 4 and (d) Tab. 5.

2.3.4. Corrosion Analysis

For electrically non-conducting coating materials, conductivity measurements of carbon fibers are easy and fast, and therefore a convenient technique for the qualitative validation of a successful coating. The carbon atoms in carbon fibers are sp^2 hybridized and the π -electrons are delocalized within the graphene layers (Fig. 2). This defines carbon fibers as electrically conductive material. The conductivity of carbon fibers was measured with a VC155 multimeter by VOLTCRAFT and clamp-type test probes KLEPS 30 by Hirschmann, which have rotating grip jaws.

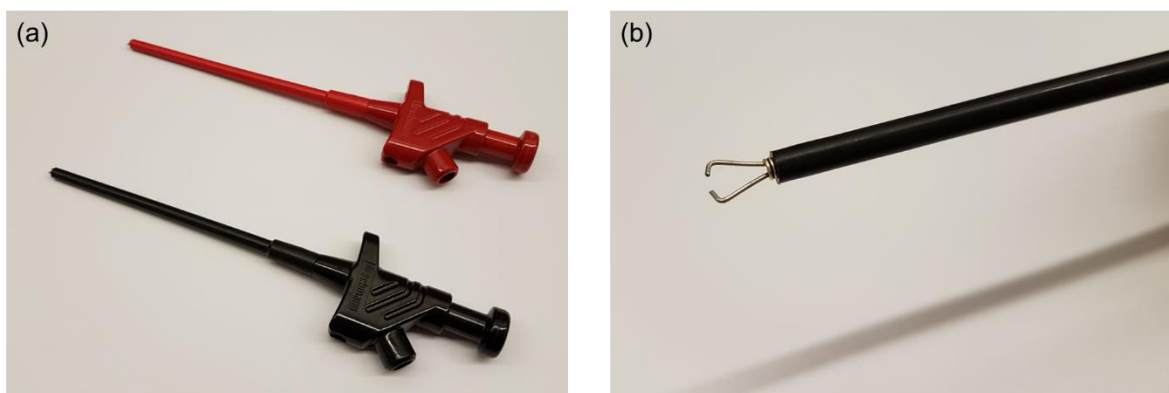


Fig. 16: Images of the clamp-type test probes with rotating grip jaws, which were used for conductivity measurements of unsized and coated carbon fibers.

Corrosion analysis of CFRP-steel composites was performed with salt spray tests. Beyond the qualitative confirmation of a successful coating with a non-conducting coating material, CFRP composites with improved corrosion behavior are in great demand. Undamaged CFRP-steel composites do not corrode, since the plastic acts as an insulator and separates the carbon fibers and the metal. As soon as damage occurs though, due to e.g. processing or external loads, electrolytes can penetrate the composite and lead to corrosion processes. The system can be described as galvanic cell: the carbon fibers act as cathode, the metal as anode and the formation of rust can be observed on the exposed metal surface.^{129–131}

The corrosion behavior of the PDMS coated carbon was analyzed in comparison to unsized carbon fibers. As metal component, cold rolled steel sheets were used. The fibers were glued to the metal with the epoxy resin system BECKOPOX EP140 and EH637. After curing, the CFRP coating was cut to expose the metal and carbon fiber surface. The composite sheets were treated for 30 days.

2.4. Impact of Coating on Fiber-Plastic Interface and Mechanical Analysis

Changes in the chemical composition of the surface of carbon fibers lead to changes in their interactions in CFRPs and therefore also to changes in the mechanical properties of CFRPs. PDMS coated carbon fibers changed from a graphitic (unsized) surface to an oxidized and then to a silicone type surface. This affects the surface chemistry, polarity and topography. Changes in chemical composition are crucial to chemical reactions between fiber surface and epoxy resin and have therefore a direct influence on the adhesion between fiber and plastic. The change in polarity affects wetting behavior and ability of the resin and can lead to an increase or decrease in adhesive bonding. A change in topography, e.g. porosity, can create mechanical interlocking and increase the adhesion between fiber and resin. The analysis of the adhesion of fiber and plastic on a micromechanical level was performed via pull-out tests. First impressions of CFRPs and the influence of the coatings on a macromechanical level were analyzed via tensile tests and bending tests.

2.4.1. Micromechanical Analysis

Micromechanical analysis is an irreversible characterization technique for the determination of the fiber-resin bond-strength on a microscopic level and can be performed via different methods.¹³² There is no general agreement which technique is best, since they are not directly comparable between each other and the microscopic results cannot be directly linked with the macroscopic results, due to different stress states and interfacial failure modes.¹³³ Pull-out and microbond tests^{134,135} are most alike to each other, since they work with a pulling force for the debonding of fiber and matrix. The sample preparation for both methods is very sensitive; single fibers have to be embedded in the matrix droplet and tested after curing. The push-out test,^{136,137} on the other hand, is suitable for cured CFRP preprints and laminates, since the measurement is not disturbed by neighboring fibers. Another approach is described as fragmentation test;^{138,139} here, single fibers are embedded in a bone shaped tensile strength testing probe.

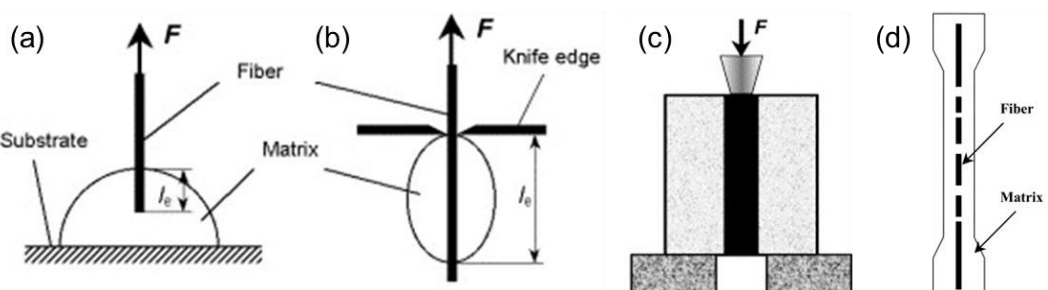


Fig. 17: Schematic illustration of different micromechanical tests: (a) pull-out test, (b) microbond test, (c) push-out test and (d) fragmentation test.¹³²

Pull-out tests of single carbon fibers embedded in epoxy resin droplets were performed for the micromechanical analysis and the characterization of the bond strength between carbon fibers and resin. This method allows a quantitative assessment of the chemical and physical interactions within CFRPs. With pull-out tests, various parameters of the coating can be observed: thickness and homogeneity of the coating, molecular mass of the polymer, reaction time and temperature.

Sample Preparation and Measurement Procedure

In this work, the pull-out test method was used for the determination of the bond strength between fiber and matrix. A test machine MTS Criterion C45.105 with a HBM load cell S2M (10 N) was used. The pull-out tests were performed at room temperature, with speeds between 0.05 mm/min and 2 mm/min and free fiber lengths of 10 mm. The sample preparation was done by hand, starting with the substrate. Paper probes were cut to 30 * 17 mm with rectangular holes of 10 * 11 mm. The length of the central hole can be adjusted and defines the free fiber length. The first epoxy resin droplet was placed right at the edge of the central hole and the single fiber was pushed into the resin. After straight alignment of the fiber, it was cut on the other side, right at the edge of the paper. The last step was the placement of the second epoxy resin droplet. The embedded length of the carbon fiber should be between 50 and 200 μm . The sample preparation has to be done within the time of the pot life of the epoxy resin; in the case of the BECKOPOX system EP140 and EH637, the pot life is 30 minutes. The pull-out tests were performed as statistical measurement series, with 30 pull-out samples for every carbon fiber sample. For the measurement, just the paper substrate of the pull-out samples were put in the clamping jaws. This way, there is no additional force introduced to the resin. After the samples were fixed in the test machine, the sides of the paper substrate were cut, so that just the carbon fiber was left between the two epoxy resin droplets.

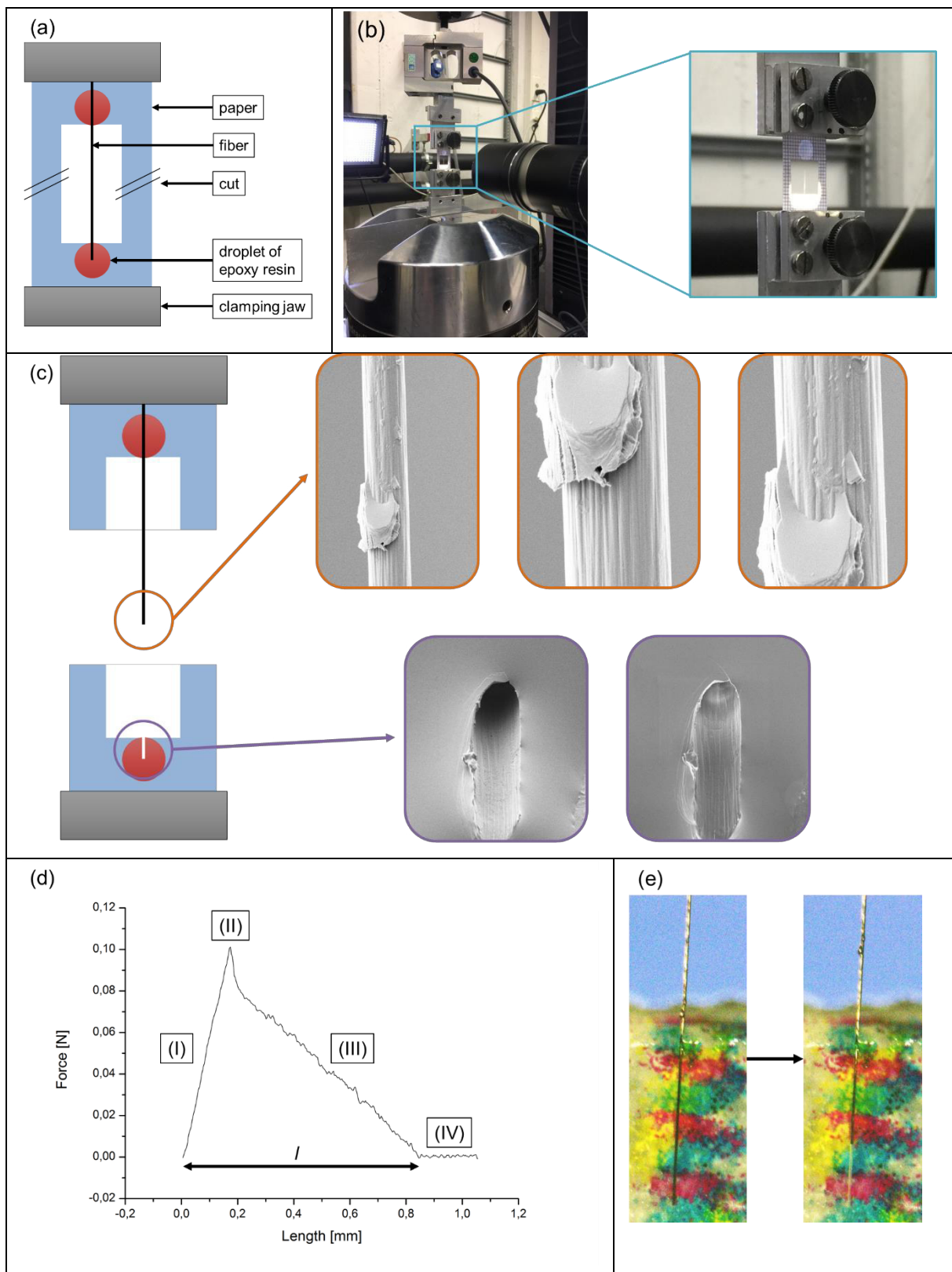


Fig. 18: Sample preparation and measurement technique of the pull-out test method. (a) Schematic illustration and (b) photographic image of sample preparation and probe holder. (c) SEM images of epoxy resin residue on fiber and of fiber shaped hole in epoxy resin droplet after pull-out test. (d) Exemplary measurement of pull-out test with an embedded fiber length *l* and four stages: (I) increase of tension, (II) maximal force, (III) frictional sliding and (IV) fully debonded interface. (e) Light-microscopic images, taken at phase (I) and at phase (III) of the pull-out test.

A typical measurement of pull-out tests is shown in Fig. 18 (d): the curve is separated in four stages. First, an increase of tension (I) in the elastic area is observed. The elongation at break of carbon fibers is reported to be between 1 and 2 %,^{16,21,24,25} which means, carbon fibers undergo an elastic deformation of 0.1 to 0.2 mm at a free fiber length of 10 mm before they break. The maximal force (II) describes the adhesion between fiber and resin. At this point, the tensile force is higher than the static friction. Due to the manual sample preparation, the embedded lengths vary between the pull-out sample, which means the maximal forces cannot be compared directly. The calculation of the interfacial shear strength takes this into account: the IFSS is defined as force per interface area (eq. (3)). After the break of the bonding between fiber and resin, the fiber is pulled out of the resin droplet. The recorded force in this stage is caused by kinetic friction (III) and decreases linearly with the decreasing contact area. The fully debonded interface (IV) is reached when the fiber is completely pulled out of the resin droplet.

$$IFSS = \frac{F_{max}}{\pi \cdot l \cdot d} \quad (3)$$

- IFSS interfacial shear strength
- F_{max} recorded maximal force
- l embedded length of the fiber
- d diameter of the fiber

Sample Preparation: Free Fiber Length

One adjustable parameter for pull-out tests is the free fiber length, which is set by the length of the rectangle hole in the paper substrate (Fig. 18 (a) and (b)). The free fiber length affects the first phase of the measurement: the increase of tension and elastic deformation of the carbon fiber. Since the elastic deformation of carbon fibers is 1 to 2 %,^{16,21,24,25} the value of elongation increases with increasing free fiber length (Fig. 19 (b), (c) and (d)): 0.02 mm elongation for 2 mm free fiber length, 0.04 mm for 5 mm and 0.1 mm for 10 mm. However, increased elongation at break does not mean increased adhesion, but just a change in the slope of the curve in the elastic area. IFSS measurements of aminated fibers did indeed vary with different free fiber lengths, but with no particular tendency and are therefore classified as statistical errors. The pull-out tests of coated carbon fibers were not affected by different free fiber lengths, whatsoever.

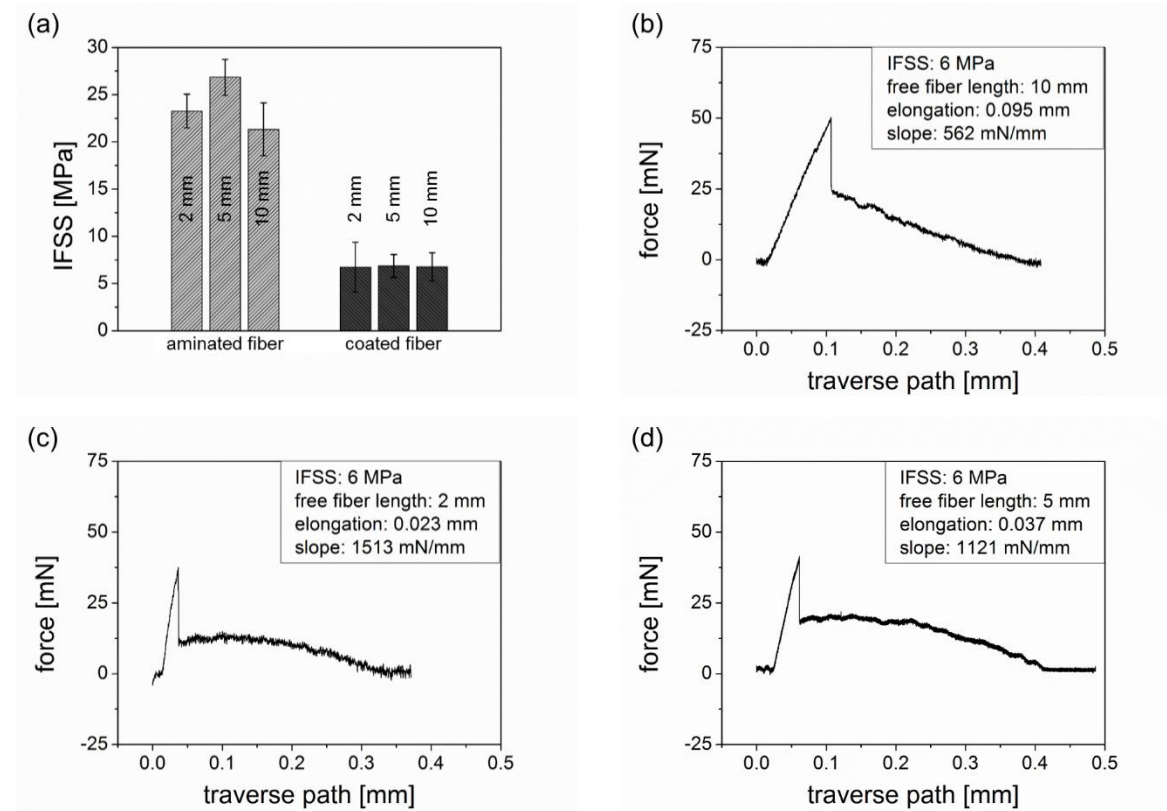


Fig. 19: Influence of free fiber length on pull-out tests. (a) Comparison of the IFSS of aminated and coated fibers tested with different free fiber lengths. (b), (c), (d) Exemplary measurements of the force elongation curves of coated fibers with different free fiber lengths but same IFSS values.

Sample Preparation: Influence of Pot Life of the Epoxy Resin

The statistical measurement series for pull-out tests were prepared as one batch for every carbon fiber sample. Meaning, the binding agent and the curing agent were mixed in the beginning of the preparation of every measurement series and used for all 30 pull-out samples. Since the epoxy resin undergoes cross-linkage as soon as it is mixed with the curing agent, the resin mixture has a pot life. With increasing preparation time, the amount of functional groups for the reaction between carbon fiber surface and epoxy resin decreases (Fig. 5 and Fig. 8). Additionally, the resin mixture increases in viscosity with increasing preparation time, which decreases the wetting ability of the resin. This results in higher debonding forces and IFSS values for the first pull-out tests within one measurement series and in lower values for the last prepared pull-out tests (Fig. 20 (a)).

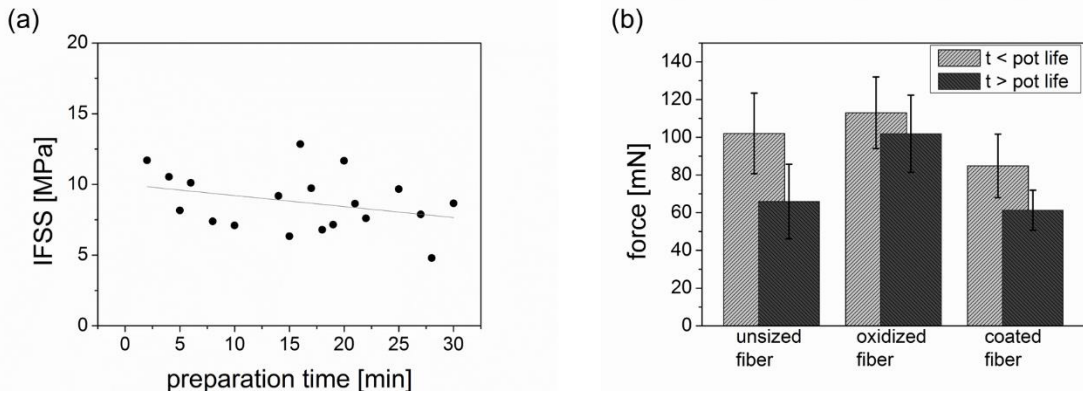


Fig. 20: Influence of pot life of the epoxy resin on pull-out tests. (a) IFSS results depending on preparation time until pot life of the epoxy resin is reached and (b) comparison of different carbon fiber samples, which were prepared before and after pot life was reached.

Measurement Procedure: Testing Speed

Mechanical testing procedure can be set by strain rate: quasi-static for low strain rates and dynamic for high strain rates.¹⁴⁰⁻¹⁴² In terms of plastic samples, the failure behavior changes strain-dependent; at low strain rates the specimens fail in a more ductile style and at high strain rates in a more brittle way.^{140,141} Even though the mechanical behavior of carbon fibers is strain-independent,¹⁴³ CFRP composites have been recorded to be sensitive to strain rates¹⁴⁴.

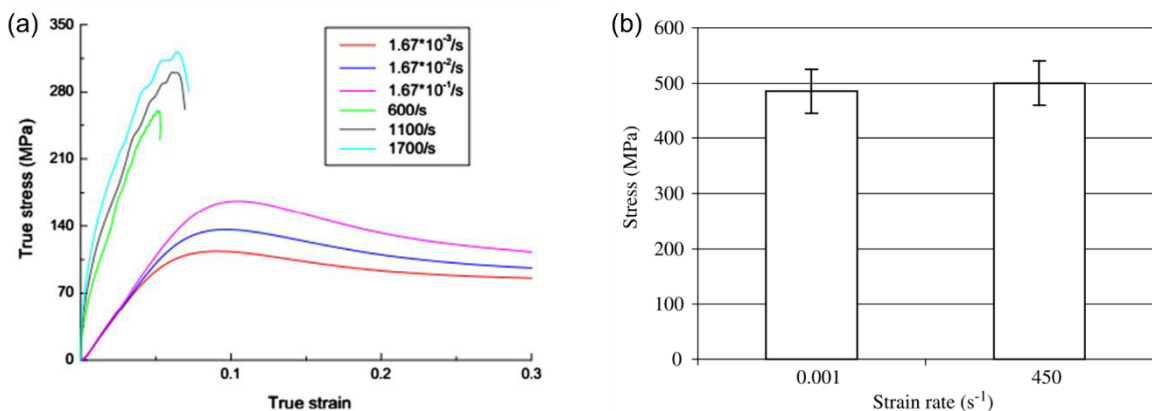


Fig. 21: Strain rate dependency of mechanical analysis. (a) Strain rate sensitivity of PMMA shown in compressive stress-strain curves.¹⁴⁰ (b) Mean stress of CFRP composites at different strain rates.¹⁴⁴

High strain rates can be used for crash simulation. This work focuses on the fiber-resin interface and the chemical and physical interaction; therefore, low testing speeds are required. This way, the system has more time for load distribution, physical effects (e.g. friction between fiber and resin) are better visible and a steady equilibrium within the contact area can be reached. The testing speeds correspond to the traverse speed, which is set between 0.05 and 2 mm/min. With free fiber lengths of 10 mm, the strain rates are therefore between 10^{-5} and 10^{-3} s^{-1} .

2.4.2. Macromechanical Analysis

After the detailed determination of the bond strength of carbon fibers and epoxy resin, macromechanical analysis was performed. The BECKOPOX system EP140 and EH637, and the polyurethane system PU3090A and PUH3090B were used as resin components. For both test methods, tensile tests and bending tests, a test machine MTS793 was used and the samples were prepared to be 100 mm long, 5 mm wide and 2 mm high. The amount of carbon fibers (unsized or coated) within the CFRP was set to 1 - 10 %. The tests are based on DIN EN ISO 527 and DIN EN ISO 14125. Since the carbon fibers were coated as loose bundles and the test samples were prepared by hand, it was not possible to create laminates or perfectly unidirectional aligned CFRPs.

Both test methods belong to the fundamental mechanical testing techniques and expose the test specimen to a controlled force until failure. Tensile tests enable the determination of the tensile strength and tensile modulus of a compound, and the bending test method is used for the determination of the bending strength and bending modulus. While the composites are exposed to a pulling force in tensile tests, they are exposed to a compression force in bending tests. Both techniques allow the assessment of the composite's plastic deformation ability, through elongation or strain.

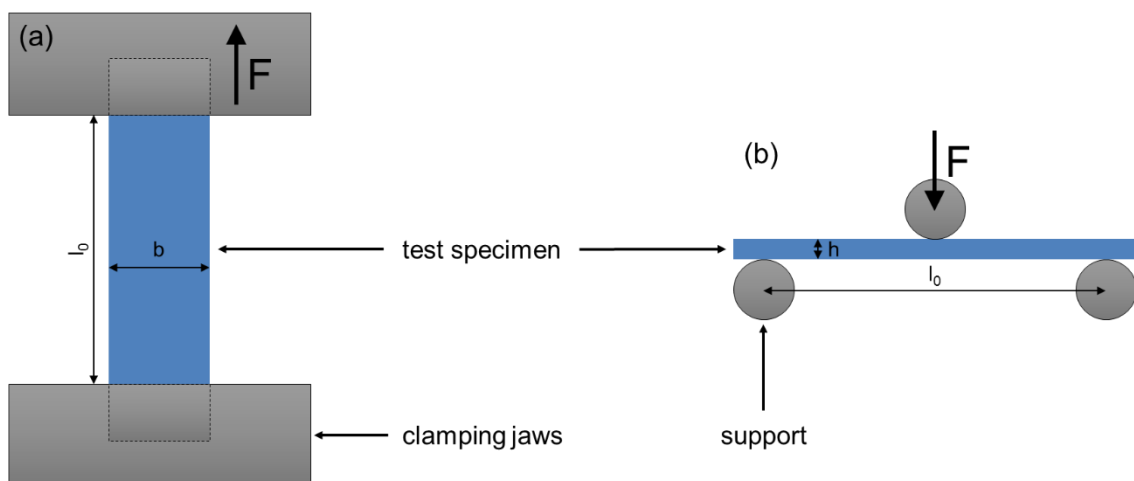


Fig. 22: Schematic illustration of mechanical testing methods. (a) Front view of tensile test and (b) side view of bending test.

Chapter 3: Covalent PDMS Coating on Carbon Fibers

Covalently bonded PDMS on carbon fibers presents a low friction, elastomeric interphase in CFRP composites. The objective focuses on energy dissipation, a better plastic deformation behavior, enhanced shock absorption and lower defect formation during manufacturing and processing, through reduction of internal stress.

Different PDMS polymers were used and analyzed concerning reaction yield, functional groups, molar masses and molecular structures. The chemical analysis focuses on chemical and physical properties, changes on the carbon fiber surface, and the effects on topography and polarity. The analysis methods include scanning electron microscopy, atomic force microscopy, contact angle measurements and corrosion analysis. The mechanical analysis focuses on the fiber-resin interactions and their effect on a micro- and macro-scale level.

PDMS has excellent properties in terms of friction¹⁰⁰ and slip behavior¹⁰⁶. It is able to form a low cohesion layer with low shear resistance and slip behavior of a viscous material when exposed to stress. Furthermore, it is described, that hydrodynamic slip is dependent on interfacial interactions. The less interactions between two surfaces, the lower the friction force. However, the interaction is ultimately related to the surface energy¹⁰¹ and is with the exception of functional groups (e.g. biterminated PDMS) existent in form of van der Waals forces. For friction and hydrodynamic slip behavior, a dependency on molar mass was found. The detailed description says, the degree of slip and energy dissipation is directly related to the degree of entanglement of polymer chains; and polymer chains are usually longer in polymers with higher molar masses. The longer the chains, the higher the energy consumption under stress and therefore, the higher the energy dissipation, the higher the hydrodynamic slip and the lower the friction resistance. Additionally, it was observed, that PDMS is able to provide a good stress transfer. Further properties like flexibility and compressibility^{109,110} underline the elastomeric character of PDMS and its ability to act as soft interphase. In addition to the remarkable mechanical properties of PDMS, the chemical¹⁰⁴ and electrical¹⁰³ stability should be mentioned. The chemical inertness ensures the formation of a protective layer for delivery and storage, and the electrical stability leads to positive influence on corrosion problems occurring in CFRP composites.

3.1. Experimental

PDMS coated carbon fibers can be obtained via different approaches; in this work the first step introduced oxygen containing functional groups on the fiber surface through oxidation. The fiber surface is then more reactive and grafting of the requested coating can be performed. It is either possible to perform a two-step synthesis and graft the PDMS layer directly on the oxidized fiber or to add an extra grafting step with a coupling agent to achieve higher yields under less harsh reaction conditions. The various PDMS species, which were used, are listed in Tab. 6 and the experimental procedure is summarized in Fig. 23.

PAN-based, high strength, unsized carbon fibers have an almost inert surface. Functional groups can be introduced through a treatment with strong acids and oxidizing agents (Fig. 23 (a)). Best results were obtained through oxidation in concentrated nitric acid at 120 °C for 3 hours, (based on Pittman's instructions^{51,52}). A gas washing bottle, filled with a saturated solution of iron sulfate, was used for the reduction of resulting nitrous gases. After the oxidation

treatment, the mixture was carefully poured onto ice and the fibers were washed with distilled water until a neutral pH was reached. The oxidized fibers contain reactive hydroxyl- and carboxyl-groups on the fiber surface (Fig. 7).

For the covalent coating of PDMS, various PDMS species were used (Tab. 6): epoxy-, amino-, acryloxy- or hydroxy-functional as either bifunctional terminated or as copolymer. Depending on the functional group, the oxidized fibers were coated directly (Fig. 23 (b)) or an additional grafting step was needed. For this, the oxidized carbon fibers were mixed into tetraethylenepentamine and heated to 200 °C for 4 hours (based on Pittman's instructions^{51,52}). After the mixture cooled down, the fibers were washed with distilled water. The resulting fibers contain reactive amine groups on the fiber surface (Fig. 23 (d)). Another way to enhance the reactivity of the fiber surface is the use of a good leaving group, like p-toluenesulfonyl chloride (Fig. 23 (c)). For that, 2 mg tosyl chloride for every 1 g of oxidized carbon fibers were mixed in water. The mixture was stirred at room temperature for 5 hours. The resulting fibers were washed with distilled water and contain tosylates on the fiber surface, instead of the less reactive hydroxyl groups.

The final step, the coating with PDMS, can be performed in solution or bulk. Functionalized carbon fibers were placed in a flask with either a mixture of a solvent and PDMS or just pure PDMS. As solvent, ethanol, methyl isobutyl ketone or mineral spirits can be used. For high temperature grafting, the use of mineral spirits is recommended. The reaction temperature was varied from 80 °C to 200 °C.

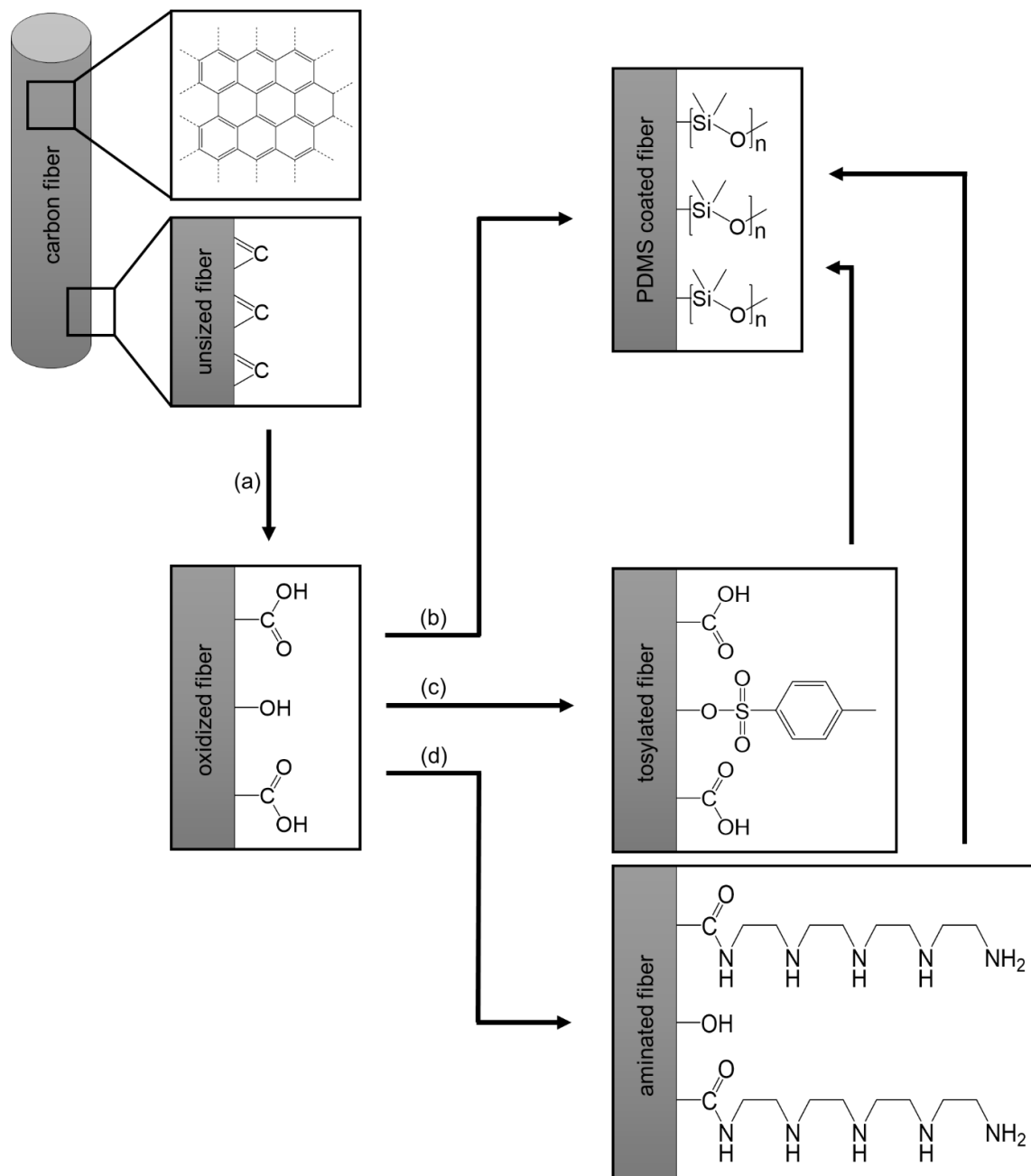
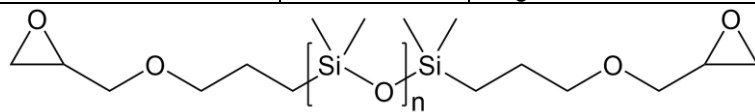
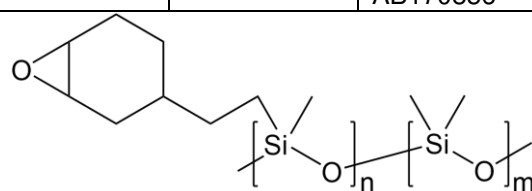
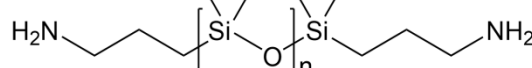
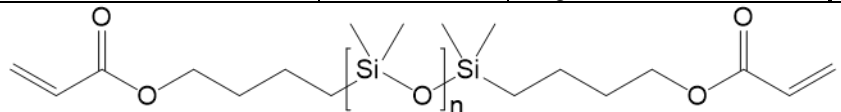
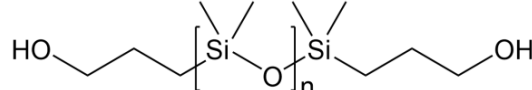


Fig. 23: Schematic overview of the experimental procedure for the covalent bonding of PDMS on carbon fibers. (a) Oxidation of the carbon fiber surface is the first step of all coating methods. Path (b) shows direct grafting of PDMS on the oxidized carbon fiber surface in the two-step-synthesis. The three-step-synthesis is described in (c) and (d) by the use of coupling agents.

Tab. 6: PDMS species for covalent bonding on carbon fibers and their structures.

sample	PDMS species	molar mass [g/mol]	supplier	reaction path (Fig. 23)
E2400	glycidyl biterminated	2400	Evonik Tegomer® E-Si 2330	(b), (d)
				
EB420	epoxy copolymer	420	ABCR AB155127	(b), (d)
EB290	epoxy copolymer	290	ABCR AB170856	(b), (d)
				
A5000	amino biterminated	5000	ABCR AB109371	(b), (c)
A30000	amino biterminated	30000	ABCR AB111873	(b), (c)
				
V2500	acryloxy biterminated	2500	Evonik Tegomer® V-Si 2250	(b)
				
OH2300	hydroxy biterminated	2300	Evonik Tegomer® H-Si 2315	(b)
				

3.2. Chemical Composition of Carbon Fiber Surface

Covalent bonding between the PDMS coating and the carbon fiber surface was confirmed by x-ray photoelectron spectroscopy. As representable examples, there are three different samples shown in Fig. 24: unsized, thin PDMS coated and thick PDMS coated carbon fibers. For both coatings, an epoxy-terminated PDMS with a molar mass of 2400 g/mol (sample: E2400) was used. The syntheses were carried out at 180 °C for 3 hours. To obtain a thick coating, the carbon fibers were mixed in pure PDMS; for a thin coating, the PDMS was diluted in mineral spirits. As expected, carbon, oxygen and nitrogen were detected in all samples (Fig. 24 (a)). Commercially available carbon fibers always contain small amounts of nitrogen, due to the manufacturing from polyacrylonitrile.^{16,21,22} The oxygen and silicon contents increase with an increasing thickness of PDMS layer, because of the introduction of more siloxane groups. On the other hand, the carbon and nitrogen contents decrease with an increasing thickness of PDMS layer. This is caused by the surface sensitivity of the XPS spectroscopy: the thicker the coating layer, the less bulk material is detected. The same can be observed for the comparison of the C1s spectra^{46,58,145} of the two different PDMS samples (c) and (d) in Fig. 24: the π - π^* signal, caused by aromatic compounds in the fiber bulk material, is just detected for a thin PDMS layer. Furthermore, the C-O signal is correlated to the connecting units and therefore it is a direct confirmation of the covalent bonding between the coating and the fiber surface.

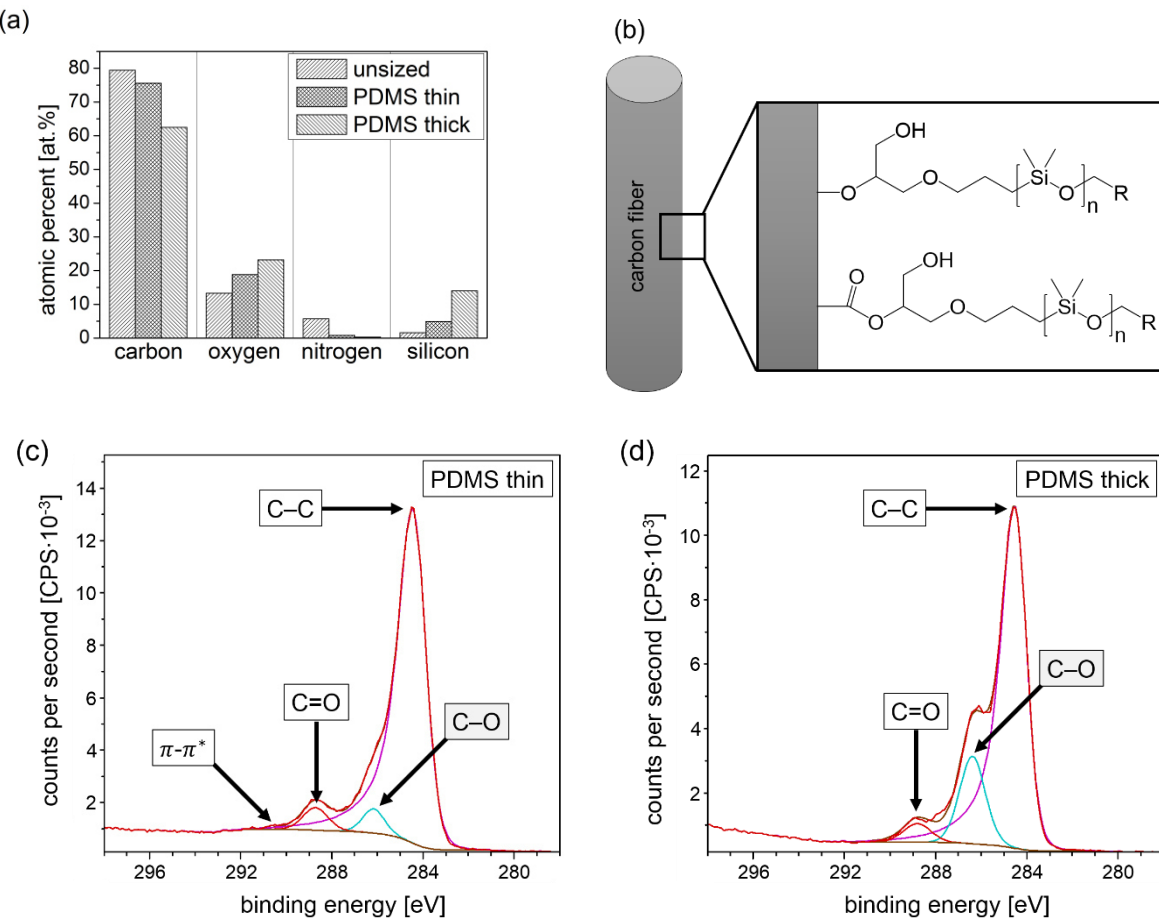


Fig. 24: XPS measurements of unsized carbon fibers, carbon fibers with a thin PDMS coating and carbon fibers with a thick PDMS coating. (a) Quantitative summary of the surface composition of unsized and PDMS coated fibers. (b) Schematic illustration of the PDMS coating on the fiber surface. (c) XPS C1s spectrum of carbon fibers with a thin PDMS coating and (d) XPS C1s spectrum of carbon fibers with a thick PDMS coating; the red line represents the curve fitting.

3.3. Physical Appearance and Nanomechanical Analysis of Carbon Fiber Surface

The topographical analysis of the fiber surface was performed with atomic force microscopy. Differences of the surface topography concerning the grafting step and the variation of the reaction parameters can be observed in terms of quality and quantity. Fig. 25 illustrates the changes of the fiber surface due to the oxidation process and the coating with PDMS.

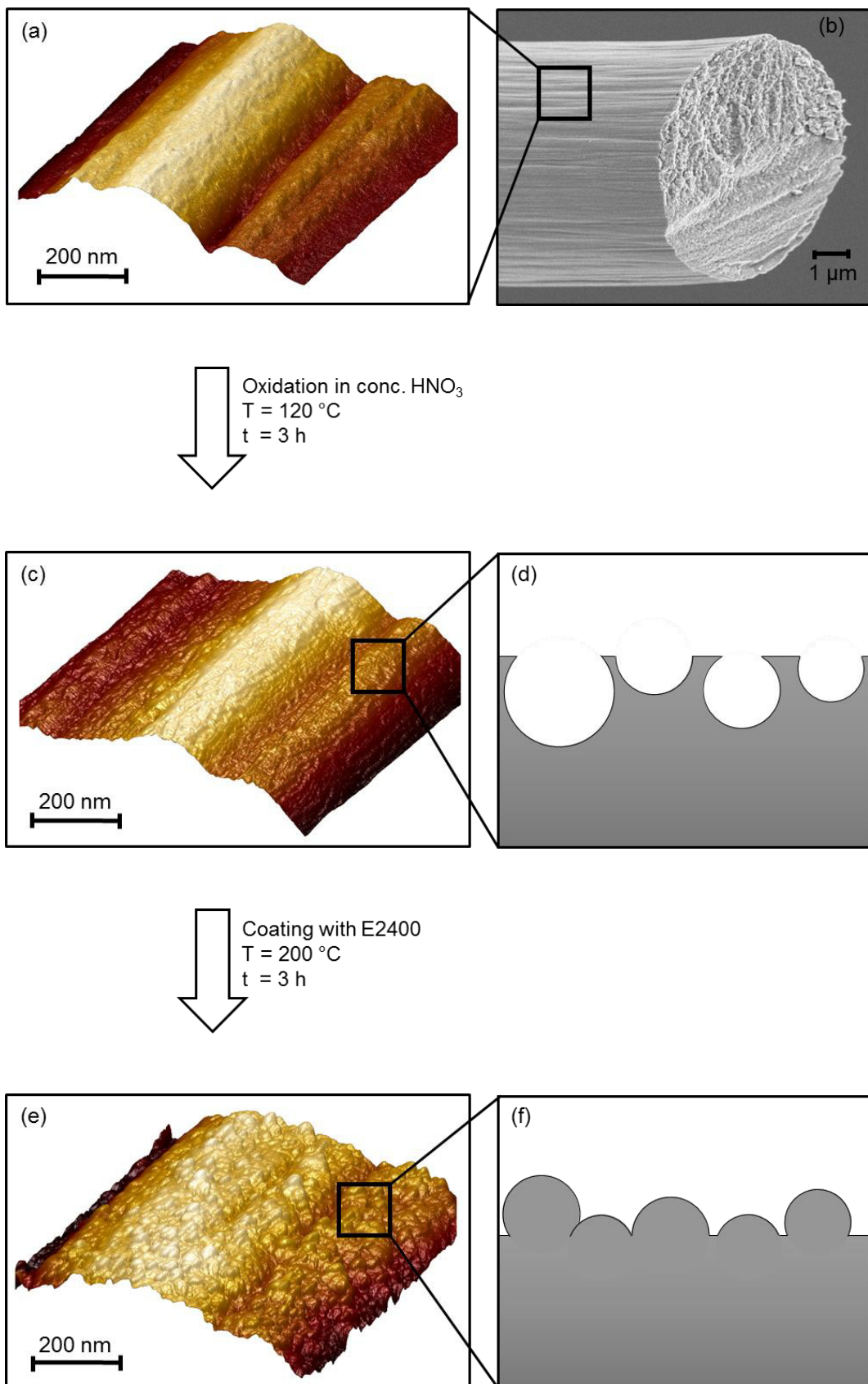


Fig. 25: (a) 3D AFM height image and (b) SEM image of unsized carbon fibers. (c) 3D AFM height image and (d) schematic illustration of the fiber surface of oxidized fibers. (e) 3D AFM height image and (f) schematic illustration of the fiber surface of E2400-PDMS coated fibers.

The surface of unsized carbon fibers (Fig. 26) is mostly inert. There are just few oxygen and nitrogen containing functional groups available on the surface of PAN-based carbon fibers. Due to its turbostratic and amorphous structure (Fig. 2), unsized carbon fibers' surface has no characteristic pattern in the nanoscale area. The typical stretch marks (Fig. 25 (b)) appear due to the spinning and drawing process during manufacturing.

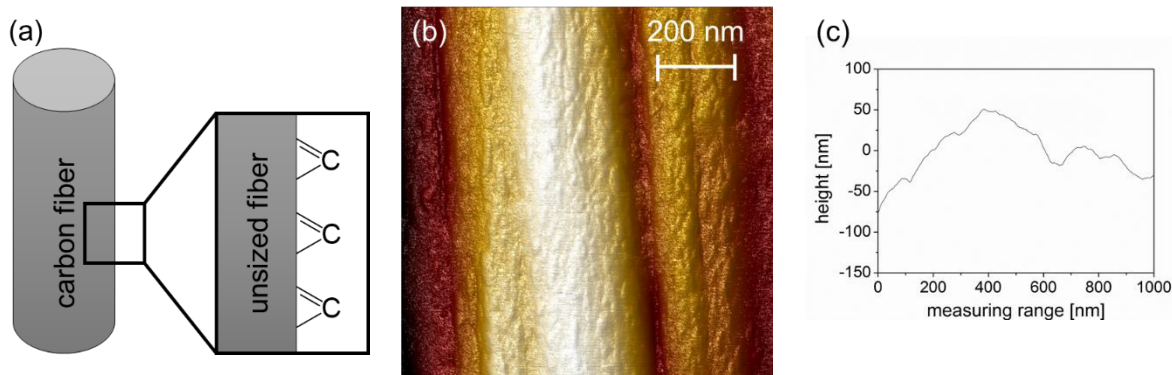


Fig. 26: (a) Schematic illustration of the chemical composition on fiber surface of unsized carbon fiber. (b) AFM height image of unsized carbon fiber and (c) graphical presentation of surface topography of unsized carbon fiber.

Oxidation of carbon fibers in concentrated nitric acid leads to a porous fiber surface. As described by Pittman et al.^{51,52} and Yue et al⁴², carbon erosion takes place, since the graphene layers are being oxidized (Fig. 7). Porosity and surface area can be analyzed by AFM measurements with the PeakForce QNM mode: the surface roughness is described by the roughness average R_a and the surface area is defined by the actually measured surface in comparison of the measuring range of $1 * 1 \mu\text{m}^2$. The porosity and the surface area of the fibers increased through the oxidation process: a R_a of 24 nm for unsized fibers and a R_a of 45 nm of oxidized fibers were detected. The detected surface area of unsized fibers was 10.1 % higher than the set measuring range, but the detected surface area of oxidized fibers was 29.2 % higher. Because of the typical curvy surface of a fiber and the stretch marks,¹¹⁶ which are typical for PAN-based carbon fibers, neither can R_a be zero nor the surface area be $1 \mu\text{m}^2$. This means, the AFM measurement technique cannot detect an ideally smooth carbon fiber surface. Nonetheless, the changes in the surface topography of carbon fibers through oxidation in nitric acid can be observed, even with the presence of stretch marks.

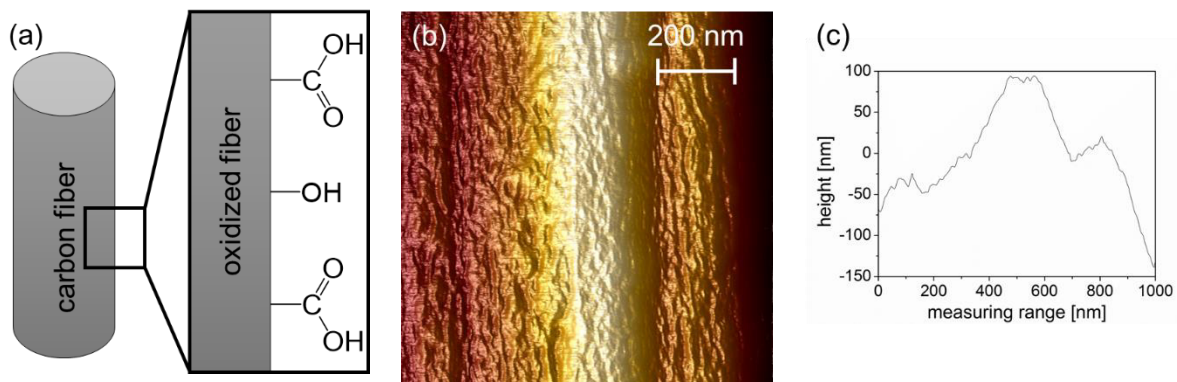


Fig. 27: (a) Schematic illustration of the chemical composition on fiber surface of oxidized carbon fiber. (b) AFM height image of oxidized carbon fiber and (c) graphical presentation of surface topography of oxidized carbon fiber.

The PDMS coating on the fiber surface is not fully cross-linked, but the polymers are covalently bonded to the carbon fiber surface. The coating does not just fill the pores of oxidized carbon fibers, but creates a new and characteristic structure on the carbon fiber surface. This surface topography depends mainly on the structure of the PDMS: biterminated PDMS forms ball-like domains (Fig. 28 (d) and (e)) and copolymer PDMS forms scale-like structures (Fig. 28 (f) and (g)) on the fiber surface. The ball-like domains can reach sizes up to 30 nm; the dimensions of the single structures of the copolymer EB420-PDMS coating are below the detection limit of the microscope. Both PDMS coatings show less rough surfaces than oxidized carbon fibers. The biterminated E2400-PDMS coated carbon fiber surface was detected to be smoother than the copolymer EB420-PDMS coated carbon fiber surface, since a R_a of 17 nm for E2400-PDMS coated fibers and a R_a of 27 nm for EB420-PDMS coated fibers were detected. Also, the detected surface area of EB420-PDMS coated fibers was detected to be 19.7 % higher than the set measuring range, the surface area difference of E2400-PDMS coated fibers is just 12.6 %. These results are surprising, since the optical comparison of both PDMS coated fibers (Fig. 28 (d) and (f)) would suggest a smoother surface for the copolymer EB420-PDMS coated carbon fibers. This is a perfect example of how stretch marks preponderate in value, due to their dimensions of several 100 nm. Since the stretch marks are more distinct in the EB420-PDMS coated specimen than in the E2400-PDMS coated carbon fiber, the optically smoother surface is detected to be rougher.

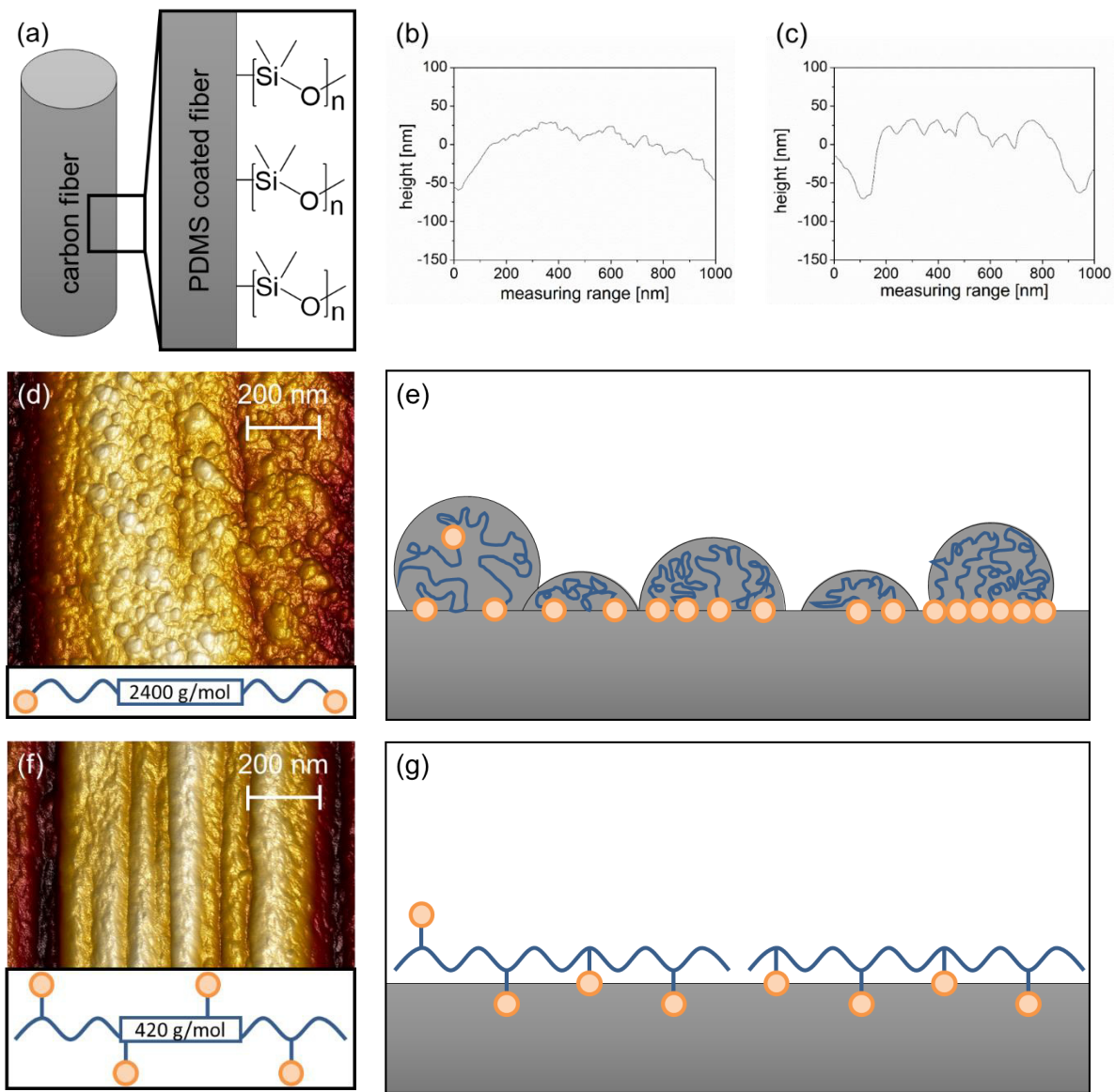


Fig. 28: (a) Schematic illustration of the chemical composition on fiber surface of PDMS coated carbon fiber. Graphical presentation of surface topography of (b) E2400-PDMS and (c) EB420 coated carbon fiber. (d) AFM height image and (e) schematic illustration of the bonding mechanism of E2400-PDMS coated carbon fiber. (f) AFM height image and (g) schematic illustration of the bonding mechanism of EB420-PDMS coated carbon fiber.

The biterminated E2400-PDMS coated carbon fiber surface is particularly interesting from the viewpoint of atomic force microscopy, since it can be analyzed in terms of nanomechanical properties. This is possible, because the coating forms domains on the carbon fiber surface, which have significantly different values in their physical and mechanical characteristics than the carbon fiber itself. The results are summarized in Fig. 29. The deformation image (Fig. 29 (b)) describes how deep the tip of the cantilever can penetrate the sample. The ball-like domains are made of PDMS, which is softer than the carbon fiber and leads to higher data values for the domains in the deformation image. In the dissipation image (Fig. 29 (c)) the dissipated energy is shown, which is calculated by the integration of the area between trace and retrace. The dissipation data of the domains have very small values, which means that there is almost no lost

energy through e.g. friction between cantilever tip and the sample. This result is consistent with PDMS being commonly used as slip additive. The adhesion image (Fig. 29 (d)) describes the negative peak force as a function of the separation between cantilever tip and sample. Like the dissipation data, there is no or just little adhesive force detected between cantilever tip and the PDMS domains. The 3D height images with the adhesion data color scale as skin is shown in Fig. 29 (e) and (f). These images show that the detected domains in the nanomechanical measurement correlate clearly with the surface topography.

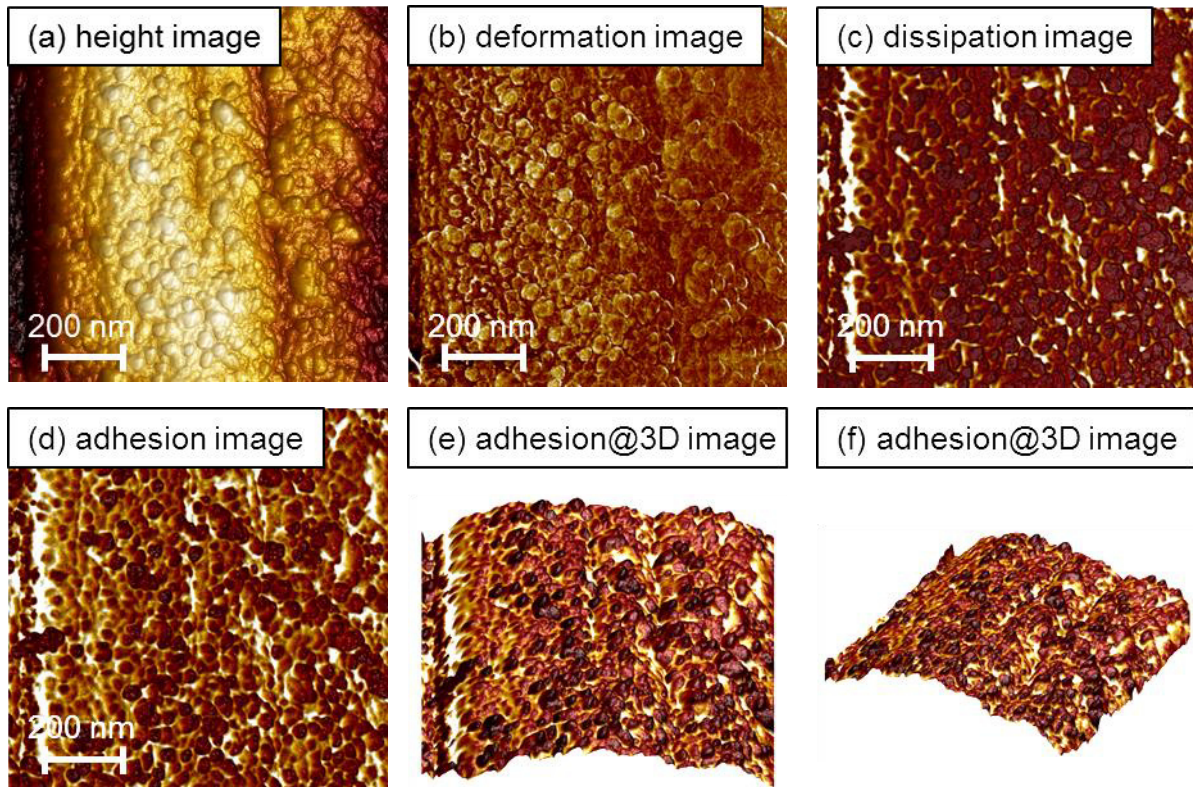


Fig. 29: AFM (a) height image, (b) deformation image, (c) dissipation image and (d) adhesion image of bitminated E2400-PDMS coated carbon fiber. (e) & (f) 3D AFM height image with adhesion data as skin.

The PDMS domains form independently from the biterminated functional groups (e.g. epoxy, amino, acryloxy or hydroxy), as long as a reaction between the carbon fiber surface and the polymer chain takes place (Fig. 30 (a) - (c)). Just changing the PDMS reagent for the coating of carbon fibers, but keeping all other reaction parameters constant, leads to similar results between samples: formation of PDMS domains of alike sizes. The slight differences are caused by the different yields of reactions, since the reaction mechanisms change with the change of functional groups in the PDMS. The size of the domains can be controlled by the temperature, since the temperature influences the yield of the reaction and thus the amount of precipitated PDMS on the carbon fiber surface (Fig. 30 (a), (d) - (f)). In the case of epoxy biterminated PDMS, the best results were obtained at high reaction temperatures. At 200 °C, the formed

PDMS domains on the carbon fiber surface are big and well defined. The PDMS domains shrink with decreasing temperature until there are no defined PDMS domains observable at 100 °C.

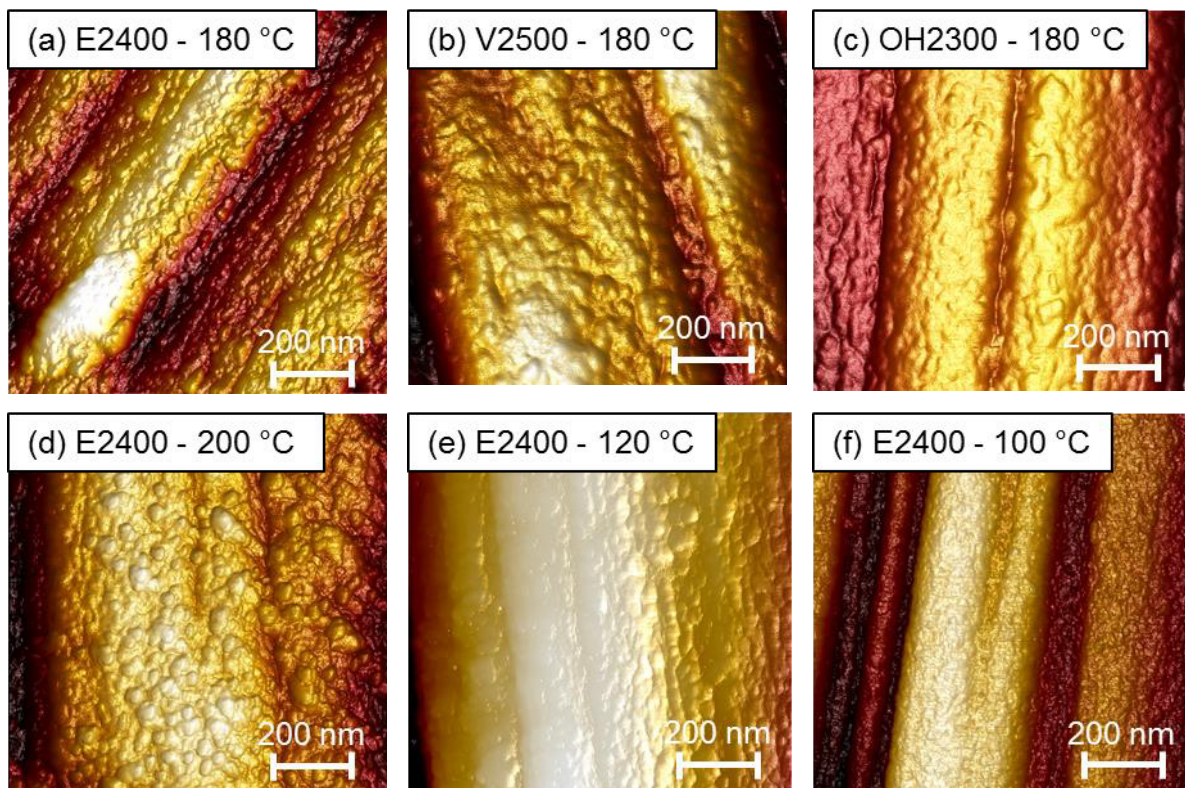


Fig. 30: AFM height images of biterminated PDMS coated carbon fibers, synthesized with different reaction parameters. Carbon fibers coated at 180 °C with PDMS with different functional groups: (a) epoxy, (b) acryloxy and (c) hydroxy. At different temperatures synthesized epoxy-PDMS coated fibers: (d) 200 °C, (a) 180 °C, (e) 120 °C and (f) 100 °C.

3.4. Polarity and Wettability of Carbon Fiber Surface

Contact angle measurement of single carbon fibers were performed with a force tensiometer. Using an adapted Wilhelmy method, the dynamic contact angle of single carbon fibers can be detected. The advancing contact angle is measured during the wetting process (immersion in water) and the receding contact angle during the de-wetting process. Modifying the carbon fiber surface through oxidation in nitric acid and coating with a PDMS polymer changes the chemical composition and thus, the polarity of the carbon fiber surface. The changes in polarity can be studied via contact angle measurements of single carbon fibers after every synthesis step (Fig. 31). Unsized fibers have an almost inert surface, with just few oxygen and nitrogen containing functions. Therefore, the measured advancing angle of 89 ° and receding angle of 42 ° corresponds to the expected wettability (Tab. 3).^{117,118,121}

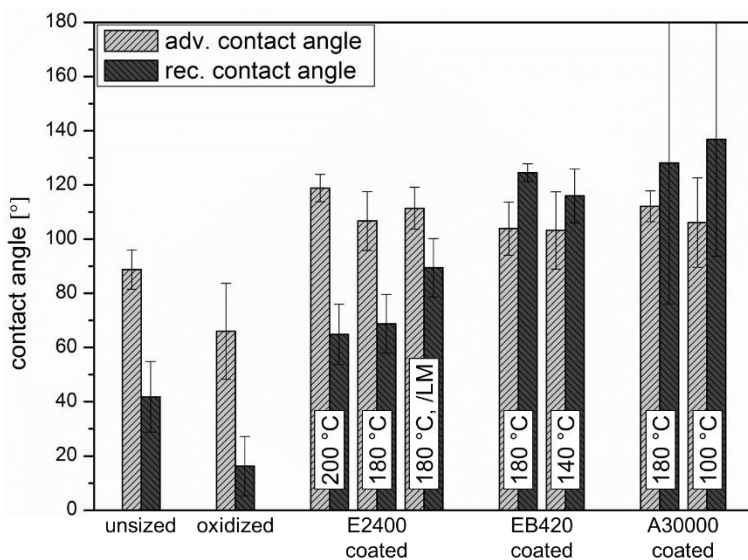


Fig. 31: Comparison of advancing and receding contact angles of unsized, oxidized and PDMS coated carbon fibers.

The oxidation process of the carbon fiber surface introduces a variety of different oxygen containing functional groups and should increase the polarity and thus, the wettability as a consequence. However, this is just partly the case: the measured advancing angles are between 50° and 90° . The reason for that seemingly high contact angle is the change of the topography through the erosion of carbon layers and thus, the increase of surface area and porosity (Fig. 7). The perimeter, which is used to calculate the contact angle, of an oxidized carbon fiber is higher than the perimeter of an ideally smooth carbon fiber. In case of a hydrophilic material, the contact angle decreases with an increasing surface area. However, the pores in the fiber surface are being flooded during the measurement and due to the pore shape, this process increases the measured force during the immersion of the sample in water. Fig. 32 illustrates the flooding of pores with different shapes during the contact angle measurement. Depending on the shape of the pore and its opening, different flooding scenarios are possible. In case (a), the water level has already risen to the height of the pore, but since the pore opening is smaller than the pore diameter, the water cannot flow into the pore. Pore (b) has an opening of the size of its diameter and thus, can be flooded easily. However, air bubbles can be trapped easily in pores like (c) and (d), and distort the measurement.

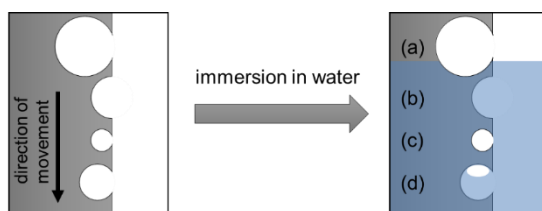


Fig. 32: Schematic illustration of the flooding of differently shaped pores in the oxidized carbon fiber surface during the wetting process of a contact angle measurement.

The analysis of PDMS coated carbon fibers show, that all PDMS coated carbon fibers are hydrophobic, regardless of functions or molecular masses of the PDMS polymers. These results are as expected, since pure PDMS is a hydrophobic material.¹⁰⁸ Comparison of biterminated E2400-PDMS and copolymer EB420-PDMS shows different values for the hysteresis (between advancing and receding angle) and confirms the results of the AFM measurements (Fig. 28): the different structures of the PDMS polymers lead to different bonding mechanisms and therefore to different roughnesses. Biterminated A30000-PDMS coated fibers are especially interesting, since they partly show ultrahydrophobic properties, due to the high molar mass of the PDMS.

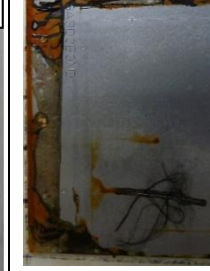
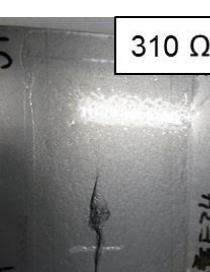
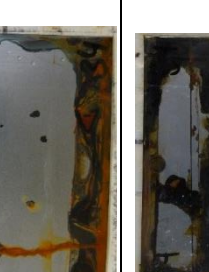
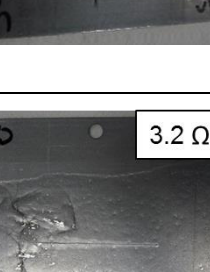
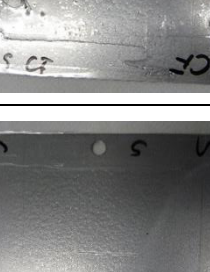
3.5. Corrosion Potential of Carbon Fibers

The challenges of high performance materials like carbon fibers, do not just refer to the interfacial behavior (e.g. adhesion) in carbon fiber reinforced plastics, but also include the electrical behavior concerning the interaction of CFRP composites with metal components. For the reinforcement of e.g. steel components with carbon fibers, an epoxy resin can be used as adhesive. The plastic is not conductive and since the metal is protected by the coating from the carbon fibers and the environment, no corrosion will take place. However, this is just true until damage occurs to the CFRP-steel compound, through e.g. processing of the compound, tension within the structure or external mechanical load. As soon as damage releases the metal and/or fiber surface, the compound can corrode. In presence of an electrolyte, the steel acts as the anode and the carbon fiber as the cathode. The contact corrosion is very effective and has destructive consequences for the entire component.

A salt spray test was performed to analyze the corrosion behavior of CFRP-steel compounds, in which PDMS coated carbon fibers were used. The results are summarized in Tab. 7. The black area presents the cathodic disbondment. The formation of rust occurs in the presence of oxygen: directly at the cut. Comparison of the steel sample (no use of carbon fibers) and the sample with unsized carbon fibers shows that the corrosion process is accelerated in the presence of carbon. The accelerating influence is best seen after 10 days. In case of the reference sample, the steel forms anodic and cathodic sub-areas, which alternate and are able to change in location. In the sample with unsized carbon fibers, the fibers act as a static cathode. The reverse case can be seen in all samples with PDMS coated carbon fibers: the corrosion process is decelerated. For the PDMS coated carbon fiber samples, three different PDMS polymers

were used: two biterminated (E2400 and A30000) and one copolymer (EB420) PDMS. The degree of deceleration varies depending on the molecular mass and the structure of the PDMS coating. A thicker PDMS coating leads to a better insulation and thus, the coated carbon fiber is less conductive. The observations are consistent: the sample with a 2400 g/mol PDMS coating shows a lower deceleration degree than the sample with a 30000 g/mol PDMS coating. Coincidentally, the sample preparation for the copolymer PDMS EB420 did not go according to standard procedure and caused a phase separation, due to poor wetting between fiber and resin. Due to this particular preparation mistake, the exact area of the formation of the galvanic couple can be observed. The cut surfaces of the fibers are not coated, due to the sample preparation method and therefore, are not insulated by a PDMS coating. The ends of the carbon fiber bundle were cut to length after the coating with PDMS, and cut in the middle after the preparation of the CFRP-steel sample for corrosion tests. In exactly these spots, the formation of rust took place (clearly visible after 3 days and after 10 days). This means, the carbon fibers themselves do not just act as the cathode, but the specifically not insulated areas of the carbon fiber surface enable redox reactions and therefore, corrosion.

Tab. 7: Comparison of corrosion tests of unsized and PDMS coated carbon fibers.

steel reference	0 d	3 d	10 d	30 d
unsized fibers	E2400-PDMS coated fibers 310 Ω	A30000-PDMS coated fibers 740 Ω	EB420-PDMS coated fibers 8000 Ω	
				
				
				
				

3.6. Fiber-Plastic Interface Characterization

For the analysis of fiber-resin interactions in CFRP composites, pull-out tests were performed. Epoxy resin BECKOPOX EP140 and EH637 was used as plastic component. Unsized, oxidized and PDMS-coated single carbon fibers were embedded in resin droplets and pulled out of the cured resin with a defined strain rate. The recorded force is characteristic for the fiber-resin interface. However, the measured forces cannot be compared directly with each other, neither within one measurement series nor with differently coated carbon fibers. This is caused by the different embedded lengths of the fibers: the longer the embedded length, the higher the contact area between fiber and resin and therefore, the higher the adhesive force. The calculation of the interfacial shear strength (eq. (3)), which depends on the recorded force and the interface area, allows the comparability between pull-out tests.

Unsized Carbon Fibers

An exemplary curve of the pull-out tests of unsized carbon fibers is shown in Fig. 33 (a); the measurement is separated in four stages: phase I describes an increase in tension and is defined as elastic area. Phase II follows after the fiber reaches the limit of the elastic deformation. At this point, there is a force equilibrium between cohesive and adhesive forces. If the adhesive forces between fiber and resin are stronger than the cohesive forces of the fiber, the fiber will break and the test is not declared “pull-out test” but “single fiber tensile test”. However, if the adhesive forces between fiber and resin are weaker than the cohesive forces of the fiber, the bonding of fiber and resin will break. The recorded force in phase III is mainly caused by friction, since the fiber has to be pulled out of the resin droplet (Fig. 33 (c)). The friction force decreases almost linearly with the decreasing contact area of fiber and resin. Phase IV describes the fully debonded interface, when the fiber is completely pulled out of the resin droplet.

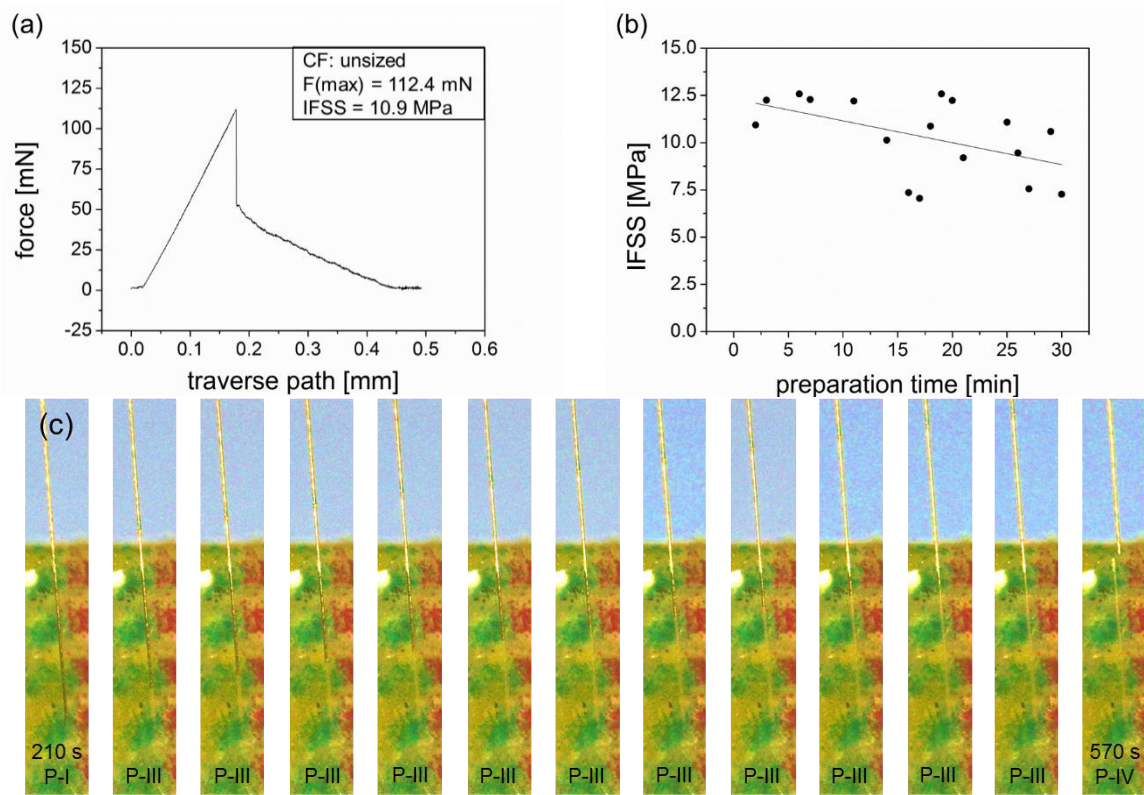


Fig. 33: Pull-out tests of unsized carbon fibers. (a) Exemplary pull-out test of a fiber, which was prepared at 18 minutes preparation time. (b) Summary of IFSS values of one measurement series. (c) In-situ light microscopic images (interval: 30 s) of the pull-out test which is shown in (a).

The pull-out sample of the exemplary measurement of Fig. 33 (a) was prepared at 18 minutes preparation time, the remaining IFSS values of that measurement series are shown in Fig. 33 (b). Even though the pot life for the epoxy resin is 30 minutes, the decrease in wetting behavior and adhesive bonding ability of the resin is clearly visible after just 10 mins. The mean IFSS of unsized carbon fibers and the epoxy resin is 10.3 ± 2.0 MPa. But, separating the samples into three categories delivers more specific results: samples which were prepared in the first 10 minutes of preparation time have IFSS values of 12.0 ± 0.6 MPa, samples which were prepared in 11 to 20 minutes of preparation time have IFSS values of 10.3 ± 2.1 MPa and samples which were prepared in the last 10 minutes of preparation time have IFSS values of 9.2 ± 1.4 MPa. The IFSS(1-10) can be seen as the most specific in terms of being the least affected by cross-linking influences like wetting behavior and bonding ability of the resin.

Cohesive failure of carbon fibers is detected as single fiber tensile tests, and cohesive failure of the resin is observed optically as cracks and chipped chunks right at the edge of the meniscus, which is formed due to wetting and capillary action. The dimensions of the resin ring, which remains on the fiber, depend on the adhesion of fiber and resin. Exemplary SEM images of resin failure at the meniscus area and resin ring formation are shown in Fig. 34.

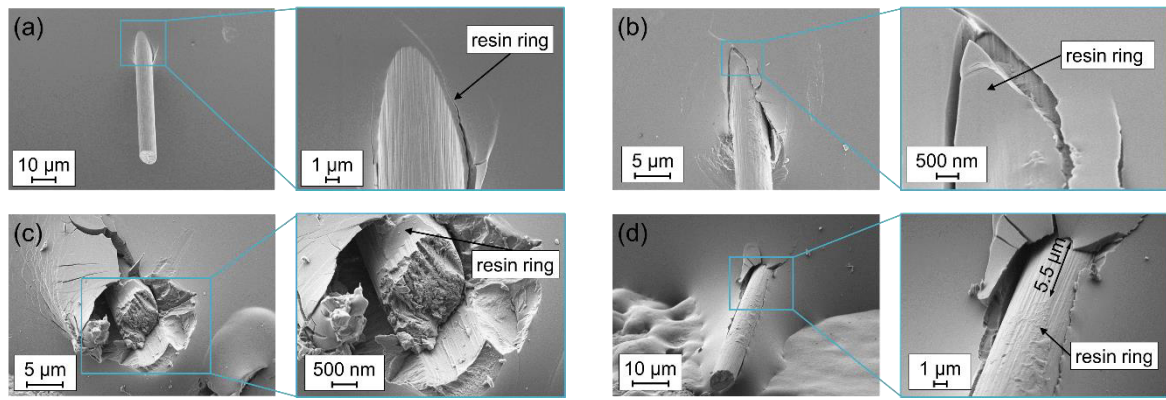


Fig. 34: Analysis of meniscus and resin ring at single fiber tensile tests of unsized carbon fibers. (a) SEM InLens images of partially debonded meniscus and the beginning of the formation of the resin ring. (b) SEM InLens images of fully debonded meniscus and formed resin ring. (c) SEM SE2 images of a severe cohesive failure of the meniscus. (d) SEM SE2 images of fully debonded meniscus and resin ring.

Optical analysis of single fiber tensile tests shows both, resin failure at the meniscus area and resin ring formation on fiber. Single fiber tensile tests occur, when the adhesive forces of fiber and resin are stronger than the cohesive forces of the fiber. This reverse force equilibrium to pull-out tests can happen due to e.g. very long embedded fiber lengths, since the bonding area, and therefore the adhesive force, increases with increasing embedded fiber length. However, as shown in Fig. 34, the resin also undergoes cohesive failure and since the meniscus area is the weakest point of the resin droplet, this is where the most harm can be observed. The exemplary SEM images show different stages of severity of resin failure. With the exception of Fig. 34 (a), the severity of resin failure can be affected by straight alignment of fiber, but more importantly, by meniscus geometry. Since the fibers are embedded at the side of the resin droplet and not on top of it, angle dependent meniscus formations like Fig. 34 (d) are possible. The sample in Fig. 34 (a) is just partially debonded. Comparing the stress values of the measurements confirm a beforehand damage to the fiber (a): stress values of samples (b), (c) and (d) are 4.2 ± 0.3 GPa and stress value of sample (a) is 1.5 GPa. That means, the acting forces on the resin in sample (a) were almost 3 GPa less than on the other samples and therefore, less damage occurred on the resin of sample (a). Interestingly, the example Fig. 34 (d) shows that the fiber slid out of the resin droplet of about 5.5 μm . Since the fiber broke before an adhesive failure (phase II) could have occurred, this sliding happened during the elastic deformation of the carbon fiber. This means, that not just the elastic deformation of the carbon fiber but also crack initiations¹⁴⁶ take place in the elastic area and influence the force measurement.

Oxidized Carbon Fibers

The intensity of resin failure increases with increasing adhesion between carbon fiber and resin. The adhesion of oxidized carbon fibers and epoxy resin is stronger than the adhesion of unsized carbon fibers and resin. The oxidation of carbon fibers increases the adhesion in three ways: chemical, physical and mechanical. The introduction of oxygen containing groups to the carbon fiber surface enables chemical reactions between the carbon fiber surface with the epoxy resin and the amine curing agent (Fig. 8). The change of polarity of the carbon fiber surface also increases its wettability and therefore, can be wetted better by the resin than unsized carbon fibers. Due to carbon erosion, which occurs through the oxidation process (Fig. 7), the porosity of oxidized carbon fibers is higher than of unsized carbon fibers. Porosity enables mechanical interlocking and therefore, enhances adhesion of carbon fiber and resin. The mean IFSS value of oxidized carbon fibers is 13.2 ± 2.1 MPa and the IFSS(1-10) is 16.2 ± 1.1 MPa. Compared to unsized carbon fibers, which have an IFSS(mean) of 10.3 ± 2.0 MPa and an IFSS(1-10) of 12.0 ± 0.6 MPa, the difference in adhesive force is 3 to 4 MPa. This difference can even be seen via light microscopy in Fig. 35. In case of successful pull-out tests (a), big chunks of resin remain on the oxidized carbon fiber. However, many samples in the measurement series undergo cohesive failure (break of fiber) and meniscus failure (break of resin) due to the increased adhesion, as seen in sample (b).

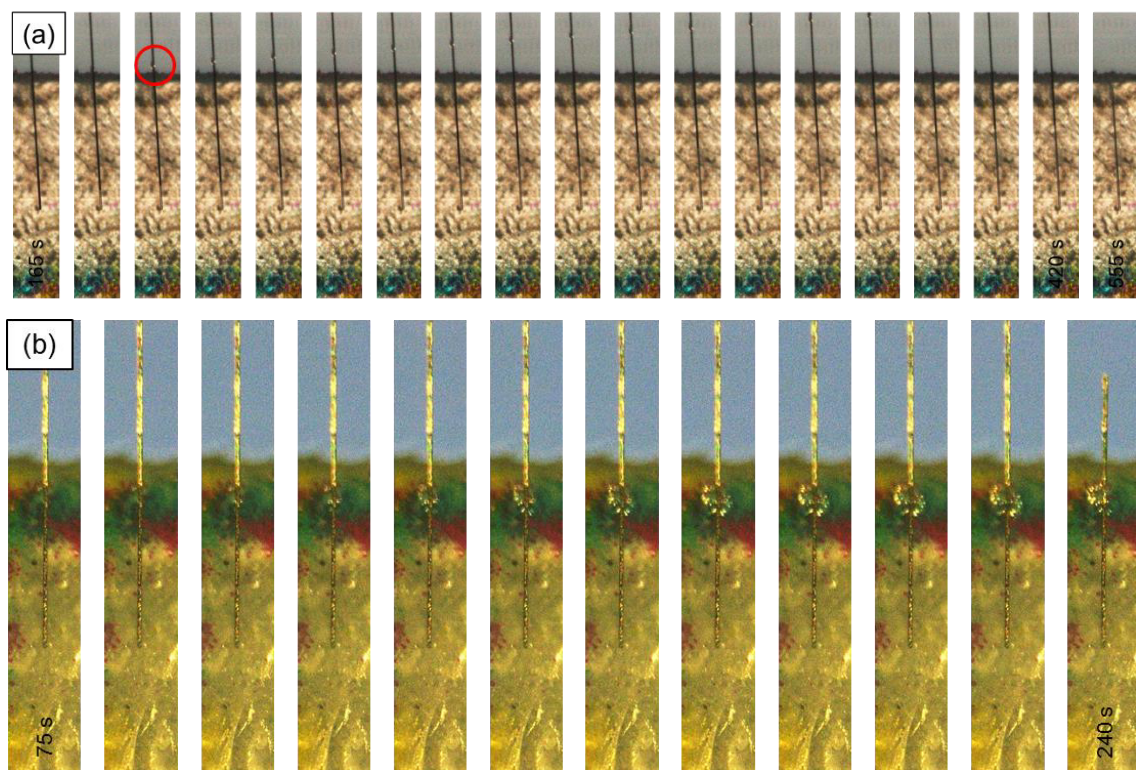


Fig. 35: Micromechanical analysis of oxidized carbon fibers. Light microscopic images of (a) a pull-out test with resin ring on fiber and (b) a single fiber tensile test with meniscus failure.

Furthermore, the increased adhesion can be observed in changed curve shapes of the pull-out tests in Fig. 36: after the adhesive failure, the carbon fibers do not slide smoothly out of the resin droplets, but are dragged out forcefully, due to increased friction. For unsized carbon fibers it was observed, that the lower the preparation time the higher the adhesive forces between fiber and resin. This is also the case for oxidized carbon fibers, sample (a) was prepared at 3 minutes preparation time and has a higher IFSS value than sample (b), which was prepared at 10 minutes preparation time. Not just the initial adhesive force is higher in sample (a), but also the friction force. A “sticky effect” can be observed in phase III: the static friction force is so high, that there is no linear decrease of kinetic friction with decreasing contact area, but instead the tension increases again while the fiber is not being pulled out. This is mainly caused by interfacial roughness and abrasion at the sliding interface,¹⁴⁷ due to the porosity of the oxidized carbon fiber surface (Fig. 7 and Fig. 25 (c) & (d)). The stick-slip behavior was observed for all oxidized carbon fibers, and its intensity correlates with the interfacial shear strength. Therefore, it also can be detected in sample (b), but in a less severe manner.

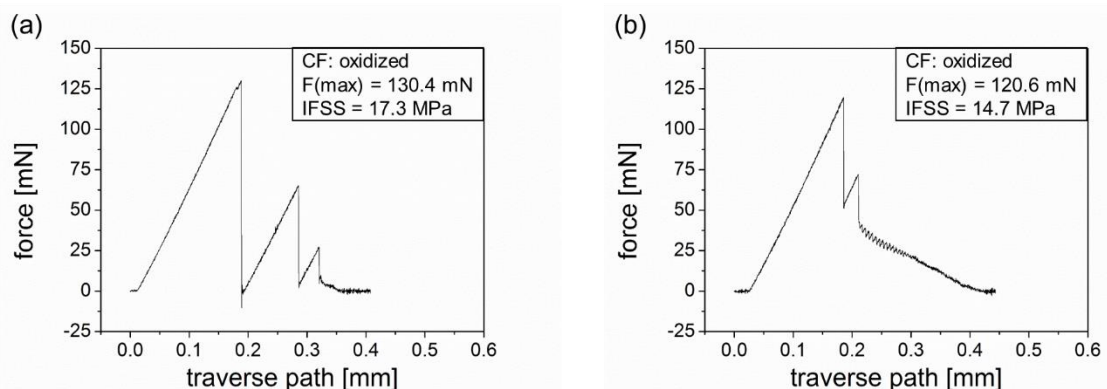


Fig. 36: Exemplary pull-out tests of oxidized carbon fibers, which were prepared at (a) 3 minutes preparation time and (b) 10 minutes preparation time.

PDMS-coated Carbon Fibers

A PDMS coating on carbon fibers eliminates the stick-slip behavior¹⁴⁷ of oxidized carbon fibers and creates a low friction sizing. The elastomeric interphase acts as a slip agent, due to its low surface energy and poor wettability,¹⁰¹ hydrophobicity,¹⁰⁸ high flexibility and compressibility^{109,110}. The PDMS coating influences the fiber-resin interaction in different ways. First, it inhibits the wetting ability of the resin already during the sample preparation. On the one hand, PDMS is chemically stable and inert, meaning it lowers the chemical reactions and interactions with the resin, compared to oxidized carbon fibers. On the other hand, the

surface energy prevents proper wetting of the fiber through the resin. This means, there is no or just few fiber-resin interactions during the curing process of the resin. Furthermore, the PDMS interphase acts as a slip agent during the pull-out test and therefore, decreases the frictional sliding in phase III and reduces interface abrasion, due to its flexibility and compressibility. The wetting behavior of the epoxy resin and the influence of PDMS can be observed optically via SEM images. Fig. 37 shows oxidized and PDMS coated carbon fibers after a pull-out test. While the oxidized carbon fibers were wetted uniformly by the resin, the PDMS coated carbon fibers show phase separation. The epoxy resin forms unique structures on the surface of the E2400-PDMS coated carbon fibers, due to the ball-like PDMS domains on the carbon fiber surface. The phase separation occurs in all PDMS coated carbon fibers, although its degree and structure differs depending on molar mass, compared to A30000-PDMS, and nanostructure of the PDMS domains, compared to EB420-PDMS.

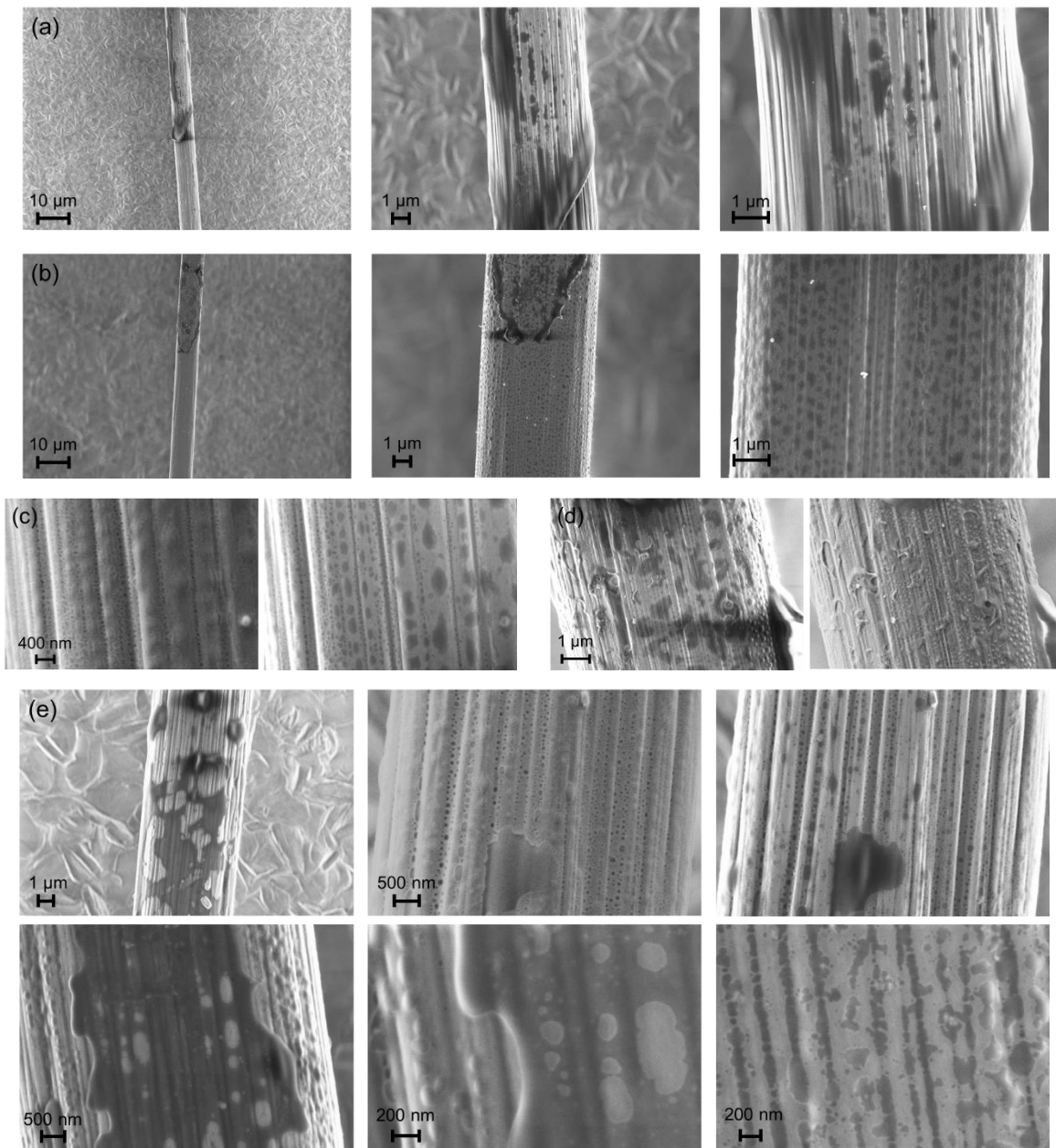


Fig. 37: Exemplary SEM images of differences in wetting behavior of epoxy resin on (a) oxidized carbon fibers, (b) E2400-PDMS, (c) A30000-PDMS, (d) EB420-PDMS (coated at 180°C) and (e) EB420-PDMS (coated at 140°C) coated carbon fibers.

Since there is no chemical reaction happening between PDMS coated carbon fibers and resin, and since the wetting behavior is strongly influenced by the PDMS coating, the pot life of the resin has just little influence on the interfacial shear strength, whatsoever. The mean IFSS value of E2400-PDMS in Fig. 38 is 8.0 ± 1.5 MPa and IFSS(1-10) is 8.6 ± 1.6 MPa. Additionally, there is no trend of IFSS values observable towards the preparation time, as it is for unsized and oxidized carbon fibers. This supports the already existing results about the PDMS coating acting as a low wettable and low friction sizing. Furthermore, a “kink” is present in the elastic area (phase I) of the pull-out tests of PDMS coated carbon fibers. The change in force in this part of

the measurements represents an onset of debonding¹⁴⁶ and does just occur in systems with low wettability or low friction.

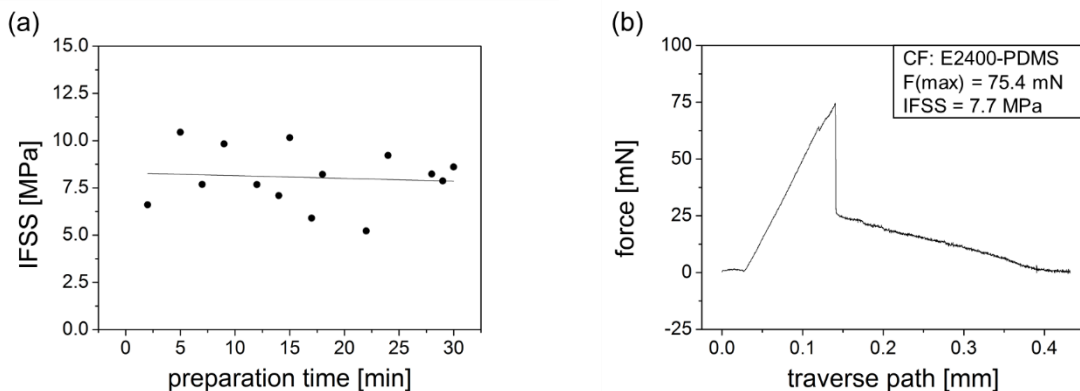


Fig. 38: Pull-out tests of E2400-PDMS coated carbon fibers, coated at 180 °C and without the use of a solvent. (a) Summary of IFSS values of the measurement series. (b) Exemplary pull-out test of a fiber, which was prepared at 12 minutes preparation time.

The interfacial shear strength of PDMS coated carbon fibers depends on reaction temperature, functional groups of the PDMS, molar mass of the PDMS and the molecular structure of the PDMS. Epoxy- and amine-terminated PDMS are especially interesting, since they mimic the functionality of an epoxy resin and an amine crosslinker. The reaction temperature and the functional groups of the PDMS both influence the reaction yield and therefore, the amount of PDMS that is deposited on the carbon fiber surface. In case of epoxy terminated PDMS, as shown in Fig. 39 (a), the reaction yield is low underneath a reaction temperature of 160 °C. The higher the reaction temperature, the higher the reaction yield and therefore, the lower the IFSS. Amine terminated PDMS polymers, on the other hand, already react at low temperatures like 100 °C, as seen in Fig. 39 (b). The reaction yield increases with increasing temperature and therefore, the IFSS values decrease. A5000- and A30000-PDMS have the same molecular structure and were coated at the same temperature, but have different IFSS values. This leads to the conclusion, that the molar mass of PDMS has direct influence on the interfacial shear strength. A summary of PDMS coated fibers with different PDMS coatings is given in Fig. 39 (c). The reaction yield depends on the functional groups of the PDMS polymers, comparing epoxy and vinyl terminated PDMS. Although epoxy copolymer EB290- and EB420-PDMS have the same functional groups like E2400, their interfacial shear strengths are significantly lower. This is caused by the scale-like PDMS structures, which are formed during the coating. They cover the carbon fiber surface more efficient than the ball-like domains, which are formed by biterminated PDMS polymers (Fig. 28). The influence of the molecular mass is demonstrated by A5000 and A30000, and by EB290 and EB420. As a remark, it has to be noted,

that a quantitative analysis of coated fibers with low reaction yields is difficult, since the coated areas are not distributed homogeneously. As shown exemplary in Fig. 39 (d), a separation of the IFSS distribution within a measurement series takes place. This is caused by heterogeneous coating of the carbon fibers: carbon fibers with a low amount of PDMS covered area mainly react as they are not coated at all. As soon as there is a sufficient amount of PDMS coating on the carbon fibers, they show the characteristic slip effect of PDMS coated carbon fibers. This separation decreases with reaction yield, since the PDMS coated area increases and the PDMS character dominates the surface properties.

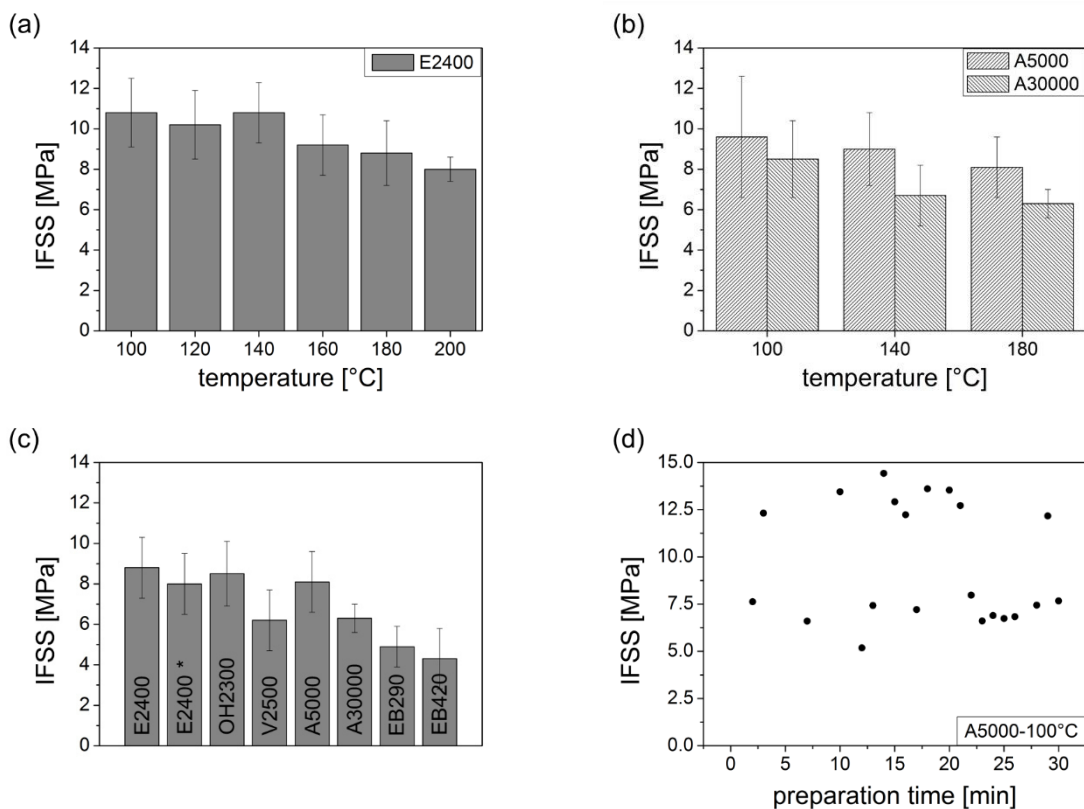


Fig. 39: Influence of reaction yield on the interfacial shear strength. (a) IFSS values of E2400-PDMS coated carbon fibers, which were coated at different temperatures. (b) IFSS values of A5000- and A30000-PDMS coated carbon fibers, which were coated at different temperatures. (c) IFSS values of PDMS coatings with different functional groups, all carbon fibers were coated at 180°C. E2400* was coated without the use of a solvent. (d) Heterogeneous distribution of the IFSS values of a measurement series of A5000-PDMS coated carbon fibers, which were coated at 100°C.

3.7. First Impressions of Carbon Fiber Reinforced Plastics

In this work, first macromechanical tests were performed. The epoxy resin BECKOPOX system EP140 and EH637 and polyurethane system PU3090A and PUH3090B were used as plastic components. The test methods include tensile tests and bending tests.

Tensile Tests: Carbon Fiber Reinforced Epoxy Resin

For the tensile tests, the CFRP test specimens are exposed to a pulling force. Due to the brittle properties of epoxy resin, the plastic just undergoes little plastic deformation. Fig. 40 illustrates the geometry of a typical test sample and the cross section of the fracture plane. The carbon fibers were not coated and therefore, show resin residues on the surface.

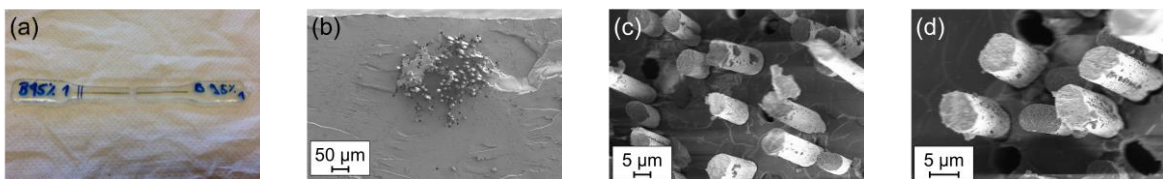


Fig. 40: CFRP tensile test samples. (a) Photographic image of test specimen. (b) SEM SE2 image, (c) & (d) SEM InLens images of cross section of the test specimen after break.

The plastic deformation behavior of the resin changes when being reinforced with fibers (Fig. 41 (a) & (b)). The exemplary measurement of pure epoxy resin shows a non-linear elastic behavior, but when being reinforced with carbon fibers the behavior changes to a linear correlation. The reinforcement causes an increase in brittleness and a decrease in elongation. The stress is calculated according to equation (4) and scales the recorded force to the specimen's dimensions. The tensile strength is defined as the maximal stress value at break and increases through the reinforcement with carbon fibers, although decreases again by the use of PDMS coated carbon fibers. These results correlate with the chemical and micromechanical analysis. The reinforcement of plastics with carbon fibers increases the composite's strength, as seen for CFRP with unsized fibers. The PDMS coating decreases the chemical and physical interactions between the fiber surface and the resin and therefore, decreases the overall strength of the compound in parallel fiber direction.

$$\sigma = \frac{F}{b \cdot h} \quad (4)$$

- σ stress [MPa]
- F recorded force [N]
- b width of test specimen [mm]
- h height of test specimen [mm]

The same tendency is observed for the elastic modulus, meaning the brittleness of the compound increases by the use of unsized carbon fibers and decreases by the use of PDMS coated carbon fibers. The elastic modulus is calculated according to equation (5) and the results correlate to the composites tendency to undergo less plastic deformation with higher strength. Meaning, the higher the increase in strength, the higher the brittleness and stiffness of the compound and the lower its elastic behavior and plastic deformation. These results correlate with the chemical and micromechanical analysis. The use of PDMS coated carbon fibers lowers the chemical and physical interactions in the fiber-resin interface and therefore, lower the brittleness of the CFRP composite. Overall, PDMS coated carbon fiber reinforced plastics are less resistant to undergo plastic deformation than unsized carbon fiber reinforced plastics.

$$E = \frac{\sigma_{max} \cdot l_0}{\Delta l} \quad (5)$$

- E elastic modulus [MPa]
- σ_{max} maximal stress [MPa]
- l_0 length of test specimen [mm]
- Δl elongation [mm]

The elongation measurement represents the plastic deformation of the compound during the tensile test. Pure epoxy resin is less brittle and more elastic than carbon fiber reinforced epoxy resin; therefore, its elongation is higher. The elongation of pure carbon fibers is 1 %,^{16,21,24,25} and since this material constant is defined by the fiber bulk, it does not change through a surface coating. However, the energy transfer of the elongation ability does transfer through the fiber-resin interface, meaning if there is a covalent bonding between fiber surface and epoxy resin within the CFRP, the composites elongation ability is not able to be higher than 1 %. The use of a PDMS coating, on the other hand, introduces a low friction interphase layer and enables the fibers and the resin to slide against each other. The ability to slip increases the overall elongation and energy dissipation of the CFRP composite.

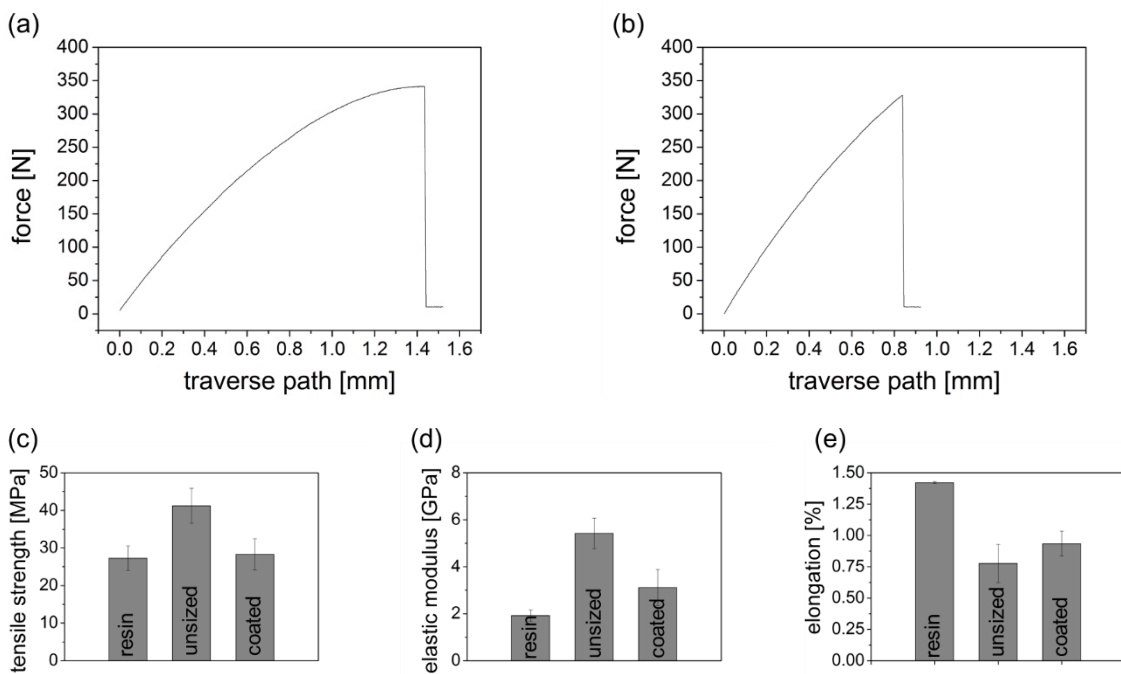


Fig. 41: Tensile test results. Exemplary measurement of epoxy resin (a) without carbon fibers and (b) with PDMS coated carbon fibers. (c) Tensile strengths, (d) elastic moduli and (e) elongation of the pure resin and of CFRPs with unsized and with PDMS coated carbon fibers.

Tensile Tests: Carbon Fiber Reinforced Polyurethane

The general brittleness of epoxy resins causes difficulties in the visual analysis of the fiber-resin interface in the fracture plane, since the fibers break really close to the fracture plane. Therefore, a PUR system was used as plastic component for the qualitative assessment of PDMS coating as slip sizing and its visibility in macromechanical tests. Polyurethane is an elastomer and the test specimen did not break in the tensile tests, but instead, slid out of clamping jaws when a certain force was reached. Carbon fiber reinforced polyurethane on the other hand, did break under the applied pulling force. This is caused by the covalent bonding between carbon fiber surface and polyurethane. Carbon fibers undergo a plastic deformation of just 1 - 2 % and after the maximum elongation of the fibers is reached, a cohesive break occurs. In case of the fibers being embedded in a plastic, the force equilibrium of adhesive and cohesive forces defines the manner of failure. There are strong chemical and physical interactions between the surface of unsized and oxidized fibers and the PUR plastic, since they can react and bond covalently. Leading to strong adhesive forces between fibers and plastic, which define the style of CFRP specimen fracture. Fig. 42 (a) - (d) illustrates SEM images of the fracture planes of unsized and oxidized carbon fiber reinforced PUR. The adhesive forces are so strong, that the PUR matrix cannot undergo plastic deformation in the interface area and breaks under

the external load. The cohesive failure of the plastic can be seen as PUR residue on the fibers. Another kind of failure behavior is observable when using PDMS coated carbon fibers for the reinforcement of PUR, which is demonstrated visually in Fig. 42 (e) - (h). Since PDMS lowers the adhesion between fibers and plastic in two ways, first, as prevention of chemical and physical interactions and second, as slip and low friction sizing, there is no residue existent on the PDMS coated carbon fibers. Most of the PDMS coated carbon fiber reinforced PUR composites did not break under external load. These results correlate with the chemical and micromechanical analysis and with the tensile tests of carbon fiber reinforced epoxy resin.

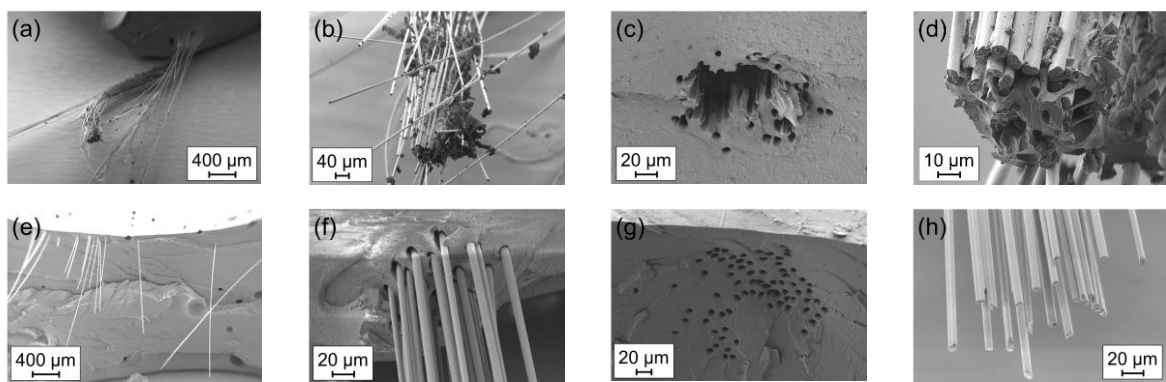


Fig. 42: Optical analysis of the fracture plane of carbon fiber reinforced polyurethane after tensile tests. (a) - (d) SEM images of unsized and oxidized carbon fiber reinforced PUR. (e) - (h) SEM images of PDMS coated carbon fiber reinforced PUR.

Bending Tests: Carbon Fiber Reinforced Epoxy Resin

The macromechanical analysis also included bending tests of carbon fiber reinforced epoxy resins. As seen in the tensile tests, the optical analysis of the fracture plane after the bending tests revealed strong adhesion for unsized and oxidized carbon fibers with the epoxy resin. Fig. 43 (a) & (b) show resin residue on the fibers and the cohesive failure of the resin, which is caused by strong fiber-resin interactions. For PDMS coated carbon fibers, the bending tests resulted in the same scenario as the tensile tests: the lower adhesion between fibers and resin prevent the cohesive failure of the resin and let the fibers slip (Fig. 43 (c) & (d)).

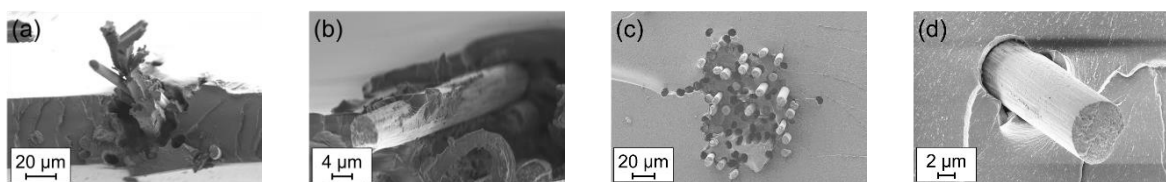


Fig. 43: Optical analysis of the fracture plane of carbon fiber reinforced epoxy resin after bending tests. (a) & (b) SEM images of oxidized carbon fiber and (c) & (d) PDMS coated carbon fiber reinforced epoxy resin.

The differences in adhesion were also observed quantitatively. The stress was calculated according to equation (6) and scales the recorded force to the specimen's dimensions. The bend strength is defined as the maximal stress value at break and increases through reinforcement of epoxy resin with oxidized carbon fibers. Since the PDMS interphase lowers the adhesion between fibers and resin, through prevention of interface interactions and as slip sizing, the bend strength of PDMS-CFRP is lower than of oxidized-CFRP. These results correlate with the chemical and micromechanical analysis and with the tensile tests of CFRP.

$$\sigma = \frac{M}{S} = \frac{3 \cdot F \cdot l_0}{2 \cdot b \cdot h^2} \quad (6)$$

- σ stress [MPa]
- M bending moment [Nmm]
- S section modulus [mm^3]
- F recorded force [N]
- l_0 support distance [mm]
- b width of test specimen [mm]
- h height of test specimen [mm]

The same tendency was observed for the elastic modulus, meaning the deformation resistance increases by the reinforcement of the epoxy resin with oxidized carbon fibers and decreases by the reinforcement with PDMS coated carbon fibers. The elastic modulus was calculated according to equation (7) and the results correlate to the composite's tendency to undergo less plastic deformation with higher strength. Meaning, the higher the increase in strength, the higher the brittleness of the compound and the higher its resistance towards plastic deformation. These results correlate with the chemical and micromechanical analysis and with the tensile tests of CFRPs. The use of PDMS coated carbon fibers lowers the chemical and physical interactions in the fiber-resin interface and therefore, lowers the brittleness of the CFRP composite. Overall, PDMS coated carbon fiber reinforced plastics are less resistant to undergo plastic deformation than oxidized CFRP composites and the pure epoxy resin.

$$E = \frac{F_{\max} \cdot l_0^3}{4 \cdot b \cdot h^3 \cdot \Delta l} \quad (7)$$

- E elastic modulus [MPa]
- F_{\max} maximal recorded force [N]
- l_0 support distance [mm]
- b width of test specimen [mm]
- h height of test specimen [mm]
- Δl deformation [mm]

The measurement of the deformation distance represents the plastic deformation of the specimens during the bending test. Even though, pure epoxy resin is less resistant towards plastic deformation, the oxidized-CFRP undergoes more plastic deformation. This is caused by the experimental setup, the CFRP composite breaks in a more ductile way than the pure resin, which breaks in a brittle way. The crack propagation stops at every single fiber and the mechanical load is then redistributed to several neighboring fibers. This way, the composite is able to not fail abruptly and undergo more deformation. The PDMS coated carbon fiber reinforced plastics show the perfect properties for this study's objective: they have the lowest resistance towards bending processes and undergo the highest deformation distances. These fibers can therefore be used for the manufacture of CFRP and are of lower risk to be damaged in processing like the state-of-the-art carbon fibers.

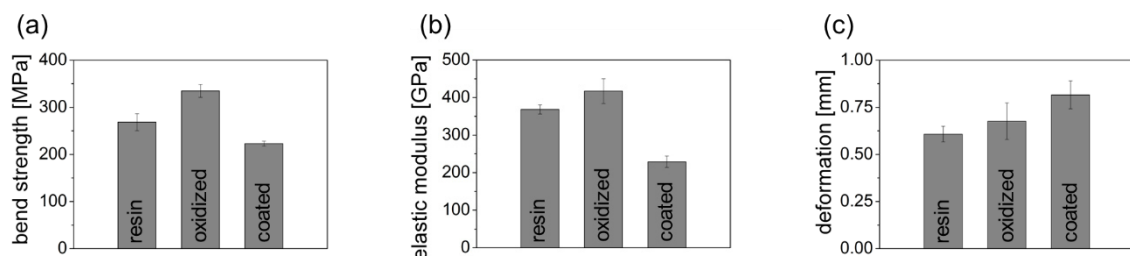


Fig. 44: Bending test results. (a) Bend strengths, (b) elastic moduli and (c) deformation distance of the pure resin and of CFRPs with oxidized and with PDMS coated carbon fibers

As a last macromechanical test to pave the way for future work, bending tests with small CFRP specimens were performed. The samples were fully loaded with carbon fibers, instead of carbon fiber contents of just 1 - 10 %. The composites were 13.4 mm long, 6.6 mm wide and 2 mm high. It was not possible to determine quantitative results, but the qualitative rateable images are shown in Fig. 45. The oxidized-CFRP specimen failed in a brittle way. The PDMS-CFRP composite, on the other hand, did not break. These are excellent results for the objective of manufacturing and processing of carbon fiber reinforced plastics and they correlate with the chemical, micromechanical and macromechanical analysis.

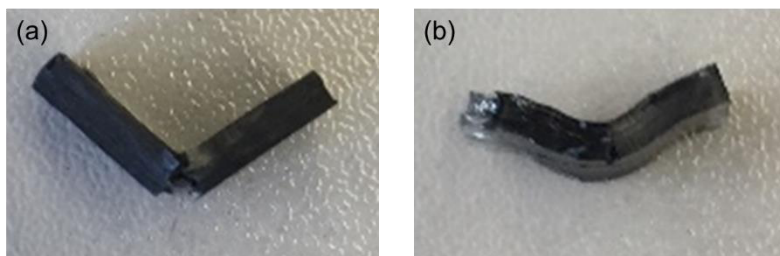


Fig. 45: Epoxy resin reinforced with the maximal load of carbon fibers. (a) Oxidized carbon fiber reinforced epoxy resin after bending test. (b) PDMS coated carbon fiber reinforced epoxy resin after bending test.

3.8. Summary

In order to create a low friction, elastomeric interphase in carbon fiber reinforced plastics, polydimethylsiloxane was covalently bonded onto carbon fibers. The objective focuses on energy dissipation, a better plastic deformation behavior, enhanced shock absorption and lower defect formation during manufacturing and processing, through reduction of internal stress. The PDMS coating was applied successfully, as shown by the chemical analysis. Different PDMS polymers were used and analyzed concerning reaction yield, functional groups, molar masses and molecular structures. The chemical analysis focuses on chemical and physical properties and changes on the carbon fiber surface and the effects on topography and polarity. The analysis methods include scanning electron microscopy, atomic force microscopy, contact angle measurements and corrosion analysis. The mechanical analysis focuses on the fiber-resin interactions and their effect on a micro- and macro-scale level.

Topographical changes due to carbon fiber surface modification and coating were observed via optical analysis with scanning electron microscopy and with atomic force microscopy, linked with a nanomechanical analysis. The carbon erosion due to oxidation was observed as an increase in porosity of the carbon fiber surface. The following coatings with PDMS polymers changed the surface topography, so that ball-like and scale-like domains, depending on the structure of the PDMS, were detected. The measured stick-slip effect on oxidized fibers via pull-out tests is caused by strong friction and was eliminated through the coating with low friction PDMS. Furthermore, the PDMS coating led to changes in polarity and thus, to wettability. These properties were determined by contact angle measurements and influence the wetting ability of epoxy resin on the carbon fibers. While unsized and oxidized carbon fibers allow a good wetting through epoxy resin, a phase separation on PDMS coated carbon fibers was observed. The strong adhesion between uncoated carbon fibers and plastic and their mechanical interlocking, and the slippery behavior of PDMS coated carbon fibers was also observed in macromechanical tests. PDMS manipulates the fiber-resin interface in three different ways: chemical, physical and mechanical. The chemical fiber-resin interactions are lowered through PDMS during the CFRP manufacture, due to the chemical inertness of PDMS. There are fewer reactions possible in the interface, because of the lack of functional groups; the main interactions are lowered to van der Waals forces. The physical interactions are predominantly influenced by the low surface energy of PDMS and the decrease of wettability of the carbon fiber surface through PDMS coating. The epoxy resin is therefore not able to efficiently wet the carbon fiber surface, which ultimately leads to a further decrease in adherence. While the chemical and physical interactions set the level of fiber-resin adhesion

during the CFRP manufacture, the mechanical influence describes the frictional behavior and the sliding ability of PDMS coated carbon fibers in the resin. The PDMS coating leads to enhanced energy dissipation in the fiber-resin interface and to hydrodynamic sliding.

Within the different PDMS coatings, a higher reaction yield led to a larger coating area and thus, to lower interfacial shear strengths. The use of PDMS with higher molar masses also decreased the interactions between carbon fibers and epoxy resin and thus, the IFSS. Interestingly, E2400-PDMS has higher IFSS values than EB420-PDMS, although its molar mass is higher. This is caused by the different molecular structures. The scale-like domains, which are formed by using the copolymer EB420-PDMS, are more efficient in covering the carbon fiber surface than the ball-like structures, which are formed by the biterminated E2400-PDMS.

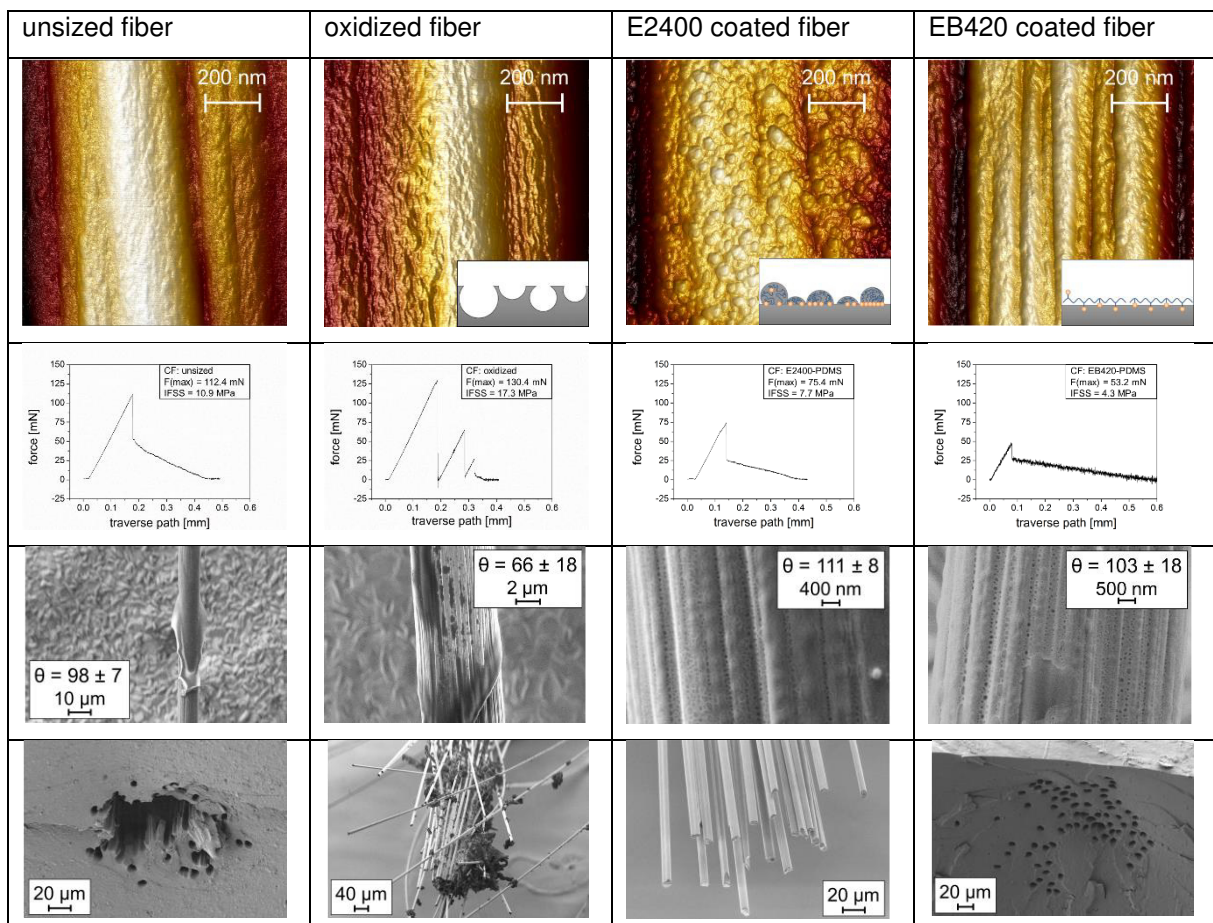
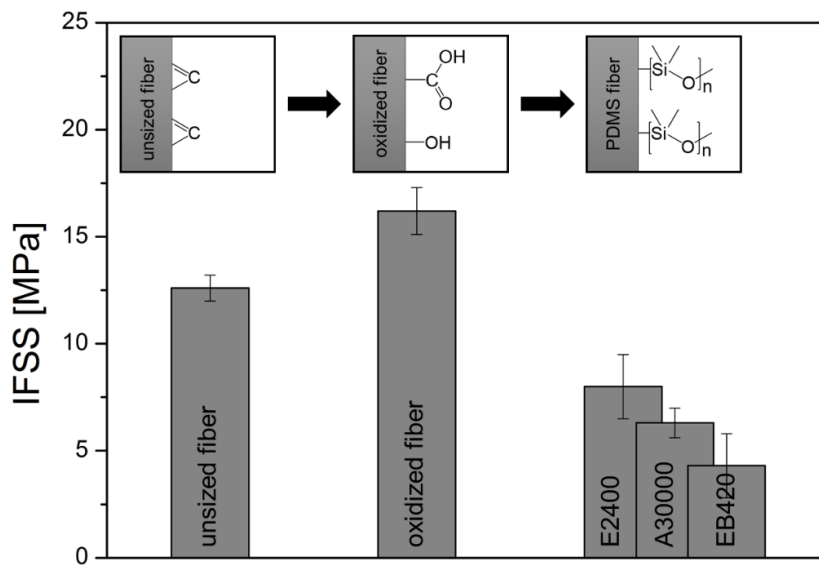


Fig. 46: Comparison of unsized, oxidized and PDMS coated carbon fibers and their IFSS values, 3D AFM height images, exemplary IFSS measurements, SEM images of wetting ability of epoxy resin on carbon fibers and CFRP tensile test.

Chapter 4: PDMS Microgel on Carbon Fibers

As shown in the previous chapter, PDMS can be successfully coated on carbon fibers and act as a low friction, elastomeric interphase in CFRPs. However, the coating process for a covalent bonding is time intensive and requires high temperatures or additional synthesis steps for the introduction of coupling agents and reactive functional groups. This is not desired for industrial manufacturing in terms of low cycle times. Therefore, a faster and more economical approach was studied: the physical adsorption of micro-sized PDMS structures via dip coating.

PDMS microgels describe colloidal emulsions of cross-linked polydimethylsiloxane spheres. Microgels^{148,149} are a well-established material in the coating industry, such as the automotive sector, due to shear thinning ability and rheological properties. Different PDMS polymers were used and analyzed concerning particle size distribution of the microgel particles, wetting ability and adhesion to carbon fibers. The analysis methods include scanning electron microscopy and pull-out tests.

4.1. Experimental

Coating of carbon fibers with a PDMS microgel requires a three-step synthesis. The carbon fiber surface had to be cleaned and activated through treatment with nitric acid and the PDMS microgel was cured with a platinum catalyst. The last step is the coating, which was performed via dip coating.

Unsized carbon fibers were treated in concentrated nitric acid at 120 °C for 3 hours, (based on Pittman's instructions^{51,52}). A gas washing bottle, filled with a saturated solution of iron sulfate, was used for the reduction of resulting nitrous gases. After the oxidation treatment, the mixture was carefully poured onto ice and the fibers were washed with distilled water until a neutral pH was reached.

The PDMS microgels were obtained through addition polymerization of vinyl and hydride functional PDMS polymers (Tab. 8). The reactions were performed at room temperature in a mixture of 18 ml NMP as solvent and 1.6 ml Fluid 190 as emulsifier. The ratio of the educts varied, depending on their functionality. A platinum-divinyltetramethyldisiloxane complex was used as catalyst and the polymerization started with its addition. The curing was completed after 1 to 3 hours. The stable PDMS microgel dispersions were then used for dip coating of the oxidized carbon fibers. The PDMS microgel coated carbon fibers were washed three times with 30 ml NMP and dried at 200 °C.

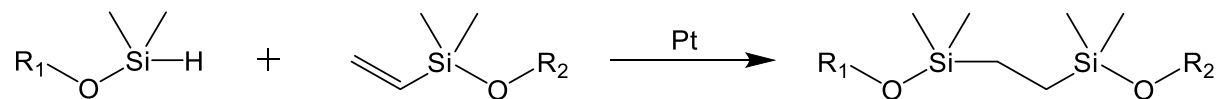
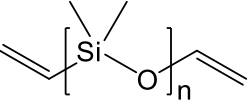
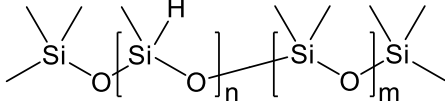


Fig. 47: General reaction procedure of PDMS microgel synthesis via hydrosilylation.

Tab. 8: PDMS species for microgel synthesis and their structures.

sample	PDMS species	molar mass [g/mol]	supplier	volume ratio to vinyl species
V800	vinyl biterminated	800	Gelest DMS-V05	---
				
HB1900	hydride copolymer	1900	Gelest HMS-071	1 : 2.7
HB6000	hydride copolymer	6000	Gelest HMS-082	1 : 2.4
HB55000	hydride copolymer	55000	Gelest HMS-064	1 : 3.2
				

4.2. Optical Analysis of PDMS Microgel Deposition onto Carbon Fibers

The assessment of the microgel coating on carbon fibers was performed visually with scanning electron microscopy. The valuation includes particle size distribution and wetting ability.

Three different PDMS microgels were synthesized and their deposition onto carbon fibers is shown in Fig. 48. The varying parameter was the molar mass of the hydride copolymer. However, the same vinyl biterminated PDMS was used for all syntheses. The particle sizes of the PDMS spheres are directly related to the size and molar mass of the PDMS species. Using HB1900-PDMS with the lowest molar mass of the selected PDMS species, leads to particle sizes, which are lower than the carbon fiber diameter. A molar mass of 6,000 g/mol forms PDMS spheres in the same size range as the carbon fiber diameters. The highest molar mass, which was used for the synthesis of PDMS microgels, was 55,000 g/mol and it led to particle sizes, which are approximately three times higher than the carbon fiber diameters.

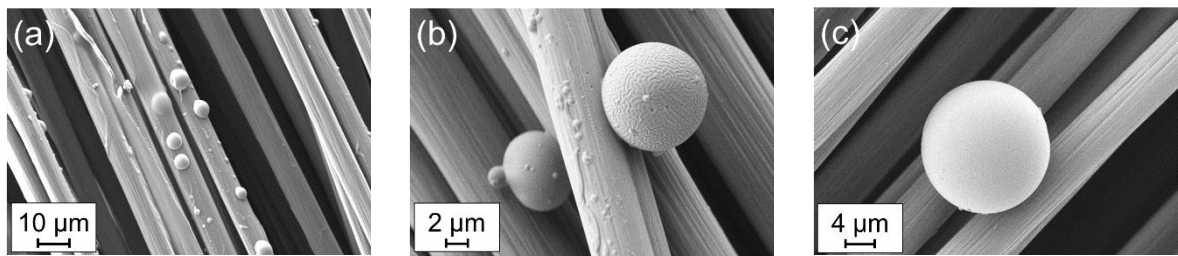


Fig. 48: SEM images of PDMS microgel on carbon fibers, synthesized from V800 and (a) HB1900, (b) HB6000 and (c) HB55000.

Furthermore, the wetting ability and therefore, the deposition of the PDMS microgel onto carbon fibers had to be ensured. As seen in Fig. 49, carbon fibers can be coated successfully with the PDMS spheres. The formed meniscus is an indication for the adhesion between PDMS particles and carbon fiber. Some PDMS particles were torn off the carbon fiber surface during sample preparation, these show impressions of the fiber on their own surface and left PDMS residue on the carbon fiber surfaces.

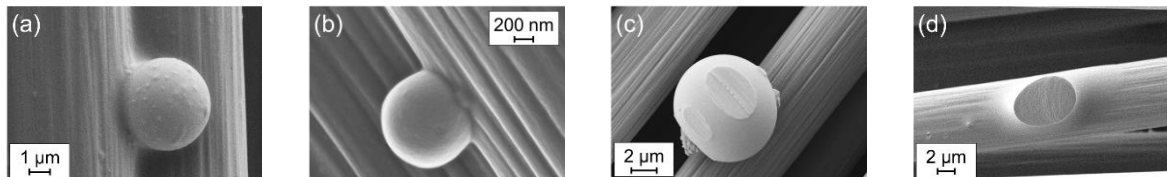


Fig. 49: SEM images of the wetting ability of PDMS microgel spheres on carbon fibers.

4.3. Fiber-Plastic Interface Characterization

For the analysis of fiber-resin interactions in CFRP composites, pull-out tests were performed. Epoxy resin BECKOPOX EP140 with EH637 was used as plastic component. Single PDMS microgel coated carbon fibers were embedded in resin droplets and pulled out of the cured resin with a defined strain rate. The recorded force is characteristic for the fiber-resin interface. The calculation of the interfacial shear strength (eq. (3)), which depends on the recorded force and the interface area, allows the comparison between pull-out tests.

None of the PDMS microgels had an impact on the interfacial shear strength between carbon fibers and epoxy resin. All three PDMS microgels, each with differently sized particles, led to similar results as oxidized carbon fibers: the IFSS of the PDMS microgel carbon fibers was measured to be 16.4 ± 1.9 MPa, which correlates to oxidized carbon fibers with an IFSS value of 16.2 ± 1.1 MPa. Meaning there was no influence of the microgel coating on oxidized carbon

fibers detected. Even though the deposition of PDMS particles was successful, the overall covered area by just few PDMS spheres is small. The poor covering ability might be the main reason for the observed performance.

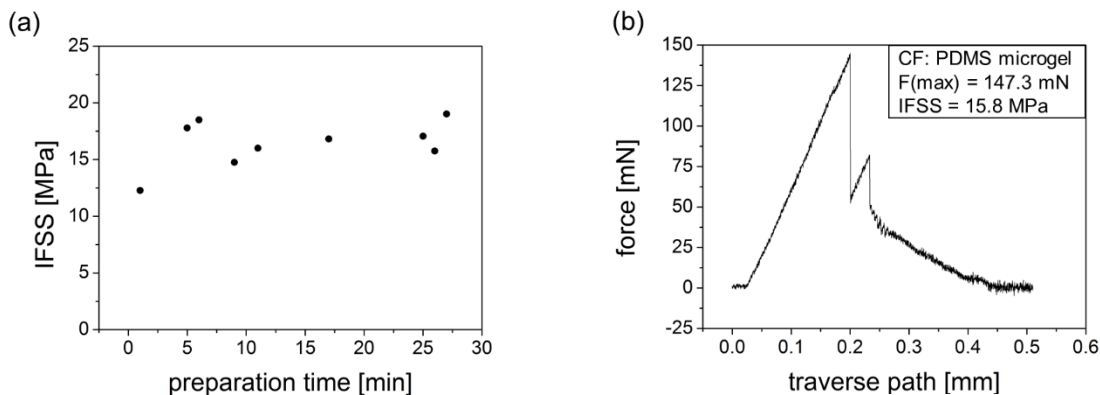


Fig. 50: Pull-out tests of PDMS microgel coated carbon fibers. (a) Summary of IFSS values of one exemplary measurement series. (b) Exemplary pull-out test of a fiber, which was prepared at 26 minutes preparation time.

The qualitative inspection of the pull-out test specimens via scanning electron microscopy defines three sections of interest (Fig.51): PDMS microgel coating (I) outside of the epoxy resin droplet, (II) within the meniscus area of the epoxy resin droplet and (III) inside the epoxy resin droplet. The PDMS microgel spheres which were outside the epoxy resin droplet for the pull-out test did not get disturbed, since they did not take part of the measurement. One of the important areas of the pull-out test is the meniscus of the resin, which is influenced by the coating of the carbon fiber. As expected, the PDMS spheres lower the wetting ability of the epoxy resin. However, the phase separation only occurs on the PDMS particles themselves and not necessarily on the surrounding area. And since the microgel covered area on the carbon fibers is very small, the effect of the PDMS particles is not detectable. The other area of interest in pull-out tests is the formerly embedded fiber. Instead of acting as a slip agent, the PDMS particles simply were torn off the carbon fiber surface. The PDMS residues of the microgel spheres are still visible after the pull-out test, but they did not contribute to sliding quantitatively.

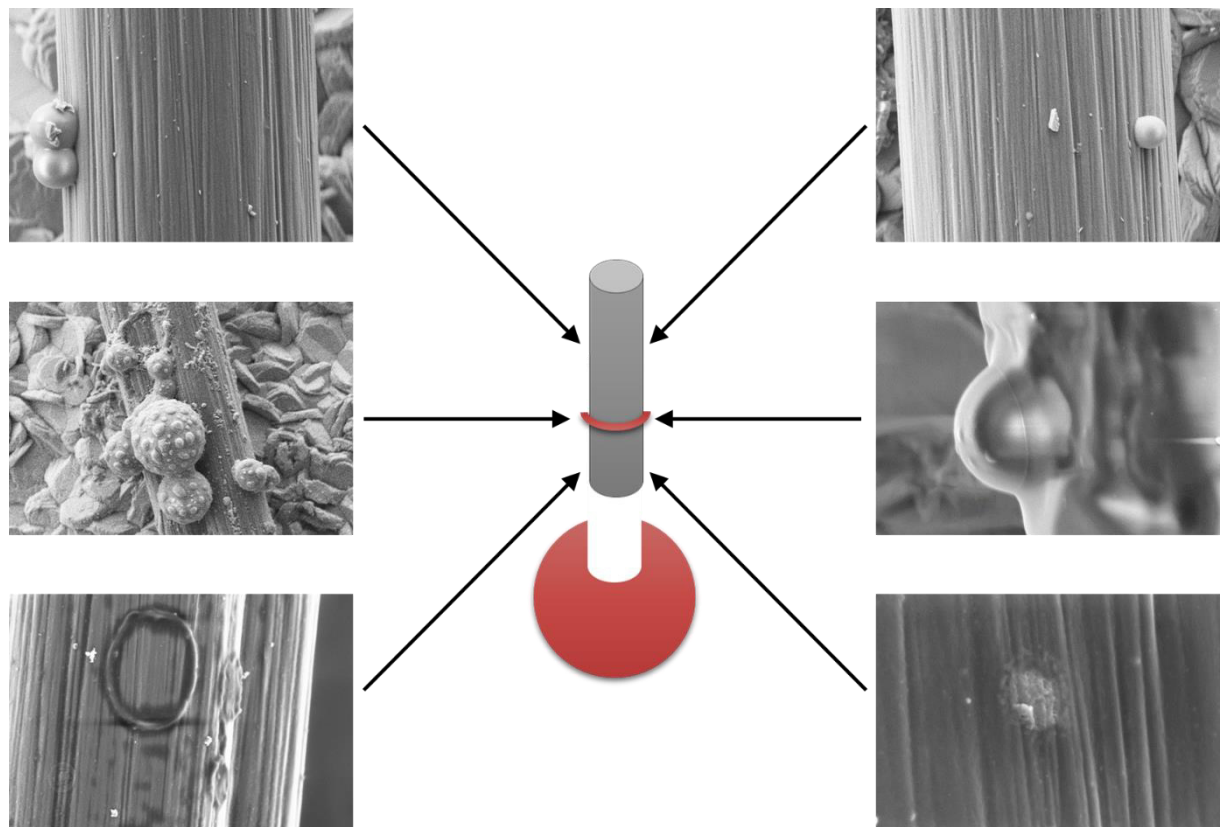


Fig.51: SEM images after pull-out tests of PDMS microgel coated carbon fibers.

4.4. Summary

PDMS microgels were successfully coated onto oxidized carbon fibers. The PDMS particle sizes of different microgels related directly to the molar masses of the used PDMS polymer educts. However, the covered area on the carbon fibers was very small and the PDMS particles did not have a quantitative influence on the interfacial shear strength in carbon fiber reinforced epoxy resins.

Next to the small coating area, the geometry of the coating also affects the fiber-resin interactions: large spherical structures on the fiber penetrate the resin deeply at the interface and do not contribute to sliding or slip effects. Therefore, a dip coating material should be tight fitting on the carbon fiber and cover the fiber surface extensively. On that account, lamellar carrier particles were chosen to be coated with PDMS and then dip coated onto carbon fibers. This system is presented in the following chapter.

Chapter 5: PDMS Janus Particles on Carbon Fibers

As shown in chapter 4, PDMS can be successfully coated on carbon fibers and act as a low friction, elastomeric interphase in CFRPs. Since, the coating process for a covalent bonding is time intensive and requires high temperatures or additional synthesis steps for the introduction of coupling agents and reactive functional groups, dip coating approaches were studied. Physical adsorptions of PDMS-structures onto carbon fibers are faster and more economical and therefore, describe methods, which are more desired in industrial-scaled manufacture.

The previous chapter focuses on dip coating with PDMS microgels. Although the physical adsorption was successful, the small coating area and the geometry of the PDMS structures prevent the PDMS phase to contribute to interfacial shear strengths of carbon fiber reinforced plastics. For that reason, lamellar particles were chosen to be used as coating material on carbon fibers. These can coat the carbon fiber surface tightly and cover more surface area. This chapter focuses on kaolinite,^{112,113} which acts as carrier particles for the PDMS phase. Meaning, the lamellar kaolinite particles first have to be coated covalently with PDMS and then are used as coating material for carbon fibers. Kaolinite clay is an aluminium silicate and defined as Janus particles,¹¹¹ due to its two-faced character.

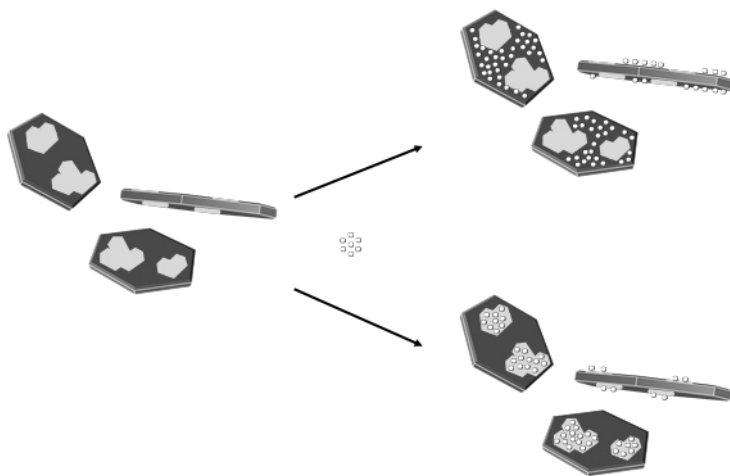


Fig. 52: Schematic illustration of the patchy two-faced Janus character of lamellar kaolinite particles.¹⁵⁰

The Janus particles were dip coated onto carbon fibers and analyzed optically via scanning electron microscopy and the effectiveness of the surface coating was determined by pull-out tests. This chapter summarizes a cooperative work project within the working group “Coatings, Materials & Polymers”. The experimental synthesis of PDMS coated kaolinite particles and the chemical analysis were performed within the doctoral thesis of Arthur Oswald¹⁵⁰ and the corresponding application procedure and mechanical analysis were performed within the present study.

5.1. Experimental

The synthesis of PDMS coated kaolinite particles was performed by A. Oswald.¹⁵⁰ The Janus particles were first treated with 3-aminopropyltriethoxysilane in order to obtain amine functions on the surface of the lamellar particles. These are more reactive than the prior available hydroxyl groups and can react directly with the epoxy biterminated polydimethylsiloxane E2400.

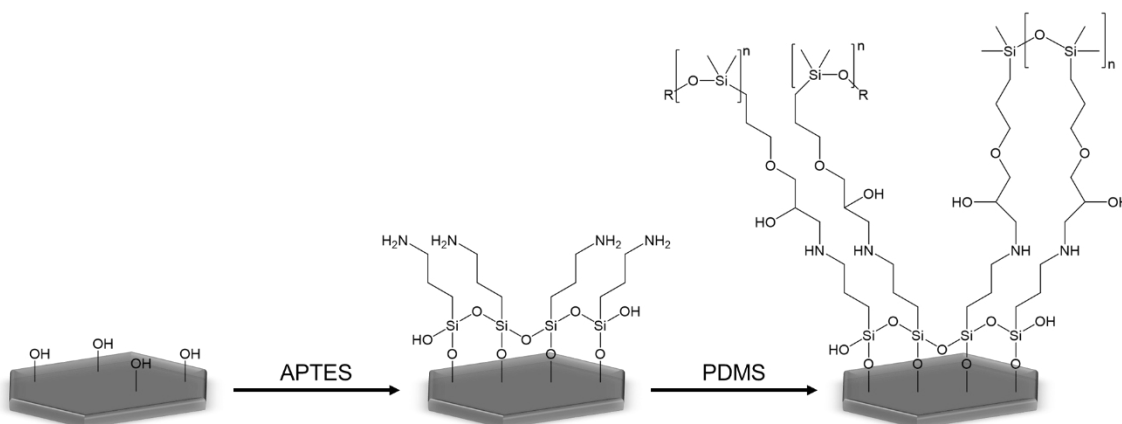


Fig. 53: Schematic illustration of the experimental procedure for the synthesis of PDMS coated kaolinite particles.

The syntheses were performed with SKT-13P kaolinite particles. The particles were dispersed in pure ethanol and 7 wt% APTES was added. The mixture was stirred at room temperature for 12 hours. The dispersion was then centrifuged two times at 4500 rpm for 5 minutes, each time 10 ml of ethanol was used for redispersion. The last dispersion was dried at 45 °C for 20 to 30 minutes until the particles appeared lucid and then treated at 120 °C for 48 hours.

For the covalent coating of APTES-Janus particles with E2400-PDMS, 0.4 wt% APTES-Janus particles were dispersed in ethanol and 30 wt% PDMS was added. The mixture was stirred at room temperature for 48 hours. The dispersion was then centrifuged two times at 4500 rpm for 5 minutes, each time 10 ml of ethanol was used for redispersion. The last dispersion was dried at 45 °C for 30 minutes.

An efficient coating of the unsized carbon fiber surface with E2400-Janus particles was performed in water. This way, a high yield of physical adsorption of the hydrophobic coated kaolinite particles was ensured. An ultrasonic bath was used for the dispersion of the E2400-Janus particles in water and the unsized carbon fibers were added to the dispersion for an hour.

5.2. Optical Analysis of PDMS-Janus Particle Deposition onto Carbon Fibers

The quality of the coating of PDMS-Janus particles and the particle distribution on carbon fibers was analyzed visually with scanning electron microscopy.

The covering ability of PDMS-Janus particles is higher than of PDMS microgel particles, comparing Fig. 48 and Fig. 54. The physical adsorption of PDMS-Janus particles on carbon fibers was overall successful, due to the setup parameters for the dip coating. Since PDMS is a hydrophobic material, the surface polarity of kaolinite decreased through the coating with PDMS. Therefore, the wetting of hydrophobic PDMS-Janus particles with water is poor. In a mixture of PDMS-Janus particles, unsized carbon fibers and water, the carbon fiber surface represent a phase, which has a lower polarity than the medium. Carbon fibers have contact angles of $90^\circ \pm 10^\circ$ (Fig. 31), meaning they are considered to be hydrophobic. Therefore, the deposition of PDMS-Janus particles on carbon fibers occurs through the PDMS phase on the particles.

However, not just the covered surface of PDMS-Janus particle coated carbon fibers is higher than of PDMS microgel coated carbon fibers, but the effectiveness of the particle's geometry is taken into account. All PDMS-Janus particles, independent of their sizes, undergo physical adsorption on the carbon fiber surface. Small particles are very tight fitting and big particles even wrap around the cylindrical fiber surface.

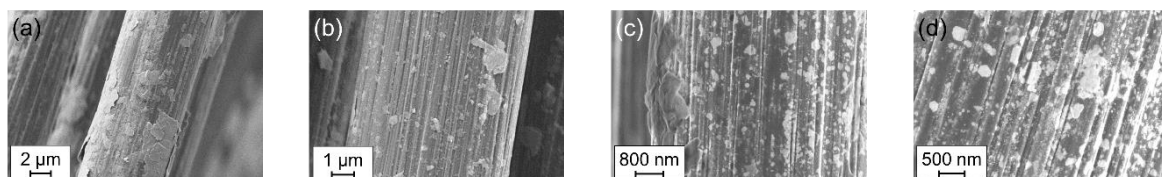


Fig. 54: Exemplary SEM images of PDMS Janus particles on carbon fibers.

5.3. Fiber-Plastic Interface Characterization

For the analysis of fiber-resin interactions in CFRP composites, pull-out tests were performed. Epoxy resin BECKOPOX EP140 and EH637 was used as plastic component. Single carbon fibers, which were coated with Janus particles, were embedded in resin droplets and pulled out of the cured resin with a defined strain rate. The recorded force is characteristic for the fiber-resin interface. The calculation of the interfacial shear strength (eq. (3)), which depends on the recorded force and the interface area, allows the comparison between pull-out tests.

Three different coatings on unsized carbon fibers were tested and are shown in Fig. 55: unmodified Janus particles, APTES-Janus particles and PDMS-Janus particles. Kaolinite particles have hydroxyl groups on the particle's surface and describe therefore, the same chemical and physical interactions in carbon fiber reinforced plastics as oxidized carbon fibers. The hydroxyl groups can take part in the curing reactions of the epoxy resin and the wetting ability of the resin is increased through the polarity of the hydroxyl groups. Additionally, the three dimensional geometry of the coating material allows mechanical interlocking with the resin and increases the interfacial shear strength even further. APTES-Janus particles coated onto carbon fibers obtain even higher IFSS values, due to the available amine groups on the particle's surface. Additionally to the physical interactions between the fiber surface and the mechanical interlocking, the chemical interactions are increased compared to unmodified Janus particles. The reaction yield between the particle's surface and the resin is higher in case of amine groups than of hydroxyl groups. This was also found to be the case for aminated carbon fibers, which were treated with tetraethylenepentamine. The interfacial shear strengths of carbon fibers, which were coated with PDMS-Janus particles, correspond with the covalent PDMS coating on carbon fibers. The characteristic stick-slip effects were observed as expected.

Tab. 9: Summary of IFSS values of carbon fibers, which were variously modified.

fiber sample	IFSS [MPa]
unsized carbon fibers	12.0 ± 0.6
oxidized carbon fibers	16.2 ± 1.1
Janus particles on carbon fibers	16.2 ± 2.1
aminated carbon fibers	21.3 ± 2.8
APTES-Janus particles on carbon fibers	21.8 ± 1.2
PDMS coated carbon fibers	8.0 ± 1.5
PDMS-Janus particles on carbon fibers	8.2 ± 0.9

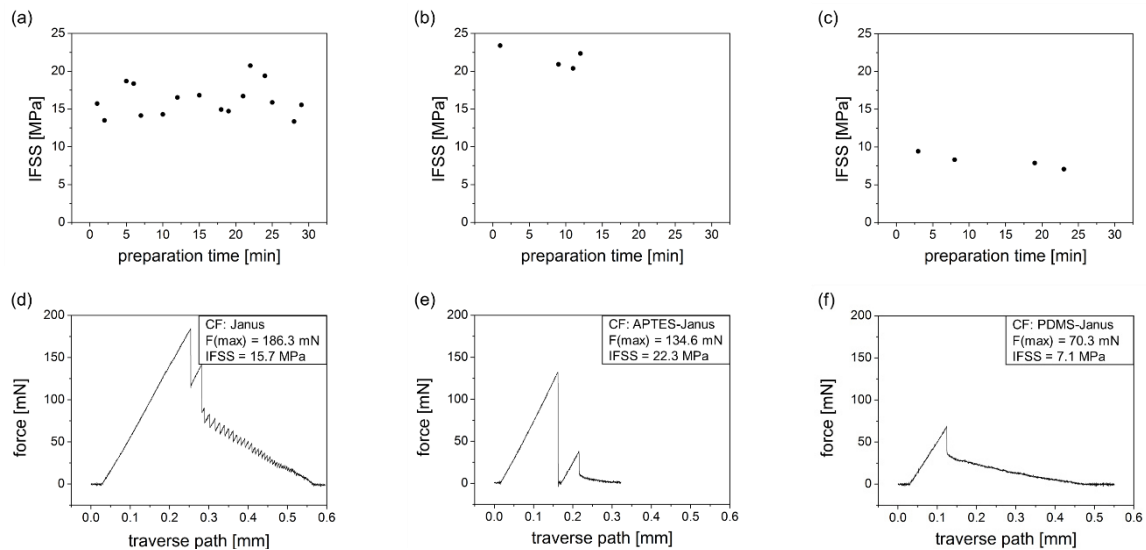


Fig. 55: Pull-out tests of Janus particles coated carbon fibers. Unmodified Janus particles coated onto carbon fibers: (a) Summary of all IFSS values of the measurement series and (d) exemplary pull-out test of a fiber, which was prepared at 1 minute preparation time. APTES-Janus particles coated onto carbon fibers: (b) Summary of all IFSS values of the measurement series and (e) exemplary pull-out test of a fiber, which was prepared at 12 minutes preparation time. PDMS-Janus particles coated onto carbon fibers: (c) Summary of all IFSS values of the measurement series and (f) exemplary pull-out test of a fiber, which was prepared at 23 minutes preparation time.

Since the PDMS phase on the Janus particles is facing the carbon fiber surface, it is expected to not find any particles left on the embedded part of the carbon fibers after the pull-out tests were performed. The adhesive force is mostly focused on the interface between kaolinite particles and epoxy resin. The pull-out test leads to a separation of carbon fiber and PDMS-Janus particles, since their interactions are weaker than the interactions between the kaolinite surface and the epoxy resin, due to the lubricating character of PDMS.

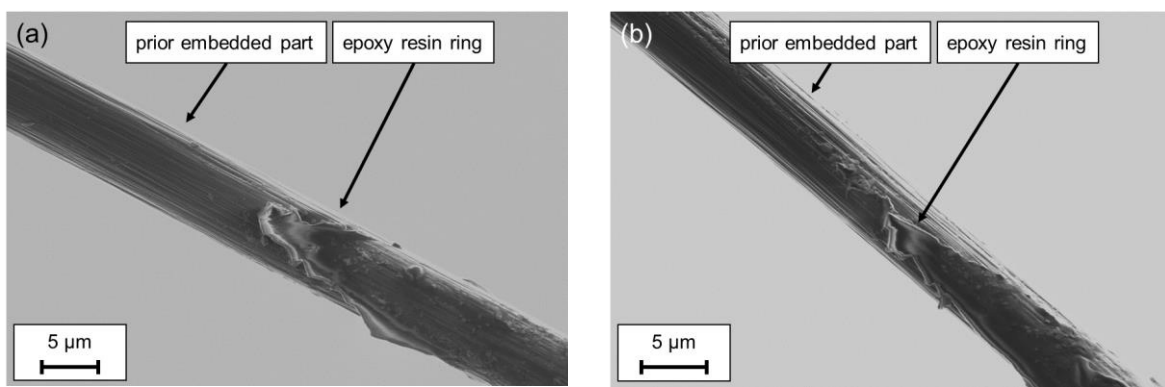


Fig. 56: Exemplary SEM images after pull-out tests of the meniscus area on carbon fibers, which were coated with PDMS-Janus particles.

5.4. Summary

PDMS-Janus particles were successfully synthesized and coated onto unsized carbon fibers. The qualitative characteristics of the coating are independent of the particle size. It was found to be an effective coating material in terms of covered area and geometry aspects. The lamellar particles fitted tightly and wrapped around the carbon fiber surface. The interfacial shear strengths correlated directly to the results of the previous chapters: oxidized carbon fibers can be replaced by Janus particles coated carbon fibers, aminated carbon fibers can be replaced by APTES-Janus particles coated carbon fibers and PDMS coated carbon fibers can be replaced by PDMS-Janus particles coated carbon fibers. The time saving and the contribution to low cycle times through the implementation of carrier particles in the manufacturing chain is a huge benefit. Without the use of dip coating with carrier particles, the increase of the IFSS of unsized carbon fibers from 12 to 16 MPa needed a 3 hour treatment in concentrated nitric acid (120 °C). A further enhancement to 21 MPa required an additional 4 hour treatment in tetraethylenepentamine (200 °C). And for the coating with PDMS, a 1 to 3 hour treatment is necessary, depending on the prior surface modifications.

All in all, the use of carrier particles is very beneficial. The beforehand surface modifications allow easy and fast dip coating processes to be integrated in industrial manufacturing chains without negative influences on cycle times and without the loss of quality.

Chapter 6: Cyclodextrin on Carbon Fibers

Previous chapters show, that PDMS can be successfully coated on carbon fibers, either covalently or on carrier particles, and act as a low friction, elastomeric interphase in CFRPs. This chapter though, focuses on a different coating material and bonding mechanism: cyclodextrin and its influence through host-guest complex formation. The complex formation was performed between the cyclodextrin, which was bonded covalently on the carbon fibers, and the epoxy resin system.

β -Cyclodextrins are cyclic oligosaccharides and can form complexes with aromatic compounds. They have a hydrophilic exterior and a hydrophobic interior, which makes them soluble in water and able to incorporate hydrophobic compounds into their cavity.^{114,115} Since they can act as host molecules for aromatic compounds like the monomers of epoxy resins (Fig. 5 (a)), polymerizations can be performed with location specificity.

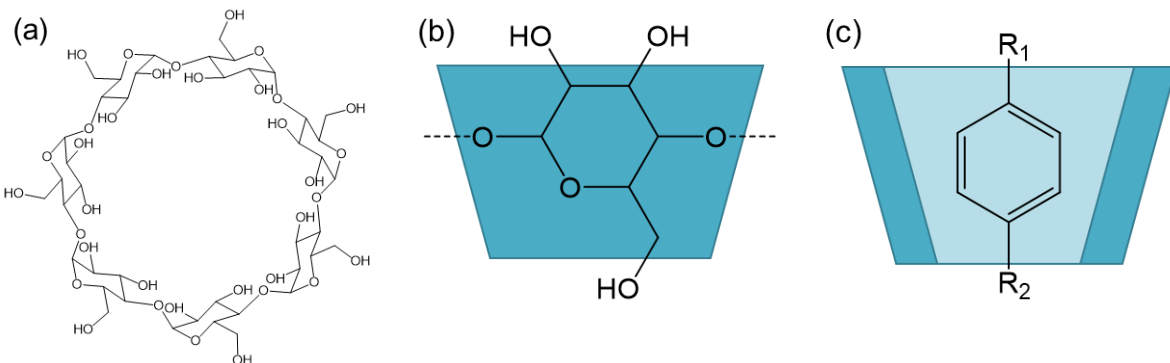


Fig. 57: (a) Molecular structure of β -cyclodextrin. (b) Schematic illustration of cyclodextrin conus and (c) inclusion complex of aromatic compound.

The chemical analysis focuses on chemical and physical properties and changes on the carbon fiber surface and the effects on composition, topography and polarity. The analysis methods include scanning electron microscopy, energy-dispersive x-ray spectroscopy and contact angle measurements. The mechanical analysis focuses on the fiber-resin interactions and is measured with pull-out tests. For that, three types of cyclodextrin coatings were tested: (I) pure β -cyclodextrin coated carbon fibers, which underwent the complex formation during the curing of the epoxy resin and β -cyclodextrin coated carbon fibers, which underwent the complex formation beforehand with either (II) the epoxy resin or (III) the amine curing agent.

6.1. Experimental

Coating of carbon fibers with cyclodextrin requires a four-step synthesis. First, the carbon fiber surface had to be activated through oxidation with nitric acid, following a treatment with tetraethylenepentamine for the introduction of amine groups. Since β -cyclodextrin has a low reactivity, it was tosylated with p-toluenesulfonyl chloride. This way, a good leaving group is available instead of the less reactive hydroxyl group. The coating process describes the reaction between aminated carbon fibers and tosylated β -cyclodextrin.

The oxidation of unsized carbon fibers was performed in concentrated nitric acid at 120 °C for 3 hours, (based on Pittman's instructions ^{51,52}). A gas washing bottle, filled with a saturated solution of iron sulfate, was used for the reduction of resulting nitrous gases. After the oxidation treatment, the mixture was carefully poured onto ice and the fibers were washed with distilled water until a neutral pH was reached. For the amination, the oxidized carbon fibers were mixed into tetraethylenepentamine and heated to 200 °C for 4 hours (based on Pittman's instructions ^{51,52}). After the mixture cooled down, the fibers were washed with distilled water. The resulting fibers contain reactive amine groups on the fiber surface and can be used directly for the coating with tosylated β -cyclodextrin.

For every 0.1 g aminated carbon fibers, 1.14 g (1 mmol) β -cyclodextrin were tosylated. β -cyclodextrin was dissolved in 50 ml water and 0.2 g (1 mmol) p-toluenesulfonyl chloride was added. The mixture was stirred at room temperature for 2 hours and the resulting gas of hydrochloric acid had to be removed constantly. After the tosylation was completed, the mixture was poured into dichloromethane. The excess solvent was removed from the precipitated solid and the product was dissolved in dimethylformamide.

The coating process was performed in DMF at temperatures between 80 and 120 °C for 4 hours. The coated fibers were then washed three times with 50 ml DMF and dried at 80 °C. Two additional samples were then prepared for the beforehand complex formation between the coated β -cyclodextrin and the aromatic parts of the resin system. One of the samples describes a beforehand complex formation between the coated β -cyclodextrin and the epoxy resin and for the other sample, the amine adduct was used for the complex formation. The beforehand complex formation was performed in water, where β -cyclodextrin coated carbon fibers and either the epoxy resin or the amine curing agent were added. The mixture was stirred at room temperature for 24 hours and later on dried at 80 °C.

6.2. Analysis of β -Cyclodextrin coated Carbon Fiber Surface

The β -cyclodextrin coating on carbon fibers was visually analyzed via scanning electron microscopy, including energy-dispersive x-ray spectroscopy. The thick coating can be observed optically, as seen in Fig. 58. Even though the coating is not homogenous, the covered area is high. There were no optical differences found between syntheses temperatures of 80, 100 and 120 °C.

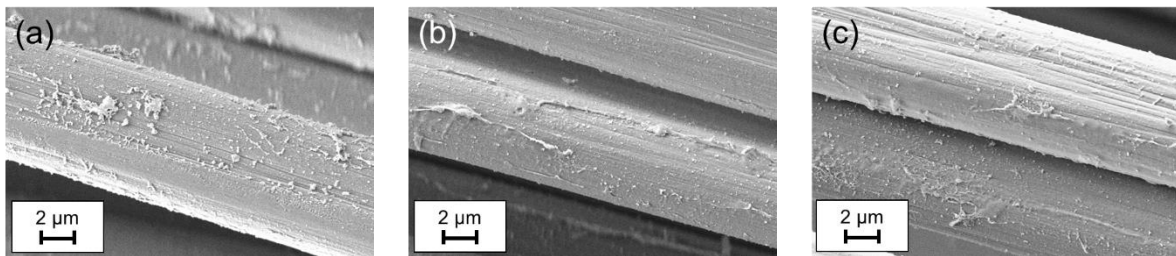


Fig. 58: Exemplary SEM images of covalently bonded β -cyclodextrin on carbon fibers.

The chemical composition was analyzed with energy-dispersive x-ray spectroscopy and is listed in Tab. 10. The $K\alpha$ lines for carbon is at 0.277 keV, for nitrogen at 0.392 keV, for oxygen at 0.525 keV and for sulfur at 2.307 keV. The element composition for carbon fibers correlates with the results of x-ray photoelectron spectroscopy (Fig. 24). Although, the nitrogen content was detected to be higher and the oxygen content to be lower than the results of the surface sensitive characterization. The reason for this is that EDX measurements detect the entire bulk material of carbon fibers, due to the penetration depth of the analytical area of 10 μm . And since there is nitrogen in the bulk and surface of carbon fibers, due to the manufacturing process (Fig. 3), and there is no oxygen in the bulk material but just on the surface of the carbon fibers, the nitrogen content is detected to be higher and the oxygen content is lower when comparing EDX and XPS measurements.

The reactivity of the carbon fiber surface was improved by a treatment with tetraethylenepentamine; therefore, an increase in nitrogen content was expected to be detected. The following coating with β -cyclodextrin was expected to increase the oxygen content, due to the high oxygen content of β -cyclodextrin itself. P-toluenesulfonyl chloride was used as a coupling agent, since it describes a good leaving group and the primary hydroxyl groups of β -cyclodextrin are low in reactivity. Sulfur was detected through EDX measurements and leads to the conclusion, that even though the reaction was set up stoichiometric, some β -cyclodextrin molecules got tosylated multiple times. The maximum amount of tosylations of β -cyclodextrin is seven times.

Tab. 10: Element composition determined by EDX measurements. [* - calculated without hydrogen and chloride content]

sample	C [at%]	N [at%]	O [at%]	S [at%]
carbon fiber	85.0	6.9	8.1	
cyclodextrin coated carbon fiber	68.0	11.3	18.0	2.7
cyclodextrin *	54.5		45.5	
tetraethylenepentamine *	61.5	38.5		
p-toluenesulfonyl chloride *	70.0		20.0	10.0

Furthermore, contact angle measurement of single β -cyclodextrin coated fibers were performed with a force tensiometer. Modifying the fiber surface changes the chemical composition and thus, the polarity of the fiber surface. The changes in polarity can be studied via contact angle measurements of single carbon fibers. Using an adapted Wilhelmy method, the dynamic contact angle of single carbon fibers can be detected. Tab. 11 summarizes the advancing contact angles. Unsized fibers have an almost inert surface, with just few oxygen and nitrogen containing functions. Therefore, the measured contact angle of 89 ° corresponds to the expected wettability (Tab. 3).^{117,118,121} The coating process of the carbon fiber surface with β -cyclodextrin increases the hydrophilicity and therefore, decreases the contact angle, due to the hydrophilic exterior of β -cyclodextrin. The complex formation with both, epoxy resin and amine curing agent, was detected with contact angle measurements and the results correspond to the analysis of the educts (Fig. 15).

Tab. 11: Comparison of contact angles of carbon fibers and β -cyclodextrin coated carbon fibers.

sample	θ [°]
carbon fiber	88.8 ± 7.3
β -cyclodextrin coated carbon fiber	54.5 ± 3.1
β -cyclodextrin complex with epoxy resin coated carbon fiber	74.2 ± 4.8
β -cyclodextrin complex with amine curing agent coated carbon fiber	71.6 ± 16.8

6.3. Fiber-Plastic Interface Characterization

For the analysis of fiber-resin interactions in CFRP composites, pull-out tests were performed. Epoxy resin BECKOPOX EP140 with EH637 was used as plastic component. Single carbon fibers, which were coated with β -cyclodextrin, with and without a prior complex formation, were embedded in resin droplets and pulled out of the cured resin with a defined strain rate. The recorded force is characteristic for the fiber-resin interface. The calculation of the interfacial shear strength (eq. (3)), which depends on the recorded force and the interface area, allows the comparability between pull-out tests.

The coating with β -cyclodextrin increases the interfacial shear strength between carbon fibers and epoxy resin drastically. Unsized carbon fibers have IFSS values of about 12 ± 0.6 MPa, while β -cyclodextrin coated carbon fibers reach IFSS values of 37.6 ± 1.8 MPa. Using beforehand complex formation with the epoxy resin or the amine coupling agent, increases the IFSS even further, to 41.0 ± 1.9 MPa. Meaning, the beforehand complex formation has a positive influence on the increase of the interfacial shear strength. These high values in adhesion cannot be explained by just functional groups, since oxidized carbon fibers (compared to the epoxy resin complex) and aminated carbon fibers (compared to the amine coupling agent complex) show IFSS values of 16.2 ± 1.1 MPa and 21.3 ± 2.8 MPa. Meaning, the bonding mechanism and complex formation have a significant impact on the adhesion between fiber and resin.

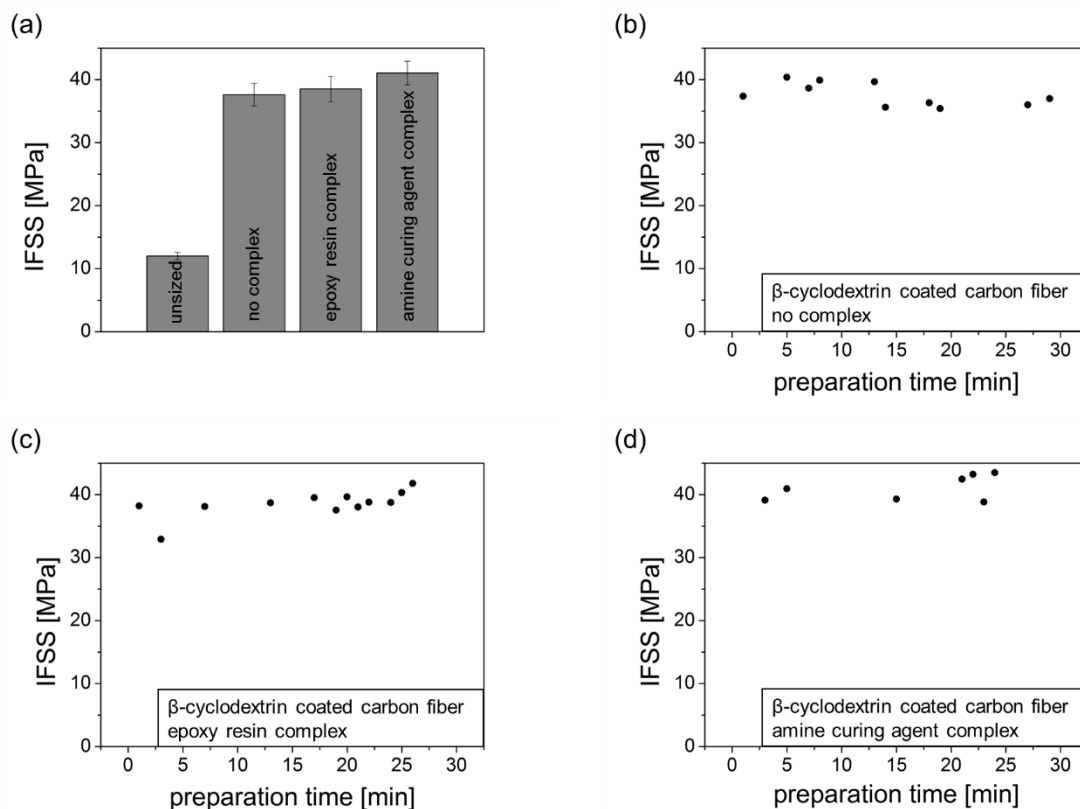


Fig. 59: Pull-out tests of β -cyclodextrin coated carbon fibers. (a) Summary of the interfacial shear strength of fibers without and with a prior complex formation. (b) Summary of the measurement series of β -cyclodextrin coated carbon fibers without prior complex formation. (c) Summary of the measurement series of β -cyclodextrin coated carbon fibers with prior complex formation with epoxy resin and (d) summary of the measurement series of β -cyclodextrin coated carbon fibers with prior complex formation with amine coupling agent.

6.4. Summary

The main objective of this study is the manipulation of energy dissipation of carbon fiber reinforced plastics through the introduction of a low friction, elastomeric interphase. However, interface design in this chapter was performed with a different bonding mechanism: the influence and interactions by cyclodextrin through host-guest complex formation. β -Cyclodextrin was bonded covalently on the carbon fiber surface and formed inclusion complexes with the surrounding plastic. The complex formation was done with the inclusion of either the epoxy resin or the amine curing agent, since both components are partly aromatic.

The cyclodextrin coating was applied successfully on the carbon fiber surface, as shown by the chemical analysis. Different states of complex formation were analyzed concerning the time of inclusion and kind of guest molecule. The analysis focuses on chemical and physical properties and changes on the carbon fiber surface and the effects on topography and polarity. The analysis methods include scanning electron microscopy, energy-dispersive x-ray spectroscopy and contact angle measurements. The mechanical analysis focuses on the fiber-resin interactions and was performed with pull-out tests.

It was possible to analyze the cyclodextrin coating visually and through element composition. The increase of reactivity of the carbon fiber surface was performed with tetraethylenepentamine and the treatment success was confirmed with the detection of an increase of nitrogen. The coating with β -cyclodextrin, on the other hand, increased the amount of oxygen. It was also observed that β -cyclodextrin was tosylated multiple times, since sulfur was detected after the coating of the carbon fibers with β -cyclodextrin. The influence of the β -cyclodextrin coating on carbon fibers was also analyzed with contact angle measurements. β -Cyclodextrin has a hydrophilic exterior and therefore, decreases the contact angles of coated carbon fibers. However, the complex formation of β -cyclodextrin with the less hydrophilic plastic components increase the contact angles of coated carbon fibers, since just the aromatic parts are part of the inclusion complex and the remaining parts of the molecules stick out and influence the overall polarity.

The ability of β -cyclodextrin to include aromatic guest molecules in its cavity has a significant impact on the interfacial shear strength of carbon fiber reinforced plastics. The complex formation itself lead to an increase of the fiber-resin adhesion from IFSS values of 12 MPa (unsized carbon fibers) to 38 MPa. It was possible to increase the interfacial shear strength even further, to 41 MPa, through a prior complex formation with one of the plastic components.

In summary, it can be stated, that the complex formation of β -cyclodextrin and the plastic components in the interface of CFRPs has a huge impact on the improvement of the interfacial shear strength. At this, an emergence can be observed, since the incredible increase in adhesion cannot be explained by the covalent use of the single components.

Chapter 7: Summary of Dissertation

This study developed from a technical issue: Is it possible to develop a CFRP component, which is optimized in its frictional behavior, while it keeps its excellent density to strength ratio? Here, an unprecedented approach was performed regarding the manipulation of the fiber-plastic interphase of CFRP composites with polydimethylsiloxane. Although CFRP compounds have remarkable mechanical properties, their deformation behavior leads to problems; including the formation of internal stress and brittle shock absorption. This is caused by the tightly bound construction of composites in combination with the low elongation ability of carbon fibers, which also makes it difficult to perform forming processes, like compression and bending. The present study shows a new approach regarding this topic, which focuses on the energy dissipation ability and elastic modulus optimization of CFRP composites.

PDMS is a well-known material in terms of low friction and its use as slip additive. Due to hydrodynamic friction, PDMS is a promising material for the objective of this study. Different coating methods were used for the coating of PDMS on carbon fibers: covalent bonding and physical adsorption of macro-sized PDMS structures. A second approach, covered by this study, describes the manipulation of the fiber-plastic interface through the interaction in complex formation.

Most research efforts within the field of carbon fiber reinforced plastics enhance the fiber-matrix adhesion. This has a positive influence of the crack propagation in a damaged CFRP composite, due to higher separation energy of fiber and plastic, and better energy transfer between them. However, enhancement of the fiber-matrix adhesion leads to increased brittleness of the compound. Though tightly bound and therefore higher in strength, the compound is less elastic and more rigid, and therefore shows low shock absorption and impact stress.^{51,52} Not only is high brittleness not desired in many applications, it creates new problems in the manufacturing chain. Processing, like bending, folding or combined forming,^{30,31} are difficult, because of the composite's low deformation performance and tendency for creasing and kinking.⁸³⁻⁸⁸

This study focuses on the modification of the carbon fiber surface and coating it with a sizing agent to manipulate the interface interactions of fiber and plastic and therefore influences the CFRP's performance. Improving the energy dissipation of CFRP composites can lead to better plastic deformation behavior, and therefore to enhanced shock absorption and to lower defect formation during manufacturing and processing. Reducing the internal stress between fiber and plastic, a ductile interphase can be applied. Ductility enables relaxation, which relieves internal stresses. If the interphase is more elastic than the fibers and the matrix, it can undergo plastic deformation, when an external load is applied. This way, the possibility of failure is lower, since the interphase is not brittle and the crack propagation cannot form local stress peaks. Meaning, the elastomeric interphase acts as a soft buffer. Next to ductility and elastomeric properties, the ideal interphase for energy dissipation should lower the friction between the components. Friction describes the force between two objects, which are in direct contact with each other. The fiber-resin adhesion and the deformation of the interphase were aimed to be modified in this work with the focus on hydrodynamic friction.

The modification of the fiber-resin interface allows the creation of an interphase with improved energy dissipation, ductile-like failure behavior, elastomeric character, enhanced plastic deformation behavior and low friction. This approach promises a reduction in internal stress, enhanced shock absorption and lower defect formation during manufacturing and processing.

PDMS was successfully coated onto carbon fibers and manipulates the fiber-resin interface in three different ways: chemical, physical and mechanical. The chemical fiber-resin interactions are lowered through PDMS during the CFRP manufacture, due to the chemical inertness of PDMS. There are fewer reactions possible in the interface, because of the lack of functional groups; the main interactions are lowered to van der Waals forces. The physical interactions are predominantly influenced by the low surface energy of PDMS and the decrease of wettability of the carbon fiber surface through PDMS coating. The epoxy resin is therefore not able to efficiently wet the carbon fiber surface, which ultimately leads to a further decrease in adherence. While the chemical and physical interactions set the level of fiber-resin adhesion during the CFRP manufacture, the mechanical influence describes the frictional behavior and the sliding ability of PDMS coated carbon fibers in the resin. The PDMS coating leads to enhanced energy dissipation in the fiber-resin interface and to hydrodynamic sliding. Within the covalent PDMS coatings, a higher reaction yield led to a larger coating area and thus, to lower interfacial shear strengths. The use of PDMS with higher molar masses also decreased the interactions between carbon fibers and epoxy resin and thus, the IFSS. Interestingly, E2400-PDMS has higher IFSS values than EB420-PDMS, although its molar mass is higher. This is caused by the different molecular structures. The scale-like domains, which are formed by using the copolymer EB420-PDMS, are more efficient in covering the carbon fiber surface than the ball-like structures, which are formed by the biterminated E2400-PDMS.

Since, the coating process for a covalent bonding is time intensive and requires high temperatures or additional synthesis steps for the introduction of coupling agents and reactive functional groups, dip coating approaches were studied. Physical adsorptions of PDMS-structures onto carbon fibers are faster and more economical and therefore, describe methods, which are more desired in industrial-scaled manufacture. The physical adsorption of PDMS microgels on carbon fibers was successful. However, the small coating area and the geometry of the PDMS structures prevent the PDMS phase to contribute to interfacial shear strengths of carbon fiber reinforced plastics. Therefore, a dip coating material should be tight fitting on the carbon fiber and cover the fiber surface extensively. On that account, lamellar carrier particles were chosen to be coated with PDMS and then dip coated onto carbon fibers. It was found to be an effective coating material in terms of covered area and geometry aspects. The lamellar particles fit tightly and wrapped around the carbon fiber surface. The interfacial shear strengths correlated directly to the previous results: oxidized carbon fibers can be replaced by Janus particles coated carbon fibers, aminated carbon fibers can be replaced by APTES-Janus particles coated carbon fibers and PDMS coated carbon fibers can be replaced by PDMS-Janus

particles coated carbon fibers. The time saving and the contribution to low cycle times through the implementation of carrier particles in the manufacturing chain is a huge benefit. All in all, the use of carrier particles is very beneficial. The beforehand surface modifications allow easy and fast dip coating processes to be integrated in industrial manufacturing chains without negative influences on cycle times and without the loss of quality.

The present study also analyzed a different coating material and bonding mechanism: cyclodextrin and its influence through host-guest complex formation. The complex formation was performed between the cyclodextrin, which was bonded covalently on the carbon fibers, and the epoxy resin system. The cyclodextrin coating was applied successfully on the carbon fiber surface. The ability of β -cyclodextrin to include aromatic guest molecules in its cavity has a significant impact on the interfacial shear strength of carbon fiber reinforced plastics. The complex formation itself lead to an increase of the fiber-resin adhesion from IFSS values of 12 MPa (unsized carbon fibers) to 38 MPa. It was possible to increase the interfacial shear strength even further, to 41 MPa, through a prior complex formation with one of the plastic components.

Bibliography

Parts of this thesis were published in Industrial & Engineering Chemistry Research. Becker-Staines, A., Bremser, W., Tröster, T., Polydimethylsiloxane as Interphase in Carbon Fiber Reinforced Epoxy Resin: Topographical Analysis and Single Fiber Pull-Out Tests. *Ind. Eng. Chem. Res.* **58**, 23143–23153 (2019). DOI: 10.1021/acs.iecr.9b05436

1. Kemp, R. Strucutral Element Aerospace. (1922).
2. Soutis, C. Carbon fiber reinforced plastics in aircraft construction. *Mater. Sci. Eng. A* **412**, 171–176 (2005).
3. Botelho, E. C., Silva, R. A., Pardini, L. C. & Rezende, M. C. A Review on the Development and Properties of Continuous Fiber / epoxy / aluminum Hybrid Composites for Aircraft Structures. *Mater. Res.* **9**, 247–256 (2006).
4. Stewart, R. Rebounding automotive industry welcome news for FRP. *Reinf. Plast.* **55**, 38–44 (2011).
5. Wilson, A. Vehicle weight is the key driver for automotive composites. *Reinf. Plast.* **61**, 100–102 (2017).
6. Meng, F., McKechnie, J. & Pickering, S. J. An assessment of financial viability of recycled carbon fibre in automotive applications. *Compos. Part A Appl. Sci. Manuf.* **109**, 207–220 (2018).
7. Meiarashi, S., Asce, M., Nishizaki, I. & Kishima, T. Life-Cycle Cost of All-Composite Suspension Bridge. *J. Compos. Constr.* **6**, 206–215 (2002).
8. Shehata, L. A. E. M., Carneiro, L. A. V & Shehata, L. C. D. Strength of short concrete columns confined with CFRP sheets. *Mater. Struct.* **35**, 50–58 (2002).
9. Orton, S. L. Development of a CFRP System to Provide Continuity in Existing Reinforced Concrete Buildings Vulnerable to Progressive Collapse. (The University of Texas at Austin (U.S), 2007). doi:3277579
10. Zhang, Q. The ‘Black Revolution’ of Sports Equipment: Application of Carbon Fiber Reinforced Plastics (CFRP). *Appl. Mech. Mater.* **440**, 69–73 (2013).
11. Sun, G. H. & Wang, J. J. The Applied Research of Fiber Reinforced Composites Materials in Sports Equipments. *Adv. Mater. Res.* **485**, 506–509 (2012).
12. Zhang, J. Study on Carbon Fiber Composite Materials in Sports Equipment. *Appl. Mech. Mater.* **329**, 105–108 (2013).
13. Tang, Z., Kotov, N. A., Magonov, S. & Ozturk, B. Nanostructured artificial nacre. *Nat. Mater.* **2**, 413–418 (2003).
14. Koohsaryan, E. & Anbia, M. Nanosized and hierarchical zeolites: A short review. *Cuihua Xuebao/Chinese J. Catal.* **37**, 447–467 (2016).

15. Moon, R. J., Martini, A., Nairn, J., Simonsen, J. & Youngblood, J. Cellulose nanomaterials review: Structure, properties and nanocomposites. *Chem. Soc. Rev.* **40**, 3941–3994 (2011).
16. Schürmann, H. *Konstruieren mit Faser-Kunststoff-Verbunden*. Springer Berlin Heidelberg New York (Springer-Verlag, 2007). doi:10.1007/b137636
17. Vosteen, F. *Composite Chronicles : A Study of the Lessons Learned in the Development, Production, and Service of Composite Structures*. (1994).
18. Witten, E., Kraus, T. & Kühnel, M. Composites Market Report 2016. *Carbon Compos.* 1–44 (2016).
19. Holleman, A. F., Wiberg, E. & Wiberg, N. *Lehrbuch der Anorganischen Chemie*. (Walter de Gruyter, 2007).
20. Qin, X., Lu, Y., Xiao, H., Wen, Y. & Yu, T. A comparison of the effect of graphitization on microstructures and properties of polyacrylonitrile and mesophase pitch-based carbon fibers. *Carbon N. Y.* **50**, 4459–4469 (2012).
21. Minus, M. L. & Kumar, S. The processing, properties, and structure of carbon fibers. *J. Miner. Met. Mater. Soc.* **57**, 52–58 (2005).
22. Zhu, D., Xu, C., Nakura, N. & Matsuo, M. Study of carbon films from PAN/VGCF composites by gelation/crystallization from solution. *Carbon N. Y.* **40**, 363–373 (2002).
23. Houtz, R. C. " Orlon " Acrylic Fiber : Chemistry and Properties. *Text. Res. J.* 786–801 (1950).
24. Mohanty, A. K., Misra, M. & Hinrichsen, G. Biofibres, biodegradable polymers and biocomposites: An overview. *Macromol. Mater. Eng.* **276–277**, 1–24 (2000).
25. Heim, M., Keerl, D. & Scheibel, T. Spider silk: From soluble protein to extraordinary fiber. *Angew. Chemie - Int. Ed.* **48**, 3584–3596 (2009).
26. Vendrely, C. & Scheibel, T. Biotechnological production of spider-silk proteins enables new applications. *Macromol. Biosci.* **7**, 401–409 (2007).
27. Osborne, J. Automotive composites-in touch with lighter and more flexible solutions. *Reinf. Plast.* **111**, 20–24 (2013).
28. Hale, J. Boeing 787 from the Ground Up. *AERO Mag.* **4**, 17–23 (2006).
29. Georgiadis, S., Gunnion, A. J., Thomson, R. S. & Cartwright, B. K. Bird-strike simulation for certification of the Boeing 787 composite moveable trailing edge. *Compos. Struct.* **86**, 258–268 (2008).
30. Schmidt, H. C. *et al.* Manufacturing Processes for Combined Forming of Multi-Material Structures Consisting of Sheet Metal and Local CFRP Reinforcements. *Key Eng. Mater.* **504–506**, 295–300 (2012).
31. Koch, S. F. *et al.* Intrinsic Hybrid Composites for Lightweight Structures: New Process Chain Approaches. *Adv. Mater. Res.* **1140**, 239–246 (2016).
32. Dau, J., Lauter, C., Damerow, U., Homberg, W. & Tröster, T. Multi-material systems for tailored automotive structural components. *18th Int. Conf. Compos. Mater.* 1–6 (2011).
33. Constantinescu, D. M., Apostol, D. A., Picu, C. R., Krawczyk, K. & Sieberer, M.

- Mechanical properties of epoxy nanocomposites reinforced with functionalized silica nanoparticles. *Procedia Struct. Integr.* **5**, 647–652 (2017).
- 34. Kumar, A., Kumar, K., Ghosh, P. K. & Yadav, K. L. MWCNT/TiO₂hybrid nano filler toward high-performance epoxy composite. *Ultrason. Sonochem.* **41**, 37–46 (2018).
 - 35. Gojny, F. H., Wichmann, M. H. G., Köpke, U., Fiedler, B. & Schulte, K. Carbon nanotube-reinforced epoxy-composites: Enhanced stiffness and fracture toughness at low nanotube content. *Compos. Sci. Technol.* **64**, 2363–2371 (2004).
 - 36. Kumar, B. G., Singh, R. P. & Nakamura, T. Degradation of Carbon Fiber-Reinforced Epoxy Composites by Ultraviolet Radiation and Condensation. *J. Compos. Mater.* **36**, 2713–2733 (2002).
 - 37. Goldschmidt, A. & Streitberger, H.-J. *BASF Handbuch Lackiertechnik*. (Vincentz Verlag, 2002).
 - 38. Solomons, T. W. G. & Fryhle, C. B. *Organic Chemistry*. (John Wiley & Sons, 2008).
 - 39. Maimí, P., Camanho, P. P., Mayugo, J. A. & Turon, A. Matrix cracking and delamination in laminated composites. Part II: Evolution of crack density and delamination. *Mech. Mater.* **43**, 194–211 (2011).
 - 40. Yu, F. ming, Okabe, Y., Wu, Q. & Shigeta, N. A novel method of identifying damage types in carbon fiber-reinforced plastic cross-ply laminates based on acoustic emission detection using a fiber-optic sensor. *Compos. Sci. Technol.* **135**, 116–122 (2016).
 - 41. Carraro, P. A., Novello, E., Quaresimin, M. & Zappalorto, M. Delamination onset in symmetric cross-ply laminates under static loads: Theory, numerics and experiments. *Compos. Struct.* **176**, 420–432 (2017).
 - 42. Yue, Z. R., Jiang, W., Wang, L., Gardner, S. D. & Pittman, C. U. Surface characterization of electrochemically oxidized carbon fibers: surface properties and interfacial adhesion. *Carbon N. Y.* **37**, 1785–1796 (1999).
 - 43. Fukunaga, A. & Ueda, S. Anodic surface oxidation for pitch-based carbon fibers and the interfacial bond strengths in epoxy matrices. *Compos. Sci. Technol.* **60**, 249–254 (2000).
 - 44. Boudou, J. P., Paredes, J. I., Cuesta, A., Martínez-Alonso, A. & Tascón, J. M. D. Oxygen plasma modification of pitch-based isotropic carbon fibres. *Carbon N. Y.* **41**, 41–56 (2003).
 - 45. Zhang, X., Huang, Y. & Wang, T. Plasma activation of carbon fibres for polyarylacetylene composites. *Surf. Coatings Technol.* **201**, 4965–4968 (2007).
 - 46. Jang, B. Z. Control of interfacial adhesion in continuous carbon and kevlar fiber reinforced polymer composites. *Compos. Sci. Technol.* **44**, 333–349 (1992).
 - 47. Lee, W. H., Lee, J. G. & Reucroft, P. J. XPS study of carbon fiber surfaces treated by thermal oxidation in a gas mixture of O₂/(O₂+N₂). *Appl. Surf. Sci.* **171**, 136–142 (2001).
 - 48. Laachachi, A. *et al.* A chemical method to graft carbon nanotubes onto a carbon fiber. *Mater. Lett.* **62**, 394–397 (2008).
 - 49. L. H. Meng, Z. W. Chen, X. L. Song, Y. X. Liang, Y. D. Huang, Z. X. J. Influence of High Temperature and Pressure Ammonia Solution Treatment on Interfacial Behavior of Carbon Fiber/Epoxy Resin Composites. *J. Appl. Polym. Sci.* **113**, 3436–3441 (2009).

50. Severini, F., Formaro, L., Pegoraro, M. & Posca, L. Chemical modification of carbon fiber surfaces. *Carbon N. Y.* **40**, 735–741 (2002).
51. Pittman, C. U., He, G. R., Wu, B. & Gardner, S. D. Chemical Modification of Carbon Nanofiber Surfaces by Nitric Acid Oxidation Followed by Reaction with Tetraethylenepentamine. *Carbon N. Y.* **35**, 317–331 (1997).
52. Pittman, C. U. *et al.* Reactivities of amine functions grafted to carbon fiber surfaces by tetraethylenepentamine. Designing interfacial bonding. *Carbon N. Y.* **35**, 929–943 (1997).
53. Zhang, X., Pei, X., Jia, Q. & Wang, Q. Effects of carbon fiber surface treatment on the tribological properties of 2D woven carbon fabric/polyimide composites. *Appl. Phys. A Mater. Sci. Process.* **95**, 793–799 (2009).
54. Zhang, X. R., Pei, X. Q. & Wang, Q. H. The effect of fiber oxidation on the friction and wear behaviors of short-cut carbon fiber/polyimide composites. *Express Polym. Lett.* **1**, 318–325 (2007).
55. Su, F. H., Zhang, Z. Z., Wang, K., Jiang, W. & Liu, W. M. Tribological and mechanical properties of the composites made of carbon fabrics modified with various methods. *Compos. Part A Appl. Sci. Manuf.* **36**, 1601–1607 (2005).
56. Tran, M. Q., Ho, K. K. C., Kalinka, G., Shaffer, M. S. P. & Bismarck, A. Carbon fibre reinforced poly(vinylidene fluoride): Impact of matrix modification on fibre/polymer adhesion. *Compos. Sci. Technol.* **68**, 1766–1776 (2008).
57. Li, J. The effect of surface modification with nitric acid on the mechanical and tribological properties of carbon fiber-reinforced thermoplastic polyimide composite. *Surf. Interface Anal.* **41**, 759–763 (2009).
58. Weitzsacker, C. L., Xie, M. & Drzal, L. T. Using XPS to Investigate Fiber/Matrix Chemical Interactions in Carbon-fiber-reinforced Composites. *Surf. Interface Anal.* **25**, 53–63 (1997).
59. Fernández, B., Arbelaitz, A., Valea, A., Mujika, F. & Mondragon, I. A comparative study on the influence of epoxy sizings on the mechanical performance of woven carbon fiber-epoxy composites. *Polym. Compos.* **25**, 319–330 (2004).
60. Ren, P., Liang, G. & Zhang, Z. Influence of epoxy sizing of carbon-fiber on the properties of carbon fiber/cyanate ester composites. *Polym. Compos.* **27**, 591–598 (2006).
61. Gnädinger, F., Middendorf, P. & Fox, B. Interfacial shear strength studies of experimental carbon fibres, novel thermosetting polyurethane and epoxy matrices and bespoke sizing agents. *Compos. Sci. Technol.* **133**, 104–110 (2016).
62. Dilsiz, N. & Wightman, J. P. Effect of acid-base properties of unsized and sized carbon fibers on fiber/epoxy matrix adhesion. *Colloids Surfaces A Physicochem. Eng. Asp.* **164**, 325–336 (2000).
63. Karsli, N. G., Ozkan, C., Aytac, A. & Deniz, V. Effects of sizing materials on the properties of carbon fiber-reinforced polyamide 6,6 composites. *Polym. Compos.* **34**, 1583–1590 (2013).
64. Wonderly, C., Grenestedt, J., Fernlund, G. & Čepus, E. Comparison of mechanical properties of glass fiber/vinyl ester and carbon fiber/vinyl ester composites. *Compos.*

Part B Eng. **36**, 417–426 (2005).

65. Tekalur, S. A., Shivakumar, K. & Shukla, A. Mechanical behavior and damage evolution in E-glass vinyl ester and carbon composites subjected to static and blast loads. *Compos. Part B Eng.* **39**, 57–65 (2008).
66. LI, J., FAN, Q., Chen, Z., Huang, K. & CHENG, Y. Effect of electropolymer sizing of carbon fiber on mechanical properties of phenolic resin composites. *Trans. Nonferrous Met. Soc. China* **16**, Supple, s457–s461 (2006).
67. Kettle, A. P., Beck, A. J., O'Toole, L., Jones, F. R. & Short, R. D. Plasma polymerisation for molecular engineering of carbon-fibre surfaces for optimised composites. *Compos. Sci. Technol.* **57**, 1023–1032 (1997).
68. Drzal, L. T. & Raghavendran, V. K. Adhesion of Thermoplastic Matrices to Carbon Fibers: Effect of Polymer Molecular Weight and Fiber Surface Chemistry. *J. Thermoplast. Compos. Mater.* **16**, 21–30 (2003).
69. Bismarck, A., Pfaffernoschke, M., Springer, J. & Schulz, E. Polystyrene-grafted carbon fibers: Surface properties and adhesion to polystyrene. *J. Thermoplast. Compos. Mater.* **18**, 307–331 (2005).
70. Yadav, A. K. *et al.* Mechanical Analysis of Nickel Particle-Coated Carbon Fiber-Reinforced Epoxy Composites for Advanced Structural Applications. *ACS Appl. Nano Mater.* **1**, 4332–4339 (2018).
71. Zhang, F. H., Wang, R. G., He, X. D., Wang, C. & Ren, L. N. Interfacial shearing strength and reinforcing mechanisms of an epoxy composite reinforced using a carbon nanotube/carbon fiber hybrid. *J. Mater. Sci.* **44**, 3574–3577 (2009).
72. Mei, L. *et al.* Multiscale carbon nanotube–carbon fiber reinforcement for advanced epoxy composites with high interfacial strength. *Polym. Polym. Compos.* **19**, 107–112 (2011).
73. Lv, P. *et al.* Increasing the interfacial strength in carbon fiber/epoxy composites by controlling the orientation and length of carbon nanotubes grown on the fibers. *Carbon N. Y.* **49**, 4665–4673 (2011).
74. Qian, H., Bismarck, A., Greenhalgh, E. S. & Shaffer, M. S. P. Carbon nanotube grafted carbon fibres: A study of wetting and fibre fragmentation. *Compos. Part A Appl. Sci. Manuf.* **41**, 1107–1114 (2010).
75. Lee, S. B. *et al.* Processing and characterization of multi-scale hybrid composites reinforced with nanoscale carbon reinforcements and carbon fibers. *Compos. Part A Appl. Sci. Manuf.* **42**, 337–344 (2011).
76. Guo, J., Lu, C., An, F. & He, S. Preparation and characterization of carbon nanotubes/carbon fiber hybrid material by ultrasonically assisted electrophoretic deposition. *Mater. Lett.* **66**, 382–384 (2012).
77. Zhang, X. *et al.* Interfacial Microstructure and Properties of Carbon Fiber Composites Modified with Graphene Oxide. *ACS Appl. Mater. Interfaces* **4**, 1543–1552 (2012).
78. Ma, Y. *et al.* Enhanced interfacial properties of carbon fiber reinforced polyamide 6 composites by grafting graphene oxide onto fiber surface. *Appl. Surf. Sci.* **452**, 286–298 (2018).
79. Kim, B. J. *et al.* Synergistic interfacial reinforcement of carbon fiber/polyamide 6 composites using carbon-nanotube-modified silane coating on ZnO-nanorod-grown

- carbon fiber. *Compos. Sci. Technol.* **165**, 362–372 (2018).
- 80. Jones, A. R., Cintora, A., White, S. R. & Sottos, N. R. Autonomic healing of carbon fiber/epoxy interfaces. *ACS Appl. Mater. Interfaces* **6**, 6033–6039 (2014).
 - 81. Thostenson, E. T. & Chou, T. W. Carbon nanotube networks: Sensing of distributed strain and damage for life prediction and self healing. *Adv. Mater.* **18**, 2837–2841 (2006).
 - 82. Thostenson, E. T. & Chou, T. W. Real-time in situ sensing of damage evolution in advanced fiber composites using carbon nanotube networks. *Nanotechnology* **19**, (2008).
 - 83. Gutkin, R., Pinho, S. T., Robinson, P. & Curtis, P. T. A finite fracture mechanics formulation to predict fibre kinking and splitting in CFRP under combined longitudinal compression and in-plane shear. *Mech. Mater.* **43**, 730–739 (2011).
 - 84. Bishara, M., Vogler, M. & Rolfes, R. Revealing complex aspects of compressive failure of polymer composites ??? Part II: Failure interactions in multidirectional laminates and validation. *Compos. Struct.* **169**, 116–128 (2017).
 - 85. Kabiri Ataabadi, A., Hosseini-Toudeshky, H. & Ziae Rad, S. Experimental and analytical study on fiber-kinking failure mode of laminated composites. *Compos. Part B Eng.* **61**, 84–93 (2014).
 - 86. Gutkin, R., Costa, S. & Olsson, R. A physically based model for kink-band growth and longitudinal crushing of composites under 3D stress states accounting for friction. *Compos. Sci. Technol.* **135**, 39–45 (2016).
 - 87. Naya, F. *et al.* Computational micromechanics of fiber kinking in unidirectional FRP under different environmental conditions. *Compos. Sci. Technol.* **144**, 26–35 (2017).
 - 88. Canal, L. P., González, C., Segurado, J. & LLorca, J. Intraply fracture of fiber-reinforced composites: Microscopic mechanisms and modeling. *Compos. Sci. Technol.* **72**, 1223–1232 (2012).
 - 89. Bishara, M., Rolfes, R. & Allix, O. Revealing complex aspects of compressive failure of polymer composites – Part I: Fiber kinking at microscale. *Compos. Struct.* **169**, 105–115 (2017).
 - 90. Lambiase, F. & Ko, D. C. Feasibility of mechanical clinching for joining aluminum AA6082-T6 and Carbon Fiber Reinforced Polymer sheets. *Mater. Des.* **107**, 341–352 (2016).
 - 91. Lambiase, F. & Paoletti, A. Friction-assisted clinching of Aluminum and CFRP sheets. *J. Manuf. Process.* **31**, 812–822 (2018).
 - 92. Lee, M. sik & Kang, C. gil. Determination of forming procedure by numerical analysis and investigation of mechanical properties of steel/CFRP hybrid composites with complicated shapes. *Compos. Struct.* **164**, 118–129 (2017).
 - 93. Lee, M. S., Kim, S. J., Lim, O. D. & Kang, C. G. Effect of process parameters on epoxy flow behavior and formability with CR340/CFRP composites by different laminating in deep drawing process. *Procedia Eng.* **81**, 1627–1632 (2014).
 - 94. Bell, J. P., Chang, J., Rhee, H. W. & Joseph, R. Application of ductile polymeric coatings onto graphite fibers. *Polym. Compos.* **8**, 46–52 (1987).
 - 95. Gerard, J. -F. Characterization and role of an elastomeric interphase on carbon fibers reinforcing an epoxy matrix. *Polym. Eng. Sci.* **28**, 568–577 (1988).

96. Wimolkiatisak, A. S. & Bell, J. P. Toughening of Graphite-Epoxy Composites with an Electropolymerized High-Temperature Thermoplastic Interphase. *J. Appl. Polym. Sci.* **46**, 1899–1914 (1992).
97. Ruina, A. Slip Instability and State Variable Friction Laws. *J. Geophys. Res.* **88**, 359–370 (1983).
98. C. Canudas de Wit, H. Olsson, K.J.Astrom & P.Lischinsky. A new model for control of systems with friction. *IEEE Trans. Automat. Contr.* **40**, 419–425 (1995).
99. Armstrong-Helouvry, B., Dupont, P. & C. Canudas de Wit. A Survey of Models, Analysis Tools and Compensation Methods for the Control of Machines with Friction. *Automatica* **30**, 1083–1138 (1994).
100. Galliano, A., Bistac, S. & Schultz, J. Adhesion and friction of PDMS networks: Molecular weight effects. *J. Colloid Interface Sci.* **265**, 372–379 (2003).
101. Chaudhury, M. K. Surface free energies of alkylsiloxane monolayers supported on elastomeric polydimethylsiloxanes. *J. Adhes. Sci. Technol.* **7**, 669–675 (1993).
102. Camino, C., Lomakin, S. M. & Lazzari, M. Polydimethylsiloxane thermal degradation part 1. Kinetic aspects. *Polymer (Guildf.)* **42**, 2395–2402 (2001).
103. Niu, X., Peng, S., Liu, L., Wen, W. & Sheng, P. Characterizing and patterning of PDMS-based conducting composites. *Adv. Mater.* **19**, 2682–2686 (2007).
104. Zhu, B. *et al.* Poly(dimethylsiloxane) Thin Film as a Stable Interfacial Layer for High-Performance Lithium-Metal Battery Anodes. *Adv. Mater.* **29**, 2–7 (2017).
105. Bergeron, V. *et al.* Polydimethylsiloxane (PDMS)-based antifoams. *Colloids Surfaces A Physicochem. Eng. Asp.* **122**, 103–120 (1997).
106. Inn, Y. & Wang, S. Q. Hydrodynamic Slip: Polymer Adsorption and Desorption at Melt/Solid Interfaces. *Phys. Rev. Lett.* **76**, 467–470 (1996).
107. Chambon, F. & Winter, H. H. Linear Viscoelasticity at the Gel Point of a Crosslinking PDMS with Imbalanced Stoichiometry. *J. Rheol. (N. Y. N. Y.)* **31**, 683–697 (1987).
108. Khorasani, M. T., Mirzadeh, H. & Kermani, Z. Wettability of porous polydimethylsiloxane surface: Morphology study. *Appl. Surf. Sci.* **242**, 339–345 (2005).
109. Kim, T. K., Kim, J. K. & Jeong, O. C. Measurement of nonlinear mechanical properties of PDMS elastomer. *Microelectron. Eng.* **88**, 1982–1985 (2011).
110. Lee, W. S., Yeo, K. S., Andriyana, A., Shee, Y. G. & Adikan, F. R. M. Effect of cyclic compression and curing agent concentration on the stabilization of mechanical properties of PDMS elastomer. *Mater. Des.* **96**, 470–475 (2016).
111. Walther, A. & Müller, A. H. E. Janus particles. *Soft Matter* **4**, 663–668 (2008).
112. Saikia, N. J. *et al.* Characterization, beneficiation and utilization of a kaolinite clay from Assam, India. *Appl. Clay Sci.* **24**, 93–103 (2003).
113. Murray, H. H. Traditional and new applications for kaolin, smectite, and palygorskite: A general overview. *Appl. Clay Sci.* **17**, 207–221 (2000).
114. Szejtli, J. Introduction and General Overview of Cyclodextrin Chemistry. *Chem. Rev.* **98**, 1743–1754 (1998).

115. Del Valle, E. M. M. Cyclodextrins and their uses: A review. *Process Biochem.* **39**, 1033–1046 (2004).
116. An, F., Zhou, P., Lu, C. & Liu, Y. Tuning the surface grooves of carbon fibers by dry-jet gel-spinning. *Carbon N. Y.* (2018). doi:10.1016/j.carbon.2018.11.009
117. *Application Report AR271e: Wettability of carbon fibers using single-fiber contact angle measurements – a feasibility study.* (2013).
118. Wang, J. *et al. Application Report AR284: Determining the wettability of carbon fiber tows from single fiber contact angle data.* (2017).
119. Qiu, S., Fuentes, C. A., Zhang, D., Van Vuure, A. W. & Seveno, D. Wettability of a single carbon fiber. *Langmuir* **32**, 9697–9705 (2016).
120. Good, R. J. *Contact Angle, Wetting, and Adhesion: A Critical Review.* *Journal of Adhesion Science and Technology* **6**, (1992).
121. Wang, J. *et al.* Wettability of carbon fibres at micro- and mesoscales. *Carbon N. Y.* **120**, 438–446 (2017).
122. Wang, S., Zhang, Y., Abidi, N. & Cabrales, L. Wettability and surface free energy of graphene films. *Langmuir* **25**, 11078–11081 (2009).
123. Rafiee, J. *et al.* Wetting transparency of graphene. *Nat. Mater.* **11**, 217–222 (2012).
124. Shih, C. J. *et al.* Breakdown in the wetting transparency of graphene. *Phys. Rev. Lett.* **109**, 1–5 (2012).
125. Shin, Y. J. *et al.* Surface-energy engineering of graphene. *Langmuir* **26**, 3798–3802 (2010).
126. Moon, I. K., Lee, J., Ruoff, R. S. & Lee, H. Reduced graphene oxide by chemical graphitization. *Nat. Commun.* **1**, 1–6 (2010).
127. Chemzstry, F., Sczence, A. & Ohz-cho, T. Modification fluorination of carbon fiber surfaces by direct. *J. Fluor. Chem.* **57**, 169–175 (1992).
128. Zhao, F., Huang, Y., Liu, L., Bai, Y. & Xu, L. Formation of a carbon fiber/polyhedral oligomeric silsesquioxane/carbon nanotube hybrid reinforcement and its effect on the interfacial properties of carbon fiber/epoxy composites. *Carbon N. Y.* **49**, 2624–2632 (2011).
129. Nguyen, T. C., Bai, Y., Zhao, X. L. & Al-Mahaidi, R. Durability of steel/CFRP double strap joints exposed to sea water, cyclic temperature and humidity. *Compos. Struct.* **94**, 1834–1845 (2012).
130. Ma, L. Experimental Study on Corrosion Resistance of Carbon Fiber Reinforced Concrete for Sea Crossing Bridge. *J. Coast. Res.* **83**, 423–428 (2018).
131. Palani, S., Hack, T., Deconinck, J. & Lohner, H. Validation of predictive model for galvanic corrosion under thin electrolyte layers: An application to aluminium 2024-CFRP material combination. *Corros. Sci.* **78**, 89–100 (2014).
132. Zhandarov, S. & Mäder, E. Characterization of fiber/matrix interface strength: Applicability of different tests, approaches and parameters. *Compos. Sci. Technol.* **65**, 149–160 (2005).
133. Pisanova, E., Zhandarov, S. & Mäder, E. How can adhesion be determined from

- micromechanical tests? *Compos. Part A Appl. Sci. Manuf.* **32**, 425–434 (2001).
- 134. Zhandarov, S. F., Mäder, E. & Yurkevich, O. R. Indirect estimation of fiber/polymer bond strength and interfacial friction from maximum load values recorded in the microbond and pull-out tests. Part I: local bond strength. *J. Adhes. Sci. Technol.* **16**, 1171–1200 (2002).
 - 135. Zhandarov, S. & Mäder, E. Indirect estimation of fiber/polymer bond strength and interfacial friction from maximum load values recorded in the microbond and pull-out tests. Part II: Critical energy release rate. *J. Adhes. Sci. Technol.* **17**, 967–980 (2003).
 - 136. Mueller, W. M., Moosburger-Will, J., Sause, M. G. R. & Horn, S. Microscopic analysis of single-fiber push-out tests on ceramic matrix composites performed with Berkovich and flat-end indenter and evaluation of interfacial fracture toughness. *J. Eur. Ceram. Soc.* **33**, 441–451 (2013).
 - 137. Sha, J. J. *et al.* Measurement and analysis of fiber-matrix interface strength of carbon fiber-reinforced phenolic resin matrix composites. *J. Compos. Mater.* **48**, 1303–1311 (2014).
 - 138. Wagner, H. D., Nairn, J. A. & Detassis, M. Toughness of interfaces from initial fiber-matrix debonding in a single fiber composite fragmentation test. *Appl. Compos. Mater. An Int. J. Sci. Appl. Compos. Mater.* **2**, 107–117 (1995).
 - 139. Kim, B. W. & Nairn, J. a. Observations of Fiber Fracture and. *J. Compos. Mater.* **36**, 1825–1858 (2002).
 - 140. Hu, W. *et al.* Experimental investigation and modeling of the rate-dependent deformation behavior of PMMA at different temperatures. *Eur. Polym. J.* **85**, 313–323 (2016).
 - 141. Chen, W., Lu, F. & Cheng, M. Tension and compression tests of two polymers under quasi-static and dynamic loading. **21**, 113–121 (2002).
 - 142. Naik, N. K. *et al.* High strain rate mechanical behavior of epoxy under compressive loading: Experimental and modeling studies. *Mater. Sci. Eng. A* **528**, 846–854 (2011).
 - 143. Zhou, Y., Wang, Y., Jeelani, S. & Xia, Y. Experimental Study on Tensile Behavior of Carbon Fiber and Carbon Fiber Reinforced Aluminum at Different Strain Rate. *Appl. Compos. Mater.* **14**, 17–31 (2007).
 - 144. Ochola, R. O., Marcus, K., Nurick, G. N. & Franz, T. Mechanical behaviour of glass and carbon fibre reinforced composites at varying strain rates. *Compos. Struct.* **63**, 455–467 (2004).
 - 145. Dilsiz, N. & Wightman, J. P. Surface analysis of unsized and sized carbon fibers. *Carbon N. Y.* **37**, 1105–1114 (1999).
 - 146. Marotzke, C. & Qiao, L. Interfacial crack propagation arising in single-fiber pull-out tests. *Compos. Sci. Technol.* **57**, 887–897 (1997).
 - 147. Jero, P. D., Kerans, R. J. & Parthasarathy, T. A. Effect of Interfacial Roughness on the Frictional Stress Measured Using Pushout Tests. *J. Am. Ceram. Soc.* **74**, 2793–2801 (1991).
 - 148. Baker, W. O. Microgel, A New Macromolecule. *Ind. Eng. Chem.* **41**, 511–520 (1949).
 - 149. Saunders, B. & Vincent, B. Microgel particles as model colloids: theory, properties and

- applications. *Adv. Colloid Interface Sci.* **80**, 1–25 (1999).
150. Oswald, A. Organized Colloids - Organization of Spherical and Lamellar Particles. (University of Paderborn).